Tinnitus-Related Hyperactivity through Homeostatic Plasticity in the Auditory Pathway

DISSERTATION

zur Erlangung des akademischen Grades
doctor rerum naturalium
(Dr. rer. nat.)

im Fach Biophysik

eingereicht an der
Mathematisch-Naturwissenschaftlichen Fakultät I
Humboldt-Universität zu Berlin

von

Herrn Dipl.-Biophys. Roland Schaette
geboren am 24.07.1977 in Wuppertal

Präsident der Humboldt-Universität zu Berlin:
Prof. Dr. Christoph Markschies

Dekan der Mathematisch-Naturwissenschaftlichen Fakultät I:
Prof. Dr. Christian Limberg

Gutachter:

1. Dr. Richard Kempter
2. Prof. Dr. Andreas Herz
3. Prof. James A. Kaltenbach, Ph.D.

Tag der mündlichen Prüfung: 12. September 2007

A spider's web is hidden in one ear, and in the other, a cricket sings throughout the night.

- Michelangelo

Contents

Chapter 1

Introduction

> *My ears hum and buzz continuously day and night. I can tell you that I lead a miserable existence.*
>
> - Ludwig van Beethoven

Tinnitus is a phantom auditory sensation, the perception of a sound in the absence of acoustic stimulation. The term 'tinnitus' derives from the Latin *tinnire*, which means 'to ring'. The perceived tinnitus sounds can be tone-like or noise-like. Common descriptions of the tinnitus percept given by patients are 'ringing', 'whistling', 'humming', 'buzzing', or 'roaring'. Tinnitus is a very common phenomenon: up to 25% of the population have experienced an episode of tinnitus at least once (Pilgramm et al., 1999). In most cases, tinnitus only lasts for a short time, but for some people tinnitus becomes a chronic sensation. In severe cases, the tinnitus sound can be heard even in the presence of loud ambient sound. The number of persons that are seriously affected by a chronic form of tinnitus is estimated to be more than a million in Germany alone (Pilgramm et al., 1999).

Tinnitus is closely related to hearing loss. The majority of tinnitus patients is also affected by hearing loss (Nicolas-Puel et al., 2002), and the perceived pitch of the tinnitus sensation corresponds to frequencies at which hearing is impaired (Henry et al., 1999). It is thus assumed that hearing loss through cochlear damage can lead to the development of tinnitus, possibly by triggering plastic changes in the auditory system. However, hearing loss does not automatically lead to tinnitus (Lockwood et al., 2002). So far, etiologic treatments of tinnitus are not available, as the mechanisms of tinnitus development in humans have remained unclear.

The fact that tinnitus is heard in the absence of acoustic stimuli indicates that it is the spontaneous activity of neurons in the auditory pathway that is perceived. This implies that the spontaneous activity must be altered such that it resembles stimulus-induced activity. Possible scenarios are that the spontaneous firing rates of some neurons are increased or their spontaneous discharge is synchronized. Animal models of tinnitus have been developed to unravel its neural basis. Behavioral studies have verified that animals can perceive tinnitus, for example after acoustic trauma or the administration of ototoxic drugs. Neurophysiological studies in animals found no signs of tinnitus-related activity in the auditory nerve (AN) after tinnitus-inducing treatment, showing that tinnitus must be generated in the central auditory system. Possible neural correlates of tinnitus were found in the auditory cortex, the midbrain, and the brainstem. The earliest stage where tinnitus-related changes in neuronal activity were found was the dorsal cochlear nucleus (DCN), which receives excitatory input from the AN. Following cochlear damage through acoustic trauma or the administration of ototoxic drugs, the

spontaneous firing rates of neurons in the DCN were significantly increased. Moreover, the increase in spontaneous firing rates was correlated with behavioral evidence for tinnitus. These results present a paradoxical situation, as cochlear damage decreases the activity of AN fibers, yet the spontaneous firing rates in the DCN are increased. The mechanisms that give rise to such tinnitus-related hyperactivity have not been clarified yet.

This thesis focuses on the development of tinnitus after hearing loss through cochlear damage. We are going to address the following main questions:

- Are there audiometric differences between patients with both tinnitus and hearing loss and patients with hearing loss, but without tinnitus?
- How is tinnitus-related hyperactivity in the auditory system generated? What are the plasticity mechanisms that give rise to tinnitus-related activity patterns?
- Can a model for the development of tinnitus-related hyperactivity after hearing loss deliver realistic predictions of tinnitus pitch from the audiograms of tinnitus patients?

To address these questions, we employ theoretical models of neuronal information processing in the auditory system that capture the effects of hearing loss and feature mechanisms of activity-dependent neuronal plasticity. Furthermore, we analyze audiometric data from patients with and without tinnitus and apply our models to the data.

Chapters 2-5 of this thesis contain an introduction and supply the reader with background information. Chapter 2 gives an overview of the mammalian auditory system, with a special emphasis on the cochlea, the auditory nerve, and the cochlear nucleus, as these are the essential parts upon which we base our models. In Chapter 3, we summarize causes and consequences of hearing loss through cochlear damage. This chapter also covers results from animal studies on how hearing loss through cochlear damage changes the responses of auditory nerve fibers and triggers plastic changes along the auditory pathway. In Chapter 4, we review results on tinnitus in humans and animals. Special emphasis is put on the relation between tinnitus and hearing loss. We summarize results from animal studies that have identified increased spontaneous firing rates or *hyperactivity* as a neural correlate of tinnitus. Mechanisms of activity-dependent neuronal plasticity as a possible link between hearing loss and tinnitus are treated in Chapter 5. We review basic findings about spike-timing-dependent plasticity and homeostatic plasticity, and summarize evidence for the occurrence of these plasticity mechanisms in the auditory system.

The presentation of our results starts in Chapter 6 with an analysis of patient data that addresses whether there are audiometric differences between patients with hearing loss and tinnitus and patients with hearing loss but without tinnitus. We find that tinnitus patients have less hearing loss, a steeper slope of the audiogram, and the edge of the audiogram is located at higher frequencies compared to patients without tinnitus.

In Chapter 7, we present a computational model for the development of tinnitus-related hyperactivity after hearing loss. The model comprises how the responses of auditory nerve fibers and cochlear nucleus neurons are altered by hearing loss. We find that cochlear damage persistently decreases the mean firing rate of AN fibers, thus reducing the excitatory input to cochlear nucleus neurons. We then analyze the effect of activity stabilization through homeostatic plasticity in cochlear nucleus neurons. When the neuronal response gain is increased to compensate for decreased excitatory input, the mean rate can be stabilized, albeit at the cost of

increased spontaneous firing rates. Hyperactivity after hearing loss could thus be a consequence of activity stabilization.

In the basic model for the development of hyperactivity we only consider excitatory input. To analyze the influence of inhibition, we extend the model in Chapter 8 in order to reproduce the basic neuronal circuit of the dorsal cochlear nucleus with its main inhibitory interneurons. By adjusting the strengths of the inhibitory projections, we can reproduce salient response properties of DCN projection neurons in our model. We find that the development of hyperactivity through homeostatic plasticity depends on the ratio of excitation and inhibition. Neurons only become hyperactive when excitation dominates over inhibition, leading to a mean rate that is above the spontaneous rate.

Finally, as an acid test, in Chapter 9 we apply our model to the data from tinnitus patients. The model is used to predict changes in the spontaneous firing rates of auditory brainstem neurons from the audiograms of tinnitus patients. We find that the resulting patterns of hyperactivity are consistent with the pitch of the patients' tinnitus sensations. Pitch prediction is only possible from the activity patterns of neurons that become hyperactive.

The implications of our results for the treatment of tinnitus and preliminary results of a clinical study that employs tinnitus treatment based on the predictions of our model are discussed in Chapter 10.

Chapter 2

Auditory System

This chapter gives a short overview over the auditory system, with special emphasis on the cochlea, the auditory nerve and the cochlear nucleus, as these are the essential parts for the models presented in this work.

2.1 Ear and Auditory Organ

The ear transforms a mechanical signal, the pressure wave of sound, into a train of action potentials in the auditory nerve. This process of mechanosensory transduction involves several stages. It starts with the outer ear, which is shaped like a collecting horn and guides the sound waves onto the tympanic membrane. The human outer ear is most sensitive at approximately 3 kHz, where it reaches an amplifier gain of around 10 dB. The next stage is the middle ear, which contains a chain of three tiny bones called ossicles. The first one, malleus, is connected to the tympanic membrane, the last one, stapes, to the round window of the cochlea. Malleus and stapes are linked by the incus. The middle ear is required for an effective transduction of the aerial sound pressure wave into movement of the fluid inside the cochlea. It acts as an impedance transformer that matches the high impedance of the cochlear fluid to the low impedance of air. Impaired function of the middle ear increases the hearing threshold by 30-50 dB (Møller, 2000).

The final transformation of the mechanical into an electrical signal is performed in the cochlea, a snail-shaped bony structure that contains the sensory organ of hearing. The cochlea contains three fluid-filled canals, the scala tympani, the scala vestibuli, and the scala media. The scala media is situated in the middle, it is separated from the scala vestibuli by Reissner's membrane, and from the scala tympani by the basilar membrane (Fig. 2.1a).

The sensory cells of the cochlea are contained in the organ of Corti, a structure that is situated atop of the basilar membrane (Fig. 2.1a). They are called hair cells because they possess tiny hair-like protrusions at their upper ends, called stereocilia (Fig. 2.1b), which contact the tectorial membrane. There are two kinds of hair cells in the cochlea, inner hair cells (IHCs) and outer hair cells (OHCs). They are arranged in rows parallel to the longitudinal direction of the cochlea, one row of inner and three rows of outer hair cells. The IHCs are the main sensory cells, and the OHCs are believed to be involved in the active processes of the cochlea (see below). The cochlear hair cells are innervated by two types of auditory nerve (AN) fibers, the thick, myelinated type-I fibers that contact the IHCs and constitute about 95% of all AN fibers, and the thin, unmyelinated type-II fibers that contact the OHCs. Each IHC is contacted by

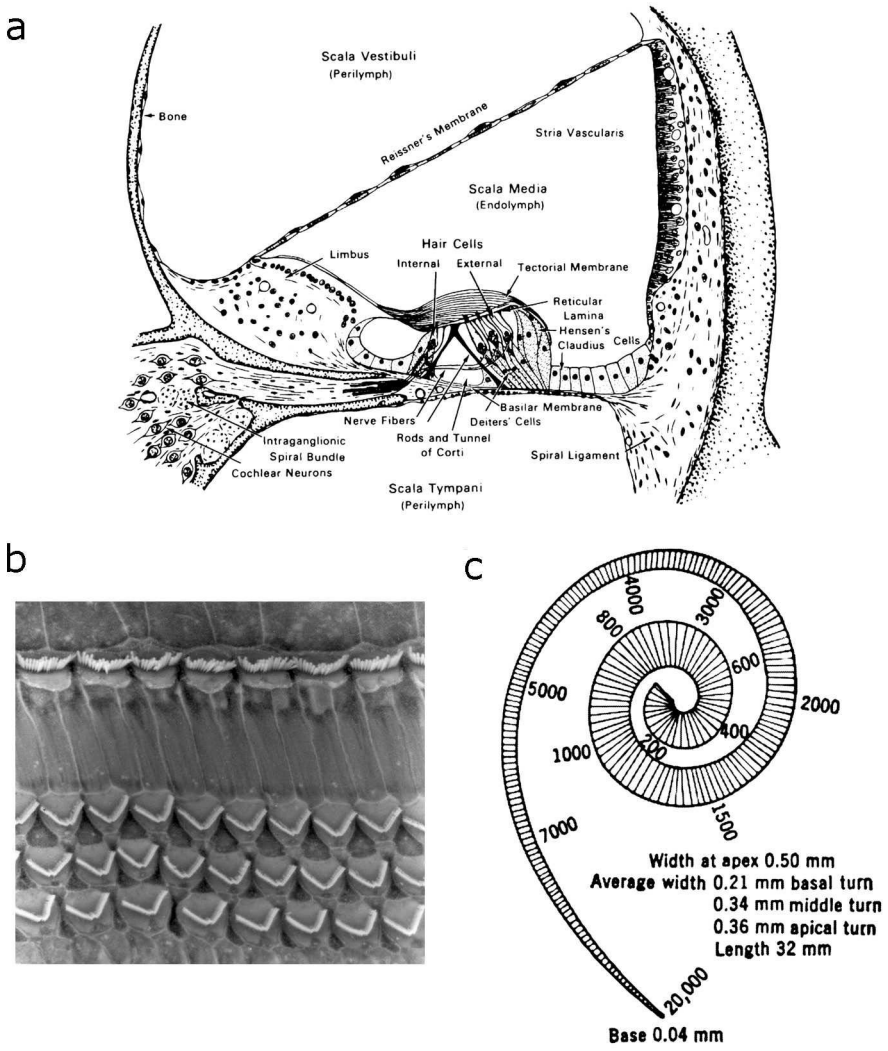

Figure 2.1: The cochlea. **a)** Cross-section through the cochlea (figure taken from Davis et al., 1953). The scala media is separated from the scala vestibuli by Reissner's membrane, and from scala tympani by the basilar membrane. The organ of Corti is located on the basilar membrane, it contains outer and inner hair cells. The auditory nerve fibers that contact the hair cells originate from spiral ganglion neurons (cochlear neurons). **b)** Raster electron micrograph picture of the surface of the organ of Corti (image courtesy of the Auditory Science Lab at the Hospital for Sick Children). One row of inner hair cells (top) and the three rows of outer hair cells (bottom, V-shaped) can be seen. The hair-like protrusions at the apical ends of the hair cells are the stereocilia which contact the tectorial membrane. **c)** Schematic picture of the basilar membrane illustrating its dimensions and the ordered representation of frequencies along its length. Low frequencies are represented at the apical end, and high frequencies at the basal end of the basilar membrane. Dimensions and frequencies are given for the average human cochlea (figure taken from Stuhlmann, 1943).

approximately 10-30 type-I AN fibers (the exact number may vary across species and along the length of the cochlea) but each type-I fiber contacts only one IHC (Ryugo, 1992). The innervation pattern of OHCs is different, each type-II fibers contacts several OHCs, and each OHC is contacted by approximately 10 type-II fibers (Ryugo, 1992). Moreover, IHCs and OHCs are also contacted by efferent fibers of the olivocochlear system.

Movement of the stapes sets the cochlear fluid into motion, leading to a displacement of the basilar membrane. A traveling wave is created inside the cochlea along the basilar membrane. Each place of the basilar membrane is tuned to a different frequency, and the resonance frequencies are ordered along the basilar membrane from high frequencies at the basal end to low frequencies at the apical end (see Fig. 2.1c). This frequency tuning arises from a combination of the basilar membrane's passive mechanical properties with active mechanisms in the OHCs. The active processes enhance the sensitivity of the basilar membrane response and sharpen its frequency tuning. The frequency spectrum of an acoustic stimulus is thus converted into a spatial pattern of vibration along the basilar membrane, as each frequency component excites a different patch of the basilar membrane. This basic principle of an ordered representation of frequencies along the basilar membrane is called *tonotopy*. It is preserved throughout the auditory system. At each processing stage one observes an arrangement of neurons ordered according to their characteristic frequency (CF, the frequency of highest sensitivity).

Vibrations of the basilar membrane are detected by the IHCs, as mechanical movement of the basilar membrane relative to the tectorial membrane leads to a deflection of their stereocilia. Deflection of the stereocilia causes ion channels to open, which transforms mechanical motion into a change in transmembrane voltage. This step converts the mechanical signal into an electrical signal. The voltage change is then passively conducted to the basal end of the IHC. Sufficient depolarization leads to transmitter release at the ribbon synapse between IHC and auditory nerve fiber, causing the auditory nerve fiber to fire an action potential. The tuning of IHCs and thus also type-I auditory nerve fibers originates from the frequency selectivity of the cochlea.

2.2 Auditory Nerve

There are two types of AN fibers, type-I fibers that contact the IHCs of the cochlea, and type-II fibers that contact the OHCs. Both fiber types project to the cochlear nucleus. Type-I fibers respond to sound and are well studied (see Ryugo, 1992, for a review), whereas little is known about the response properties of type-II fibers (Robertson et al., 1999; Reid et al., 2004), their targets in the cochlear nucleus (see, e.g., Berglund et al., 1996) and their role in auditory processing. In the following, we will only treat type-I fibers that comprise 95% of all auditory nerve fibers, and refer to them simply as auditory nerve fibers.

The response threshold of a single AN fiber depends on the frequency of the stimulus. The frequency with the lowest response threshold is called the characteristic frequency (CF) of that particular fiber. The tuning curve, i.e. the curve of threshold against frequency, usually has a narrow tip centered at the CF, and a large response area at frequencies below the CF. Thresholds rise very steep above the CF. Typical tuning curves are shown in Fig. 2.2.

Many AN fibers are spontaneously active, they produce action potentials also in the absence of acoustic stimuli. The spontaneous discharge rates and the response thresholds of AN fibers are related. Fibers with a high spontaneous rate (usually more than 20 Hz) have the lowest

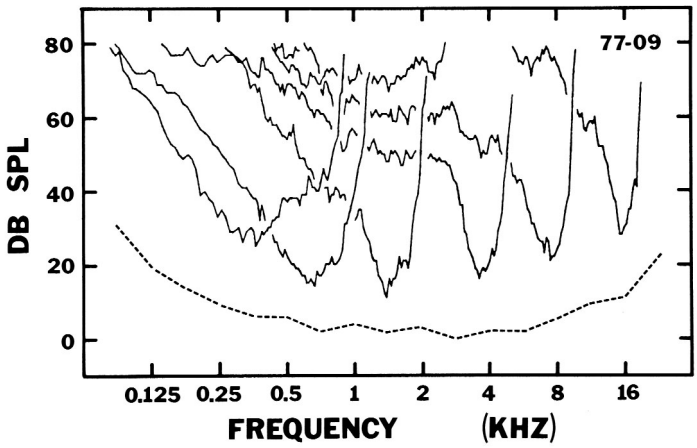

Figure 2.2: Threshold tuning curves of chinchilla auditory nerve fibers (figure taken from Ryugo, 1992). The frequency at which the lowest response threshold is observed is called the 'characteristic frequency'. The width of the tuning curves decreases for higher characteristic frequencies, the tuning is said to get 'sharper'.

response thresholds (around 0-10 dB) at CF, whereas units with lower spontaneous rate tend to have higher thresholds (Liberman, 1978). Above the response threshold, the discharge rate of AN fibers grows monotonously with increasing stimulus intensity, and reaches a plateau for high sound intensities. The dynamic range of single AN fibers is usually below 15 dB, although fibers with low spontaneous rate (less than 1 Hz) sometimes have larger dynamic ranges (Taberner and Liberman, 2005). Typical rate-intensity functions are shown in Fig. 2.3.

2.3 Overview over the Central Auditory System

The central auditory system consists of an ascending and a descending part. The ascending pathway comprises projections from the periphery to more central structures, whereas the descending pathway contains feedback projections.

2.3.1 Ascending Pathway

The auditory system is organized hemispherically in that each processing stage of the pathway is present on both sides of the brain. We now describe the major ascending pathways (Fig. 2.4). The auditory nerve terminates in the cochlear nucleus (CN), the first central processing stage of the ascending auditory pathway. Several pathways diverge from the different divisions of the CN, with the dorsal cochlear nucleus (DCN) projecting mainly to the contralateral inferior colliculus (IC) and the ventral divisions of the CN projecting to the olivary nuclei and the medial nucleus of the trapezoid body of both sides, and to the contralateral lateral lemniscus (LL). From the olivary nuclei, there are ascending connections to the nuclei of the LL and the IC. The IC is a central hub of the ascending auditory pathway (Casseday et al., 2002; Pollak et al., 2003), almost all ascending pathways converge in the IC. There are, however, some exceptions like the direct projection from the CN to the auditory thalamus that bypasses the IC (Malmierca et al., 2002; Anderson et al., 2006). The IC projects to the medial geniculate

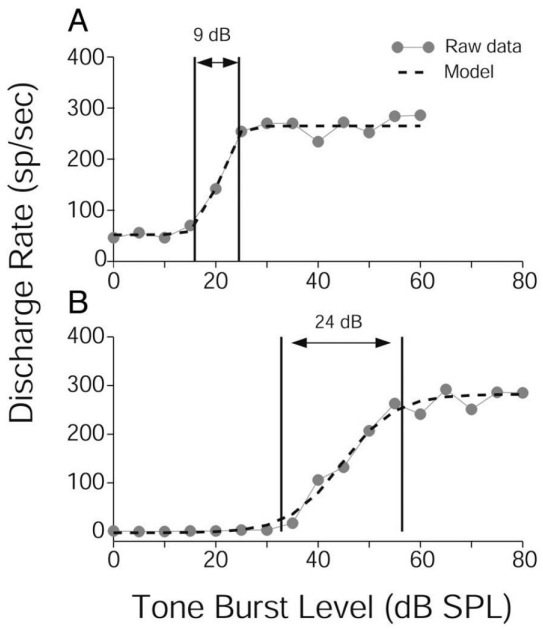

Figure 2.3: Rate-intensity functions of mouse AN fibers (figure taken from Taberner and Liberman, 2005, used with permission). **a)** Rate-intensity function (gray dots) of a fiber with a low threshold and a high spontaneous rate (49.7 Hz). The dotted line is a model fit that was used to determine the dynamic range (10-90% of the maximum driven discharge rate), which is 9 dB for this fiber. **b)** Rate-intensity function of a high-threshold, low spontaneous rate fiber.

body (MBG), which is located in the thalamus. From there, projections to the auditory cortex emerge. Major targets are the primary and secondary auditory cortex, the insular cortex, and the posterior auditory field (Winer, 1992).

The ascending auditory pathway is characterized by strong binaural interactions. The olivary nuclei, for example, receive projections from the ipsi- and the contralateral CN. Moreover, there are also commissural connections at many processing stages, connecting the cochlear nuclei of both sides (Cant and Gaston, 1982), the inferior colliculi (Pollak et al., 2003), and of course the auditory cortices via the corpus callosum (Winer, 1992).

Along the auditory pathway, an increasing specialization of the neuronal responses is generally observed. Whereas many responses of neurons in the ventral cochlear nucleus (VCN) still resemble the responses of AN fibers, already in the DCN more complex response properties emerge. In the olivary nuclei, neurons are sensitive to interaural time- and level differences. These response properties are important for sound localization in the horizontal plane. In the IC, neurons are also sensitive to the elevation of sound sources (Schnupp and King, 1997), which is important for the representation of auditory space. Cortical neurons have been shown to be sensitive to many specialized features, like frequency-modulation of stimuli (Nelken, 2002) or the pitch of complex tones (Bendor and Wang, 2005). Specialization of the neuronal response along the auditory pathway is thought to be the basis of feature extraction. Convergence of different sorts of inputs from a variety of cell types in lower processing centers as well as interaction of excitation and inhibition is needed for such complex responses. The basic tonotopic organization, however, is preserved at all stages of the auditory pathway.

2.3.2 Descending Pathway

The auditory system is also characterized by an abundance of descending projections. The auditory cortex projects, for example, to several lower regions of the auditory pathway: the MGB, the IC, the ventral nucleus of the trapezoid body, the lateral superior olive, and even as far peripherally as the CN (Smith and Spirou, 2002). Further descending connections go from

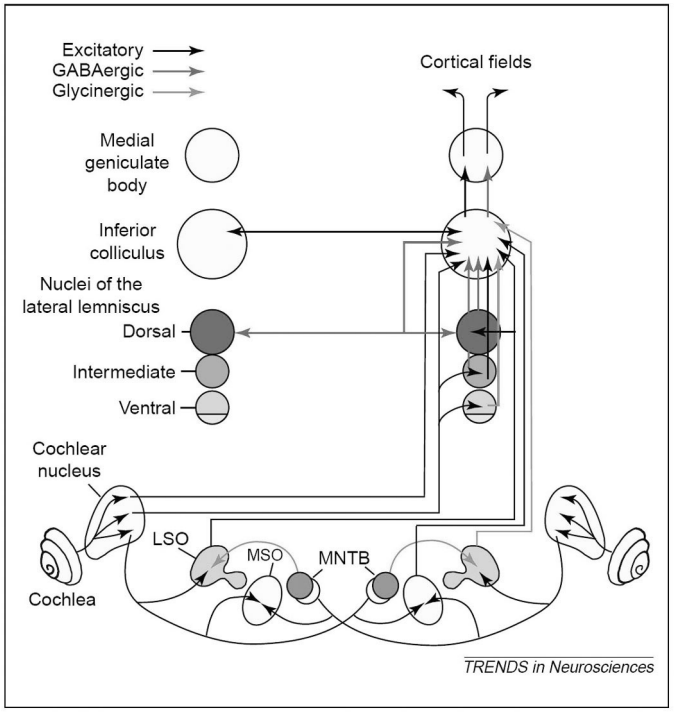

Figure 2.4: Schematic diagram of major pathways of the ascending auditory system (figure adapted from Pollak et al., 2003, used with permission from Elsevier). Each step of the auditory pathway is organized tonotopically. This organization principle is derived from the mapping of frequency along the cochlea. In the cochlea, hair cells, which are the primary sensory cells, transform acoustic signals into nerve impulses, that are then relayed to the cochlear nucleus via the auditory nerve. From there, several parallel pathways diverge. They involve the lateral superior olive (LSO), the medial superior olive (MSO), the medial nucleus of the trapezoid body (MNTB), and the nuclei of the lateral lemniscus, and then converge onto the inferior colliculus. The inferior colliculus projects to the medial geniculate body, a thalamic structure, which finally transmits the information to the auditory cortex. Excitatory connections are denoted by black and inhibitory connections by gray arrows. Top-down connections of the 'descending' pathway, e.g. from the cortex to the thalamus, IC and cochlear nucleus, are not shown.

the IC to the olivary nuclei and to the DCN (Møller, 2000). An important efferent pathway is the olivocochlear system, which provides feedback signals to the cochlea. The olivocochlear fibers originate from neurons in the olivary nuclei and project to OHCs and IHCs in the cochlea. This feedback can modulate the responses of AN fibers. Electrical stimulation of fibers of the olivocochlear bundle increases the response threshold of AN fibers, decreases the spontaneous firing rate, and shifts rate-intensity functions to higher sound intensities (Winslow and Sachs, 1987; Guinan and Gifford, 1988).

2.4 Cochlear Nucleus

The cochlear nucleus has two major divisions, the ventral cochlear nucleus, and the dorsal cochlear nucleus. All auditory nerve fibers terminate in the CN, synapsing on the various neuron types of the CN. The innervation pattern preserves the cochleotopic arrangement of the AN fibers. Fibers originating from the apex of the cochlea innervate more ventral parts of all divisions of the CN, whereas fibers coming from basal parts of the cochlea innervate more dorsal regions, preserving a tonotopic organization.

In anatomical studies, a variety of cochlear nucleus neurons have been identified, for example fusiform, giant, cartwheel, radial, and multipolar cells. Physiologically, CN neurons can be characterized by their response to acoustic stimuli. A common classification scheme for CN neurons divides the neurons into response types based on the shape of their response map, their spontaneous rate, their noise-response, and the shape of their rate-intensity function. In the following, we will briefly summarize the five main response types that are recorded from CN neurons, schematic illustrations of the corresponding response maps are shown in Fig. 2.5. Type-I neurons are characterized by a response map with a single excitatory area, and their responses are very similar to the responses of auditory nerve fibers. These neurons are spontaneously active, respond to tones and noise, and have a monotonic rate-intensity function. Type-I neurons are mainly found in the VCN. The response map of type-II neurons also contains a central excitatory region, but there may also be inhibitory sidebands. Type-II neurons are not spontaneously active, do not respond to noise and have nonmonotonic rate-intensity functions. These neurons are exclusively found in the DCN. Type-III neurons display a response map with a central excitatory area and inhibitory sidebands. In contrast to type-II neurons, they are spontaneously active and respond to noise. These neurons can be found in DCN and VCN. Type IV neurons show mainly inhibitory responses, but they have some excitatory areas, with a prominent, low-threshold excitation region. Type V neurons show only inhibitory responses at low sound pressure levels, and possess a small excitatory area at high sound pressure level. They are spontaneously active and only found in the DCN. (see Rhode and Greenberg, 1992, and references therein). Neurons in the CN have also been classified according to their post-stimulus time histograms (PSTHs) in response to acoustic stimuli. A rich repertoire of response types has been observed, for example neurons whose PSTHs are very similar to those of AN fibers (primary-like response), repetitively firing chopper units, onset units that only fire at the beginning of a stimulus presentation, and many more (see Rhode and Greenberg, 1992, for a review).

Interestingly, binaural interactions already take place at the level of the cochlear nucleus. There is a commissural projection from the contralateral CN that directly connects the cochlear nuclei of both sides (Cant and Gaston, 1982; Shore et al., 1992), and excitatory as well as

inhibitory responses to contralateral stimulation have been observed (Mast, 1970, 1973; Shore et al., 2003; Davis, 2005; Sumner et al., 2005). In the following, we are going to treat the complex anatomy and physiology of the DCN in more detail.

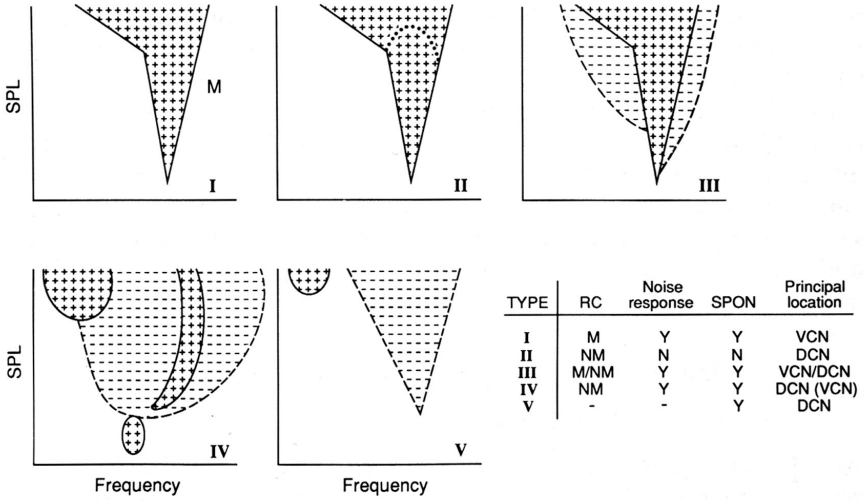

TYPE	RC	Noise response	SPON	Principal location
I	M	Y	Y	VCN
II	NM	N	N	DCN
III	M/NM	Y	Y	VCN/DCN
IV	NM	Y	Y	DCN (VCN)
V	-	-	Y	DCN

Figure 2.5: Schematic response maps of cochlear nucleus neurons (figure taken from Rhode and Greenberg, 1992, used with permission). Response maps are obtained by stimulating a neuron with pure tones of varying frequency and intensity. Excitatory responses are denoted by '+', inhibitory responses by '-'. SPL = sound pressure level; RC = rate curve for characteristic frequency tones, which is either monotonic (M) or nonmonotonic (NM); SPON = spontaneous activity. The dotted line in the response map of type-II neurons denotes the point where nonmonotonic rate-intensity functions reach their maximum.

2.4.1 Dorsal Cochlear Nucleus

The dorsal cochlear nucleus is organized in three layers (Fig. 2.6, see Cant, 1992; Young and Davis, 2002, for a review). The uppermost layer is called the molecular layer, it contains several types of inhibitory interneurons including cartwheel, Golgi, and stellate cells. The next layer is the pyramidal cell layer, which contains the cell bodies of pyramidal cells (also called fusiform cells) and granule cells. The apical dendritic trees of the pyramidal cells extend into the molecular layer, and their basal dendrites into the deep layer, where they are contacted by AN fibers. The granule cells receive inputs from the somatosensory system through mossy fibers. The granule cell axons form a system of parallel fibers in the molecular layer and constitute its main input. The deep layer contains a variety of neuron types, including giant and vertical cells. The main input to the deep layer is formed by AN fibers and projections from the VCN.

Pyramidal cells are the major projection neurons of the DCN. Their axons leave the DCN through the dorsal acoustic stria, and project directly to the contralateral IC. Moreover, there are also direct projections from the DCN to the medial geniculate body, these projections originate from fusiform and giant cells (Malmierca et al., 2002; Anderson et al., 2006). The DCN also receives efferent projections directly from the cortex (Weedman and Ryugo, 1996; Jacomme

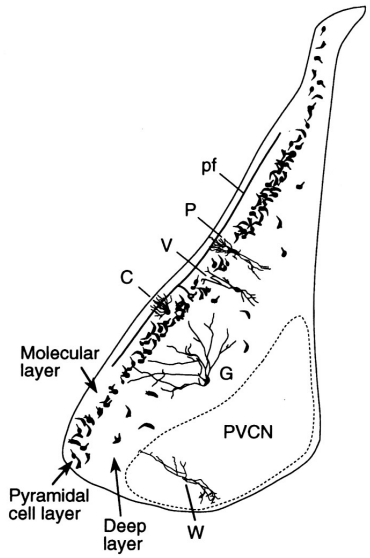

Figure 2.6: Sketch of a frontal section of the dorsal cochlear nucleus (figure taken from Young and Davis, 2002, reproduced with permission). The dark shapes are the somata of DCN principal cells (pyramidal and giant cells). The typical locations of the cell bodies of pyramidal cells (P), cartwheel cells (C), vertical cells (V), giant cells (G) are illustrated by drawings of individual neurons. The parallel fibers (pf) in the molecular layer originate from granule cells in the pyramidal cell layer. Moreover, the location of wide-band inhibitor neurons (W) in the VCN is shown.

et al., 2003), and a variety of inputs from the somatosensory system (Davis et al., 1996b; Kanold and Young, 2001; Zhou and Shore, 2004; Shore, 2005).

In cats, DCN projection neurons mostly show type IV response properties (Young, 1980), whereas in gerbils the majority of DCN fusiform cells shows type-III response characteristics (Davis et al., 1996a; Ding et al., 1999). Based on a series of physiological studies, a basic circuit diagram has been proposed to account for major interactions in the DCN that shape the responses of type-IV neurons (Fig. 2.7c, see Young and Davis, 2002, for a review). It contains two types of inhibitory interneurons, one with type-II response properties, and wide-band inhibitors (WBI). The type-II neurons have been identified as the tuberculoventral cells in the deep layer of the DCN. They are not spontaneously active, have a non-monotonous rate-intensity function in response to pure-tone stimuli, and give only weak or no responses to broad-band noise (Spirou et al., 1999, see also Fig. 2.7a). The WBIs are believed to be the onset-C (also called radiate or D-multipolar) neurons of the VCN. WBI neurons strongly responds to broad-band noise. They are not spontaneously active and only weakly respond to pure tones (Fig. 2.7b). The response thresholds of both the WBI and the type-II neurons are generally higher than those of type-IV units (Young and Davis, 2002). The AN provides excitatory input to all neurons of this circuit. The main properties of type-IV responses can be explained by inhibition from type-II neurons in conjunction with inhibition from WBI-neurons that also inhibit the type-II units (Fig. 2.7d). Modeling studies show that the response characteristics of projection neurons in this basic DCN circuit can be tuned to different response types by adjusting the strengths of the inhibitory connection (Zheng and Voigt, 2006a).

Interestingly, DCN principal cells remain spontaneously active after the cochlea has been destroyed (Koerber et al., 1966), demonstrating that intrinsic neuronal mechanisms or additional excitatory inputs are also involved in the generation of DCN spontaneous activity. Moreover, blocking inhibition through the application of the GABA-antagonist bicuculline or the glycine antagonist strychnine increases the spontaneous firing rate of DCN principal cells, demonstrating that they are subject to tonic inhibition (Davis and Young, 2000).

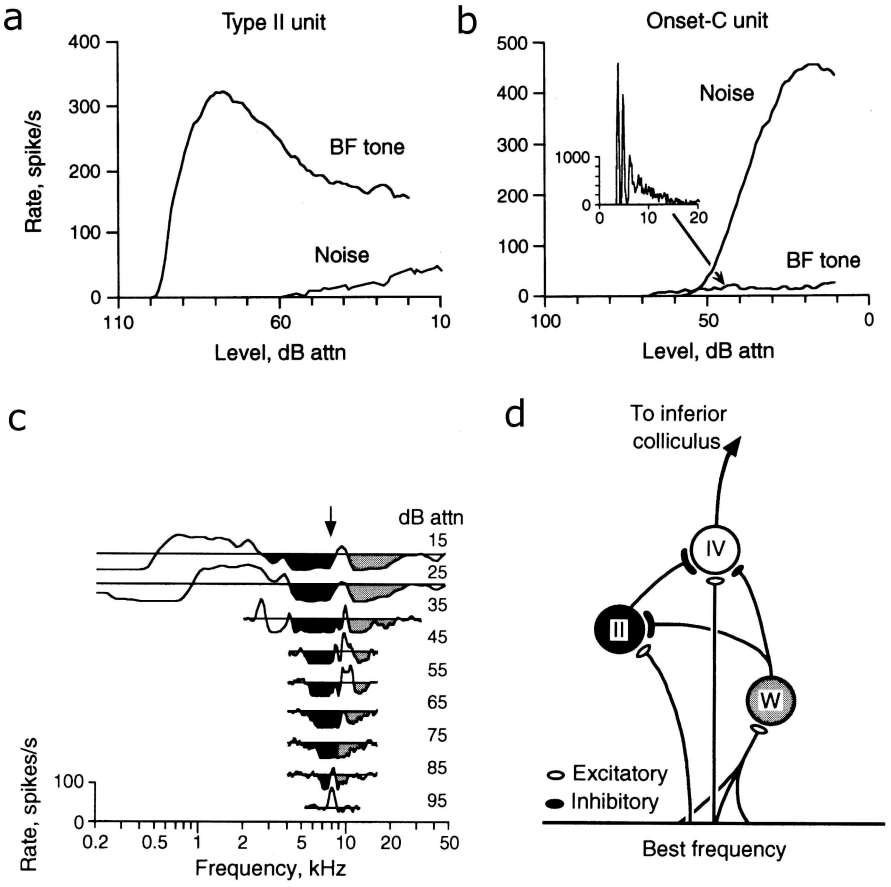

Figure 2.7: Physiology of DCN neurons (figure adapted from Young and Davis, 2002, used with permission). **a)** Type-II neurons usually have a non-monotonous rate-intensity function for pure tones. Broad-band noise only evokes weak responses at high intensities. **b)** Onset-C neurons of the VCN are believed to be the source of wide-band inhibition in the DCN. They strongly respond to broad-band noise and only have a weak response to pure tones. **c)** Typical response map of a type-IV unit of the DCN. There is a narrow excitatory area around the neuron's best frequency (arrow), surrounded by strong inhibitory side-bands (shaded areas). Black denotes the inhibitory influence of the type-II unit, and gray stands for inhibition that is assumed to come from the wide-band inhibitor (see b). **d)** Qualitative model for the generation of type-IV responses. The best-frequency axis stands for the characteristic frequency of auditory nerve fibers from the cochlea. Type **IV** neurons are pyramidal/fusiform cells, which project to the inferior colliculus, type **II** and **W** (wide-band inhibitor) are local inhibitory interneurons. Neurons are connected through excitatory (open ellipses) and inhibitory synapses (filled ellipses).

Chapter 3

Hearing Loss

Hearing loss can be caused by a variety of factors, and different stages of the auditory pathway can be affected. The main types of hearing loss are conductive hearing loss and sensorineural hearing loss. Conductive hearing loss is caused by an impairment of the sound conducting apparatus of the middle ear, for example through perforation of the tympanic membrane, interruption or fixation of the ossicular chain. Conductive hearing loss increases hearing thresholds by approximately 30-50 dB. Sensorineural hearing loss comprises impaired function of the sensory cells in the cochlea and of neurons in the central auditory system. It is thus subdivided into cochlear and retrocochlear hearing loss. Cochlear hearing loss is caused by damage to or loss of cochlear hair cells. Noise overexposure, acoustic trauma, age-related changes, and ototoxic side-effects of certain drugs are common causes for cochlear hearing loss. Retrocochlear hearing loss is caused by impaired neural function in central auditory structures. One of the most common kinds of retrocochlear hearing loss is impaired neural conduction in the auditory nerve, caused for example by acoustic tumors (Møller, 2000). Other types are caused by disorders of central auditory processing. In the following, we will focus on cochlear hearing loss, as this is the most common kind of hearing loss among tinnitus patients (Nicolas-Puel et al., 2002). We will review cochlear damage, its effects on auditory nerve responses, and plastic changes in the central auditory system caused by hearing loss.

3.1 Cochlear Hearing Loss

3.1.1 Noise-Induced Hearing Loss

Exposure to loud noise, like for example from industrial machines, amplified music, or gunshots, can lead to hearing loss. Depending on the intensity of the noise and on the exposure duration, hearing loss is either temporary, recovering within minutes or hours to days, or permanent. The underlying pathology in noise-induced hearing loss is damage to or loss of cochlear hair cells. Intense sound exposure puts cochlear hair cells under mechanical and metabolic stress, which may damage the hair cells and even lead to complete hair cell loss. For low noise doses, reversible disorder of the stereocilia of outer and inner hair cells in the cochlea has been observed (Gao et al., 1992). For high intensities, irreversible stereocilia damage occurs (Liberman, 1984; Kaltenbach et al., 1992; Gao et al., 1992), together with complete hair cell loss (Kaltenbach et al., 1992; Wang et al., 2002b; Chen and Fechter, 2003; Emmerich et al., 2005, see also Fig. 3.1). The severity and spatial extent of stereocilia damage and hair cell loss

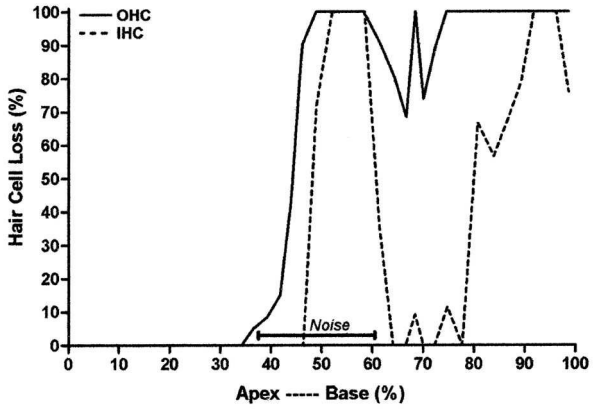

Figure 3.1: Cochleogram of a rat that was exposed to octave-band noise (9.6-19.2 kHz) at 115 dB SPL for 4 hours (figure taken from Chen and Fechter, 2003, used with permission). OHCs are lost in the basal half of the cochlea, whereas IHC loss is confined to the region most strongly stimulated by the noise (indicated by the bar) and to the basal end of the cochlea.

depend on the spectrum of the traumatizing stimulus, its intensity, and the exposure duration (Kaltenbach et al., 1992; Emmerich et al., 2005). OHCs seem to be more vulnerable than IHCs. After acoustic trauma, OHC loss is typically observed in large parts of the basal turns of the cochlea, whereas IHC loss is restricted to smaller areas (Wang et al., 2002b; Chen and Fechter, 2003). For both stereocilia damage and hair cell loss, the damage is usually more severe in basal parts of the cochlea, apical parts are affected to a much lesser degree (Kaltenbach et al., 1992; Chen and Fechter, 2003).

In humans, noise-induced hearing loss typically increases hearing thresholds in the high-frequency range (see Fig. 6.1 on page 38 for examples), and its earliest clinical manifestation is usually a dip in the audiogram around 4 kHz (Møller, 2000).

3.1.2 Age-Related Hearing Loss

For many people, aging is accompanied by a worsening of their hearing ability, more than 40% of men and 30% of women older than 75 years report a hearing problem, compared to less than 5% under 45 (Lockwood et al., 2002). The average hearing threshold of 50-year old men at 6 kHz, for example, is around 20 dB above the normal threshold of young, healthy individuals, and rises to more than 50 dB threshold elevation for 75-year old men (Spoor, 1967). Typically, age-related hearing loss (presbycusis) is characterized by gradually sloping hearing loss toward higher frequencies (Spoor, 1967). Age-related changes in the cochlea that are responsible for the decline in hearing ability are a degeneration of hair cells and atrophy of the stria vascularis (Gates and Mills, 2005). In humans, damage to hair cell stereocilia as well as hair cell loss have been observed, especially in the basal turn of the cochlea (Soucek et al., 1986). Such changes are also observed in animal models of presbycusis (Adams and Schulte, 1997; Francis et al., 2003).

In addition to cochlear changes, age-related changes in the AN, including degeneration of AN fibers, may contribute to presbycusis (Keithley and Feldman, 1979; Nadol, 1979; Møller, 2000). Moreover, there might also be changes in the central auditory system, as indicated by the fact that the ability of old subjects to detect gaps in stimuli is worse than that of young subjects with similar hearing loss (Schneider and Hamstra, 1999).

3.1.3 Hearing Loss through Ototoxic Drugs

Many drugs have ototoxic side-effects, for example aminoglycoside antibiotics (e.g. streptomycin, kanamycin, and gentamycin) or chemotherapeutics used in cancer therapy like cisplatin and carboplatin. Administration of cisplatin and aminoglycoside antibiotics can lead to OHC loss, IHCs are only affected to a lesser degree (Dallos and Harris, 1978; Kaltenbach et al., 2002; van Ruijven et al., 2004, 2005). Moreover, cisplatin may also damage AN fibers (van Ruijven et al., 2004, 2005). In contrast to that, low doses of carboplatin lead to selective IHC loss in chinchillas (Wang et al., 1997; McFadden et al., 1998). OHC loss is only observed after high carboplatin doses (Wang et al., 1997). In the guinea pig, on the other hand, the effects of carboplatin on OHCs are similar to those of cisplatin (Saito et al., 1995), and the effects of carboplatin in the human cochlea have not been clarified yet. Ototoxic substances interfere with the metabolism of hair cells, leading to metabolic exhaustion and oxidative stress through an increase in the level of oxygen free radicals (Sha and Schacht, 1999). This may cause the observed hair cell death. Hearing loss through drug-induced OHC loss can be as high as 50-60 dB. It usually begins at high frequencies, and progresses gradually toward lower frequencies (Møller, 2000).

3.2 Changes in AN Activity after Cochlear Damage

Damage to or loss of cochlear hair cells alters the response properties of the affected auditory nerve fibers. We are now going to review how different kinds of cochlear damage influence AN responses.

3.2.1 Effect of Noise-Induced Stereocilia Damage on AN Responses

Damage to the stereocilia of IHCs decreases the effectivity of the transduction of basilar membrane motion into depolarization of the IHCs. Damage to the stereocilia of OHCs on the other hand, impairs the function of the cochlear amplifier. In a series of experiments, Liberman and co-workers examined the effects of noise-induced stereocilia damage on auditory nerve responses. Stereocilia damage was induced through acoustic trauma. After the recordings had been obtained, the AN fibers were labeled and traced back to the cochlea to correlate the observed changes in physiology with cochlear damage (Liberman, 1984; Liberman and Dodds, 1984a,b; Liberman and Kiang, 1984). Damage to the stereocilia of IHCs and OHCs generally leads to higher response thresholds of the affected AN fibers. Threshold increases of 60-80 dB are found for severe stereocilia damage. When only IHC stereocilia are affected, tuning of the AN fibers is preserved, the threshold curve is simply shifted to higher intensities. Damage to OHC stereocilia, on the other hand, leads to impaired tuning and increased thresholds of AN fiber responses. The loss of IHC stereocilia decreases the spontaneous discharge rate of the affected AN fibers, a reduction of approximately 50-70% is observed after the loss of all tall IHC stereocilia. The maximum driven discharge rate of AN fibers after stereocilia damage, however, remains unchanged. Examples of AN rate-intensity functions after noise-induced stereocilia damage are shown in Fig. 3.2. The shape of AN rate-intensity functions can be altered after noise-induced stereocilia damage in that some rate-intensity functions are shallower than normal (Heinz and Young, 2004)

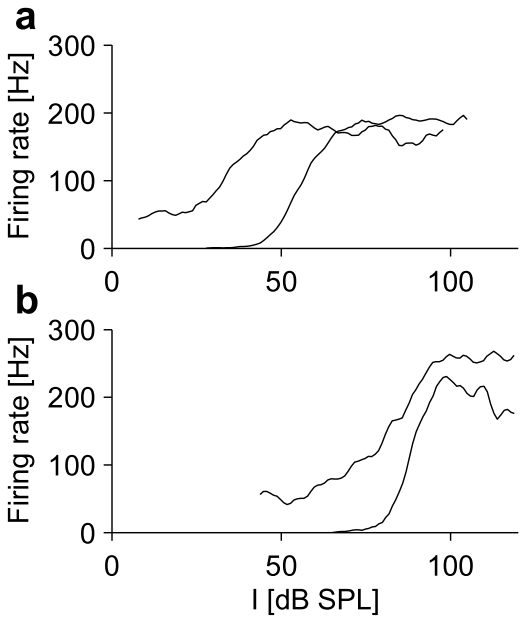

Figure 3.2: Rate-intensity functions of AN fibers after acoustic trauma (figure based on data from Heinz and Young, 2004, used with permission). Cats were exposed to a 50 Hz-wide noise band centered at 2 kHz at 103-108 dB, exposure duration was 4 hours. **a)** Rate-intensity functions of two AN fibers (CFs around 1 kHz) from a cat that had mild hearing loss after the exposure. **b)** Rate-intensity functions of two AN fibers (CFs around 1 kHz) from a cat that had moderate to severe hearing loss after the exposure.

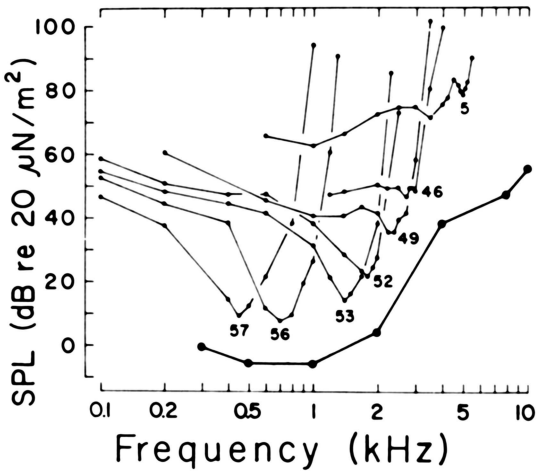

Figure 3.3: Behavioral audiogram (thick line) and threshold tuning curves of AN fibers (thin line) of a chinchilla after OHC loss through kanamycin treatment (figure taken from Dallos and Harris, 1978, reproduced with permission). In the high-frequency range, hearing thresholds are elevated due to OHC loss. AN fibers with high CFs (5 and 46 for example) display broadened tuning curves and elevated response thresholds, whereas AN fibers with low CFs (e.g. 56 and 57) have normal thresholds and sharp tuning.

3.2.2 Effects of Selective OHC Loss on AN Responses

The OHCs are involved in the active processes inside the cochlea that increase the sensitivity and sharpen the tuning of the basilar membrane response. Moreover, due to these active processes, the response of the basilar membrane is nonlinear, with compression at high sound intensities (see Geisler, 1998; Møller, 2000, for a review). Selective loss of OHCs impairs the function of the cochlear amplifier and thus leads to increased response thresholds and impaired tuning of AN fiber responses (Dallos and Harris, 1978, see also Fig. 3.3). Moreover, AN rate-intensity functions are steeper than normal after OHC loss (Schmiedt and Zwislocki, 1980). The spontaneous and the maximum discharge rate of AN fibers, however, are not affected by OHC loss, as these are determined by the status of the IHCs, which remain fully functional. (Dallos and Harris, 1978; Schmiedt and Zwislocki, 1980).

3.2.3 Effects of Selective IHC Loss on AN Responses

Each type-I AN fiber contacts only one IHC (Ryugo, 1992). The death of inner hair cells therefore deprives the corresponding AN fibers of their input. After selective IHC loss through carboplatin administration, fewer acoustically responsive are encountered, and the compound action potential of the AN is reduced approximately in proportion to the amount of IHC loss (Wang et al., 1997). The remaining responsive AN fibers are characterized by normal or near-normal response thresholds and normal, sharp tuning curves, as expected for intact OHCs. The shape of the observed rate-intensity functions after carboplatin treatment is normal, too. The spontaneous and the maximum discharge rate, however, are slightly reduced (Wang et al., 1997).

3.3 Plastic Changes in the Central Auditory System after Hearing Loss

Plastic changes have been observed at various levels of the auditory pathway after hearing loss. Such changes could be caused by a plastic adaptation to an altered input signal, as hearing loss strongly alters the responses of AN fibers to acoustic stimuli. In the following, we review changes in neural responses that have been observed after hearing loss.

3.3.1 Reorganization of Tonotopic Maps after Hearing Loss

The basic organization principle of the auditory system is tonotopy, i.e. frequencies are represented in an ordered fashion from low to high frequencies at each processing stage of the auditory pathway. However, when the cochlea is mechanically lesioned in adult animals to produce high-frequency hearing loss, plastic reorganization of these tonotopic maps has been observed in the primary auditory cortex (Robertson and Irvine, 1989; Rajan et al., 1993; Irvine and Rajan, 1997) and the medial geniculate body (Kamke et al., 2003). Neurons that, given their location, would normally be expected to have best frequencies within the frequency-range affected by the lesion were observed to have acquired new best frequencies corresponding to the borders of the lesion. Response thresholds at these new best frequencies were low, indicating a true plastic reorganization and not only an unmasking of residual inputs. The normal tonotopic organization with an ordered representation of frequencies was thus disrupted and the frequencies at the borders of the lesion overrepresented. Such changes have also been observed after acoustic trauma (Noreña and Eggermont, 2003, 2005). Interestingly, reorganization after hearing loss through acoustic trauma could be prevented by additional acoustic stimulation (Noreña and Eggermont, 2005), indicating that the plastic changes might be caused by a response to sensory deprivation.

In contrast to the auditory cortex and thalamus, reorganization of the tonotopic map after mechanical cochlear lesions or acoustic trauma has not been observed in the IC (Irvine et al., 2003) or DCN (Kaltenbach et al., 1992; Meleca et al., 1997; Rajan and Irvine, 1998a) of adult animals. Although neurons showed altered frequency tuning, high response thresholds indicated that only responses to residual pre-lesion inputs were observed. In juvenile animals, however, reorganization in the IC could be triggered through cochlear damage (Harrison et al., 1998).

3.3.2 Altered Neuronal Responses

Apart from reorganization of tonotopic maps, hearing loss triggers a variety of plastic changes in the central auditory system. The resulting changes in the responses of auditory neurons are more complex than the changes in auditory nerve activity. Inhibitory neurotransmission, for example, is altered at various stages of the auditory pathway for different kinds of hearing loss. Most studies reported a decrease in inhibition. Excitatory neurotransmission is also subject to plastic changes after hearing loss, in most cases increased excitatory responses have been reported. We are now going to give an overview over changes at different stages of the auditory pathway.

In the dorsal cochlear nucleus, unilateral deafening through cochlear ablation lead to a decrease in the amount of glycine released after electrical stimulation (Potashner et al., 2000; Suneja et al., 1998a), and also the number of glycine receptors was decreased (Suneja et al., 1998b). Changes were observed in the DCNs of both sides and were interpreted as a downregulation of glycinergic neurotransmission. In the VCN, a large increase in the percentage of excitatory responses to contralateral stimulation with broadband noise was observed after ipsilateral ossicle removal (Sumner et al., 2005). Normally, responses to contralateral stimulation are predominantly inhibitory (Needham and Paolini, 2003), thus this result suggests either a decrease in inhibition, an increase in excitation, or both.

In the olivary nuclei and the nuclei of the trapezoid body, decreased levels of glycine (as indicated by decreased glycine immunoreactivity) have been measured after bilateral deafening (Buras et al., 2006).

A variety of changes has also been observed in the IC after hearing loss. In the IC of young rats, bilateral cochlear ablation shifted the reversal potential of inhibitory postsynaptic currents to more depolarized values, indicating decreased efficiency of inhibition, and strongly increased the size of excitatory postsynaptic currents (Vale and Sanes, 2002). Moreover, glutamic acid decarboxylase (GAD) levels were decreased in the IC after unilateral cochlear ablation (Mossop et al., 2000) or acoustic trauma (Milbrandt et al., 2000). As GAD is an important enzyme needed for the synthesis of GABA, this finding has also been interpreted as a downregulation of inhibition. Note however that another study found increased GABA release in the IC after ossicle removal (Suneja et al., 1998a). After acoustic trauma, the maximum amplitude of evoked response potentials was increased in the IC and in the primary auditory cortex, in contrast to a decrease that was observed in the AN and CN (Wang et al., 2002a). This finding has been interpreted as a sign of increased central response gain. Similar changes were reported for the auditory cortex of chinchillas after selective IHC loss. Although evoked response potential amplitudes were slightly decreased in the IC, they were enhanced at the level of the auditory cortex (Qiu et al., 2000). These results demonstrate that the response gain can be regulated at various stages of the auditory system. In recordings from single neurons of the auditory cortex, a loss of surround inhibition was evident even for minor noise-induced hearing loss, where the threshold increase was less than 25 dB (Rajan, 1998). Interestingly, the changes occurred without a reorganization of the tonotopic map. After bilateral deafening an increased intrinsic excitability of cortical neurons was observed, together with increased thalamocortical and intracortical excitatory responses and decreased GABAergic inhibitory synaptic responses (Kotak et al., 2005).

3.4 Degeneration of Neurons in the Auditory Pathway after Hearing Loss

Hearing loss can also cause a degeneration of AN fibers and a loss of neurons in the central auditory pathway. After loss of cochlear hair cells, for example, a reduction of the number of spiral ganglion neurons and therefore AN fibers is observed (Lim, 1976; Kiang et al., 1976). Hair cell loss induced by acoustic trauma, ototoxic drugs, or direct mechanical lesions all lead to similar degeneration patterns. Although spiral ganglion cells are more resistant to acoustic trauma and ototoxic drugs than hair cells (Lim, 1976), their long-term survival seems to depend on the presence of IHCs (Kiang et al., 1976). A reduction of the number of spiral ganglion cells and auditory nerve fibers is also observed with age (Keithley and Feldman, 1982; Dazert et al., 1996). However, it is unclear whether this reduction is also caused by hair cell loss or is independently induced through age-related changes (Keithley and Feldman, 1982).

Degeneration of neurons after acoustic trauma also occurs in central auditory structures. In the cochlear nucleus and the superior olivary complex, for example, apoptotic cell death has been found after auditory nerve degeneration induced by acoustic trauma (Aarnisalo et al., 2000). Even the auditory thalamus and the auditory cortex are affected by noise-induced hearing loss. The cell density in these structures was found to be reduced after acoustic trauma (Basta et al., 2005).

Summary and Conclusions

Hearing loss changes the response properties of auditory nerve fibers. Different kinds of cochlear damage have distinct effects on AN activity. Hearing loss through cochlear damage also triggers plastic changes in central auditory neurons. Increased excitatory and decreased inhibitory synaptic transmission have been observed at many stages of the auditory pathway. Moreover, a plastic reorganization of the tonotopic maps of the auditory cortex and thalamus may occur. Some of these changes might be involved in the development of tinnitus. The following chapter gives an overview over the characteristics of tinnitus, the relation between tinnitus and hearing loss, and tinnitus-related changes in neuronal activity that have been observed in animal models of tinnitus.

Chapter 4

Tinnitus

4.1 Tinnitus in Humans

Tinnitus is the perception of a sound in the absence of an external acoustic stimulus. The word tinnitus is of Latin origin and means 'ringing in the ears'. This is the most common description of the tonal sensation experienced by many tinnitus patients, but the sound can also have fundamentally different qualities like for example a buzzing, humming, whistling, roaring or some other noise-like characteristics.

Tinnitus can be classified in 'subjective' (sound can only be heard by the patient) and 'objective' (sound can also be heard by other persons). Objective tinnitus occurs much less frequent than subjective tinnitus. Objective tinnitus is produced by a physical source within the body that activates the cochlea by air and/or bone conduction, and could thus also be called *somatosound* (Dobie, 2004). Objective tinnitus is often due to anomalies or malformations of blood vessels in the vicinity of the ear, which leads to a pulsatile sensation (Waldvogel et al., 1998). Surgical treatment of these conditions can lead to an improvement of the tinnitus. In most of the cases, however, tinnitus is a subjective phenomenon where no physical generator for the acoustic sensation can be found. As this study focuses on subjective tinnitus only, we will simply use the term 'tinnitus' for subjective tinnitus.

The tinnitus sensation can be characterized by two psychophysical variables, pitch and loudness. Tinnitus pitch is determined by presenting comparison stimuli (usually pure tones or narrow-band noise) that are varied in frequency until the perceived pitch is similar to that of the tinnitus sensation. When the tinnitus percept consists of more than one frequency, patients are usually asked to match the comparison stimulus to the pitch of the dominant component of the tinnitus sensation. Tinnitus sensations are mostly high-pitched, around 80% of the subjects match their tinnitus to frequencies above 2.5 kHz (Henry et al., 1999). Low-pitched tinnitus is usually associated with Menière's disease (Nicolas-Puel et al., 2002). The results of tinnitus pitch matching, however, can be highly variable (Burns, 1984; Henry et al., 2004). The range of pitch matching results of individual subjects in repeated tests can be more than 2 octaves (Henry et al., 2004).

Another approach to characterize the tinnitus sensation has been taken by Noreña et al. (2002), who asked patients to judge the contribution of comparison tones to their tinnitus sensation. The resulting 'tinnitus spectra' were spanning large ranges at high frequencies and corresponded to the patients' hearing loss.

To determine the tinnitus loudness, a tone or noise of similar pitch is varied in intensity

until it is perceived just as loud as the patient's tinnitus. The resulting matching intensity is usually found to be less than 10 dB above the patient's hearing threshold at that frequency (Reed, 1960). Surprisingly, the measured tinnitus loudness in dB sensation level is not related to self-reported tinnitus severity (Andersson, 2003; Dobie, 2004)

4.1.1 Epidemiology of Tinnitus

The prevalence of tinnitus in the general population has been reported to be around 10% (Hoffman and Reed, 2004, and references therein). Tinnitus is more common in men than in women (Lockwood et al., 2002). Moreover, the prevalence of tinnitus increases with age (Lockwood et al., 2002; Hoffman and Reed, 2004) and with hearing loss (Chung et al., 1984; Hoffman and Reed, 2004). In Germany, it is estimated that about 2.9 million persons have a chronic form of tinnitus (Pilgramm et al., 1999). While in most cases surrounding noise is sufficient to mask the tinnitus, 17% of the tinnitus patients hear it even in the presence of very loud external sound. Approximately 1.5 million people in Germany are substantially affected by their tinnitus, and the symptoms can be so severe that the persons are unable to lead a normal life (Pilgramm et al., 1999).

4.1.2 Tinnitus and Hearing Loss

Tinnitus and hearing loss are related. Up to 90% of the tinnitus patients are also affected by hearing loss (Nicolas-Puel et al., 2002). In epidemiological studies, hearing loss has been identified as a risk factor for tinnitus (Sindhusake et al., 2003, 2004), and the prevalence of tinnitus has been found to increase with the severity of hearing impairment (Chung et al., 1984; Hoffman and Reed, 2004). Moreover, in noise-exposed workers, those with tinnitus were found to have worse hearing than those without tinnitus (Phoon et al., 1993), and patients with unilateral tinnitus usually perceive it in the worse ear (McShane et al., 1988; Ochi et al., 2003).

In most patients, hearing loss affects the high-frequency range, and tinnitus pitch is usually matched to frequencies at which hearing is impaired (Henry et al., 1999, see also Fig. 4.1). Moreover, the tinnitus spectrum (see above) coincides with the frequency-range at which hearing loss is present. There are, however, also tinnitus patients who have normal or near-normal audiograms. These might have restricted cochlear damage or hearing impairment at frequencies above 8 kHz, both of which are not detected by conventional clinical audiometry: In tinnitus patients with normal audiograms, reduced distortion product otoacoustic emissions were observed, indicating impairment of OHC function (Shiomi et al., 1997). Restricted notches in high-resolution audiograms were also found (Sirimanna et al., 1996), and psychophysical techniques (Moore et al., 2000) revealed 'cochlear dead regions', i.e. regions with IHC loss in tinnitus patients with normal hearing (Weisz et al., 2006). Moreover, elevated hearing thresholds were found above 8 kHz in such patients (Roberts et al., 2006). Altogether this indicates that tinnitus might always be related to cochlear damage. However, not all kinds of hearing loss must lead to tinnitus, as demonstrated by the much higher prevalence of hearing loss compared to tinnitus (Lockwood et al., 2002).

Interestingly, a majority of subjects with normal hearing and no tinnitus perceived phantom sounds when subjected to prolonged periods of silence (Heller and Bergman, 1953; Tucker et al., 2005). Tinnitus emerged quickly, usually in less than 4 minutes. Most common descriptions of tinnitus were 'ringing', 'pulse', 'humming', 'heartbeat', and 'buzz' (Tucker et al.,

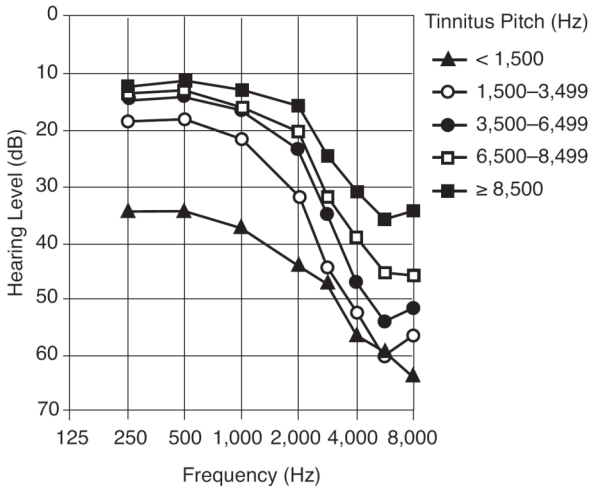

Figure 4.1: Relation between tinnitus pitch and hearing loss (figure taken from Henry et al., 1999). Tinnitus pitch was determined in 1033 patients. Then, patients were grouped by pitch and the mean audiogram was determined for each group. On average, all tinnitus patients had hearing loss. With increasing hearing loss, patients tended to have a lower tinnitus pitch.

2005), which are very similar to the tinnitus sounds described by tinnitus patients. When subjected to prolonged silence, the auditory system is subjected to sensory deprivation. This could challenge it with a situation similar to hearing loss, thus triggering a temporary tinnitus sensation.

4.1.3 Somatosensory Influences on Tinnitus

Some patients can modulate their tinnitus pitch or loudness by performing certain voluntary movements, like for example forceful head and neck contractions (Levine et al., 2003), oral-facial movements (Pinchoff et al., 1998), or jaw movements (Lockwood et al., 1998). Another form of somatosensory influence on tinnitus is gaze-evoked tinnitus, where extreme lateral gaze can trigger a tinnitus sensation. Gaze-evoked tinnitus develops in some patients after resection of acoustic neuromas (Giraud et al., 1999). Such somatosensory influence on tinnitus has given rise to the hypothesis that the interaction of somatosensory and auditory information in certain parts of the auditory pathway like for example the dorsal cochlear nucleus might be important for tinnitus generation and modulation (Levine, 1999; Levine et al., 2003).

4.1.4 Origin of Tinnitus

As tinnitus is perceived in the absence of an external acoustic stimulus, its basis may be the perception of the spontaneous activity of the auditory system. Somehow, the spontaneous activity must be altered in such a way that it can be perceived. The earliest hypotheses about tinnitus assumed a peripheral origin of the underlying neural activity, possibly caused by hyperactive hair cells or some other change in auditory nerve activity. These hypotheses, however, can not explain why sectioning the auditory nerve had little impact on tinnitus in the majority of patients or even worsened it (House and Brackmann, 1981; Jackson, 1985). Moreover, also removing efferent feedback to the cochlea by sectioning the vestibular nerve was found to have no consistent effect on tinnitus, tinnitus could be better or worse after the operation (Baguley et al., 2002). Therefore, the relevant changes must occur more centrally in the auditory system. In humans, tinnitus-related changes have been studied using imaging techniques. Using magnetic source imaging, a reorganization of the tonotopic map has been observed in the auditory

cortex of tinnitus patients (Mühlnickel et al., 1998). The location of neural activity evoked by stimulation at the tinnitus frequency was found to deviate from the location expected for a normal tonotopic map. The amount of deviation was correlated to subjective tinnitus distress. It has to be noted, though, that evidence for reorganization was only found in 4 out of 10 tinnitus subjects (compare Fig. 2 of Mühlnickel et al., 1998). Patients with gaze-evoked tinnitus were studied using the positron emission tomography scan technique. When the patients elicited their tinnitus through eye-movements, increased blood flow was observed in temporo-parietal auditory association areas, but not in the primary auditory cortex (Giraud et al., 1999). Similarly, in 'normal' tinnitus subjects, a change in tinnitus loudness through lidocaine administration was found to be associated with a significant change in neural activity in the right temporal lobe in auditory association cortex (Reyes et al., 2002).

4.2 Animal Models of Tinnitus

Studies on tinnitus in humans have identified tinnitus-related changes in brain activity in the auditory system. However, as only imaging techniques could be employed, the results are limited to large-scale effects. To identify neural correlates of tinnitus on the level of single neurons or small populations of neurons, animal studies have been conducted.

4.2.1 Behavioral Models of Tinnitus

Verifying that animals actually experience tinnitus after acoustic trauma or the administration of ototoxic drugs is an important prerequisite in the search for neural correlates of tinnitus in animals. Behavioral studies have addressed this problem using various paradigms. Generally, animals were trained to behave differently in the presence or absence of acoustic stimuli. After tinnitus-inducing manipulations, the animals were tested again. If they behaved in silence as if an external stimulus was present, this was interpreted as behavioral evidence for tinnitus, i.e. the perception of a sound in the absence of acoustic stimulation. It could thus be demonstrated that animals such as rats, hamsters, or chinchillas can experience tinnitus after salicylate treatment (Jastreboff et al., 1988; Jastreboff and Sasaki, 1994) and after exposure to intense sound (Heffner and Harrington, 2002; Brozoski et al., 2002; Kaltenbach et al., 2004; Heffner and Koay, 2005). Not all acoustically traumatized animals displayed behavioral signs of tinnitus (Kaltenbach et al., 2004), similar to the fact that noise-trauma or hearing loss does not always lead to tinnitus in humans (Lockwood et al., 2002). Moreover, the strength of the behavioral evidence for tinnitus after noise trauma was related to the amount of hearing loss as measured by the shift of the auditory brainstem response (Heffner and Koay, 2005).

4.2.2 Neurophysiological Correlates of Tinnitus

In animals with behavioral evidence for tinnitus, increased spontaneous firing rates were found in the DCN (Brozoski et al., 2002; Kaltenbach et al., 2004). The degree of increase of the spontaneous firing rates was correlated to the behavioral tinnitus score (Kaltenbach et al., 2004). Increased spontaneous firing rates were thus interpreted as a neural correlate of tinnitus.

Most animal studies on tinnitus, however, only used manipulations known to induce tinnitus in humans without further behavioral testing, assuming that observed changes in the activity

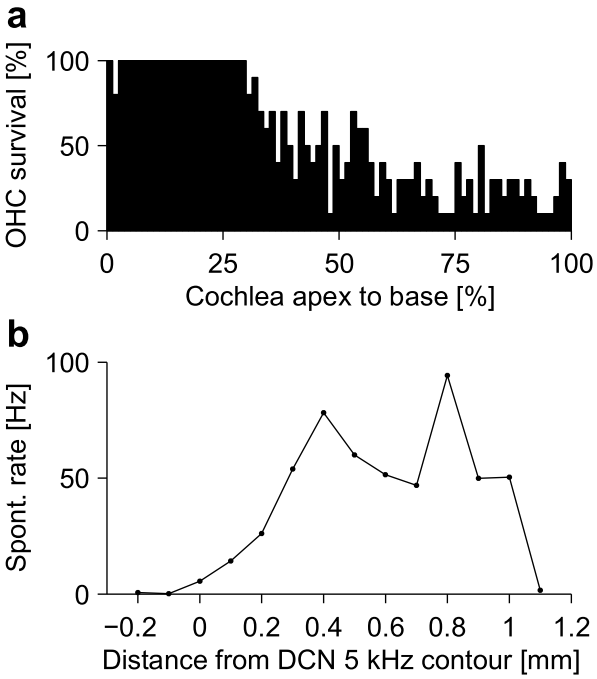

Figure 4.2: Relation between cisplatin-induced hair-cell loss and hyperactivity in DCN neurons (figure based on data from Kaltenbach et al., 2002, used with permission). **a)** Cochleogram showing cisplatin-induced OHC loss in the basal parts of the cochlea. The IHCs are not affected (not shown). **b)** Spontaneous multi-unit activity along the tonotopic axis of the DCN. The spontaneous firing rate is significantly increased in high-frequency regions of the DCN.

of auditory neurons might be related to tinnitus. Various brain regions have been studied after acoustic trauma or salicylate administration. Changes in neural activity or responsiveness were found in the auditory cortex (Seki and Eggermont, 2002, 2003), in the inferior colliculus (Jastreboof and Sasaki, 1986; Chen and Jastreboff, 1995; Ma et al., 2006), and the earliest processing change where tinnitus-related changes have been observed was the DCN.

Tinnitus-Related Changes in the Auditory Brainstem and Midbrain

Following intense sound exposure (Kaltenbach and McCaslin, 1996; Kaltenbach et al., 1998, 2000; Kaltenbach and Afman, 2000; Brozoski et al., 2002), cisplatin (Rachel et al., 2002) or salicylate (Chen et al., 2003) treatment, the spontaneous firing rates of neurons in the DCN were significantly elevated. Hyperactivity after acoustic trauma occurred in neurons spanning a characteristic frequency range of approximately an octave (Kaltenbach et al., 2000). The structure of the activity patterns was generally peak-like, thus resembling tone-evoked activity (Kaltenbach and Afman, 2000). The spread of activity along the tonotopic axis was slightly larger than for activity evoked by a pure tone. Hyperactivity developed between two and five days after hearing loss, and persisted for at least 180 days (Kaltenbach et al., 2000). Moreover, firing rates continued to be elevated even after partial or complete ablation of the cochlea (Zacharek et al., 2002) or sectioning of the top-down connections from IC and cortex (Zhang et al., 2003). This demonstrates that the maintenance of hyperactivity is an intrinsic property of the brain stem auditory structures. Apparently, hyperactivity developed only in those parts of the DCN that received input from the damaged parts of the cochlea (Kaltenbach et al., 2002, see also Fig. 4.2). Intracellular recordings revealed that the fusiform cells, the main projection neurons of the DCN which project to the inferior colliculus, develop increased spontaneous firing rates after acoustic trauma (Brozoski et al., 2002). The increase in spontaneous activity could thus also influence the spontaneous activity of neurons in the IC.

Increased spontaneous firing rate after acoustic trauma have also been observed in the IC

(Ma et al., 2006). The increase in spontaneous firing rate was strongest in neurons with characteristic frequencies close to the frequency of the traumatizing tone. Moreover, also salicylate application in vivo (Jastreboof and Sasaki, 1986; Chen and Jastreboff, 1995) and in vitro (Basta and Ernst, 2004) increased the spontaneous firing rates of neurons in the IC. The salicylate-induced increase of spontaneous firing rates could be counteracted by injecting lidocaine (Manabe et al., 1997), similar to the suppressive effect of lidocaine on tinnitus in humans.

Tinnitus-Related Changes in the Auditory Cortex

Tinnitus-related changes have also been observed in the primary auditory cortex. Following acoustic trauma, the spontaneous firing rates were significantly increased (Seki and Eggermont, 2003; Noreña and Eggermont, 2006). In contrast to the slow time course in the DCN, the increase was already evident several hours after the acoustic trauma (Noreña and Eggermont, 2003). The synchrony of the spontaneous neuronal discharge across neurons was also increased (Komiya and Eggermont, 2000; Seki and Eggermont, 2003; Noreña and Eggermont, 2003). Moreover, the increase in synchrony was significantly correlated to changes in the spontaneous firing rate (Noreña and Eggermont, 2003). Increased synchrony in addition to increased spontaneous firing rates could facilitate the misinterpretation of the activity as being sound-evoked. In addition to that, synchronized activity is more likely to be transmitted to higher brain areas that are involved in conscious perception, because synchronized spikes are more likely to evoke action potentials in postsynaptic neurons.

It has also been proposed that reorganization of the tonotopic map in the auditory cortex after hearing loss could be involved in the generation of tinnitus (Rauschecker, 1999; Eggermont and Roberts, 2004). The overrepresentation of edge frequencies after reorganization of the tonotopic map together with a loss of intracortical inhibition could lead to a tinnitus percept (Rauschecker, 1999). Interestingly, an enhanced acoustic environment could prevent the changes in tonotopic map organization (Noreña and Eggermont, 2005) and spontaneous firing rate (Noreña and Eggermont, 2006) that are normally observed in the auditory cortex after acoustic trauma. An ‘enhanced acoustic environment’ means that there is additional acoustic stimulation at high frequencies where hearing loss is expected after acoustic trauma.

4.2.3 How Are Increased Spontaneous Firing Rates Generated?

The occurrence of tinnitus is related to substantial changes in the activity of auditory neurons at the level of the brain stem, the midbrain and the cortex. The exact mechanism that is responsible for the increase of the spontaneous firing rates, however, has not been identified yet. The time course of the development of tinnitus-related changes in the DCN suggests the involvement of neural plasticity. A variety of plastic changes has been observed in various stages of the auditory system after hearing loss (see section 3). As far as the development of increased spontaneous firing rates is concerned, hypotheses involving loss of inhibition have been put forward, but so far none of these hypotheses has been proven. Possibly the simplest situation is encountered in the DCN. There is good evidence that the development and maintenance of hyperactivity after acoustic trauma or cisplatin administration is an intrinsic property of the DCN. Moreover, as acoustic trauma and hair cell loss through ototoxic drugs lead to similar effects, the initial trigger is most likely not the acoustic trauma itself, but altered auditory nerve activity after cochlear damage. Hearing loss through acoustic trauma or ototoxic drugs

increases the response threshold of the affected auditory nerve fibers. Some fibers may even be totally deprived of input because of IHC loss. This leads to diminished excitation or even deafferentiation of a large number of neurons in the DCN. Paradoxically, the spontaneous firing rate of the DCN's principal cells (Brozoski et al., 2002) is increased. Are inhibitory inputs weakened or is the responsiveness of these neurons increased by a homeostatic mechanism? In any case, activity-dependent plasticity (see Chapter 5) has the potential to play a major role in the observed changes.

4.3 Models of Tinnitus Generation

Evidence that tinnitus is independent of a generating sound provided the basis for the 'neurophysiological model' by Jastreboff and Hazell (Jastreboff and Hazell, 1993; Jastreboff, 1999; Jastreboff and Jastreboff, 1999), from which the 'Retraining Therapy' has been derived. The hypothesis for the explanation of the persistence of tinnitus in this model is a failure of habituation mechanisms. Normally, the auditory system evaluates stimuli and suppresses the unimportant ones. The 'neurophysiological model' assumes that the tinnitus sensation is associated to negative emotions like stress or fear. The resulting activation of structures of the limbic system that mediate emotions and attention creates a feedback loop: Attention is diverted to the tinnitus sensation if it is associated with negative emotions. Thereby, the signal is amplified, which in turn increases the emotional reaction, which leads to an even stronger tinnitus. A vicious cycle is formed through constant self-conditioning.

The 'neurophysiological model' focuses on psychological learning processes. It does not rely on the pathological processes which are initially responsible for the generation of tinnitus, nor does it consider the effects of plasticity mechanisms on the level of brain stem neural networks. In the 'auditory brain stem model' (Gerken, 1996), the network architecture of the auditory brain stem is taken into account in more detail. The model focuses on the IC, where patterns of lateral inhibition are found. This lateral inhibition exaggerates unevenness in the spontaneous or driven output of the cochlea across frequencies, like for example 'audiometric edges' created by hearing loss. The resulting activity peaks are proposed as a basis for a tone-like tinnitus sensation.

Lateral inhibition is also an important ingredient of the model by Langner and Wallhäusser-Franke (1999). It is based on experimental studies where strong correlations between the activation of the auditory cortex, the DCN, and the amygdala have been found in animals with tinnitus. Similar to Gerken's model, irregularities in the auditory nerve activity after hearing loss are assumed to be enhanced by lateral inhibition. A central auditory gain control mechanism (influenced by the amygdala and the formatio reticularis) tries to compensate for the hearing loss, which in turn further amplifies the already enhanced irregularities, which are then interpreted as tinnitus.

To account for cortical correlates of tinnitus like increased spontaneous firing rates and synchrony, a spiking neuron model has been proposed by Dominguez et al. (2006). The main assumption of the model is that reduced excitatory input from the periphery after hearing loss could lead to a compensatory change in the strength of lateral connections in the auditory cortex. When excitatory connections are strengthened and inhibitory connections are weakened, increased spontaneous firing rates and an increase in the synchrony of the neuronal discharge are observed in the model. However, the model does not evaluate how hearing loss could lead to

the assumed changes in synaptic strengths and which mechanisms of neuronal plasticity could be involved.

Summary and Conclusions

Tinnitus is a common phenomenon that is usually associated with hearing loss. Hearing loss, on the other hand, does not always lead to tinnitus. The occurrence of tinnitus might therefore depend on more specific features of hearing loss, like for example the shape of the patient's audiogram. The question whether specific forms of the audiogram are more likely to cause tinnitus than others will be addressed in this thesis in chapter 6.

Tinnitus has been found to lead to altered activity patterns in the auditory system of humans. In animals, increased spontaneous firing rates have been identified as a neural correlate of tinnitus. These have been found at all stages of the auditory system after acoustic trauma or administration of tinnitus-inducing ototoxic drugs. The mechanisms that lead to the development of increased spontaneous firing rates, however, have not been identified yet. The question how neural plasticity after hearing loss could lead to increased spontaneous firing rates in the cochlear nucleus will be addressed in Chapter 7 using a computational model.

Many hypotheses and models of tinnitus generation have been put forward, but so far none of these has been shown to produce testable predictions that are consistent with patient data. In Chapter 9, we will apply the model presented in Chapter 7 and extended in Chapter 8 to data from tinnitus patients. We will test whether the model is able to realistic predictions of tinnitus pitch from the audiograms of tinnitus patients.

Chapter 5

Mechanisms of Activity-Dependent Neuronal Plasticity

Hearing loss triggers a variety of plastic changes at different stages of the auditory pathway, and some of these changes might also be involved in the generation of aberrant spontaneous activity patterns that could give rise to the phantom auditory sensation of tinnitus. However, it is not known which kind of neural plasticity is responsible for the development of tinnitus-related hyperactivity after hearing loss. Many neuronal properties like for example the strength of synaptic connections can be altered in an activity-dependent fashion. Hearing loss strongly alters the activity of the auditory nerve and thus the input signal to the central auditory system, possibly triggering activity-dependent plasticity. In this chapter, we therefore review basic mechanisms of activity-dependent neuronal plasticity, focusing on long-term potentiation and depression of synaptic strength and on homeostatic plasticity. Special emphasis is put on results from the auditory system.

5.1 Long-Term Potentiation and Depression

The magnitude of the postsynaptic response that is evoked by presynaptic activity is usually called the strength or efficacy of the synaptic connection. The synaptic strength is not fixed once and for all after a synaptic contact between two neurons has been established, as certain patterns of neuronal activity can alter synaptic strengths (Bliss and Lomo, 1973). Synaptic strength can be increased (potentiation) or decreased (depression). If it is possible to trigger a lasting change in synaptic strength, one speaks of long-term potentiation (LTP) and long-term depression (LTD).

5.1.1 Excitatory Synapses

Recent investigations have revealed that the amount and direction of the change in synaptic strength at excitatory synapses can depend on the precise timing of postsynaptic action potentials with respect to presynaptic input spikes on a time scale of several milliseconds. LTP is induced if presynaptic firing precedes a postsynaptic spike within this time window, and LTD occurs if the timing is reversed (Markram et al., 1997; Zhang et al., 1998; Bi and Poo, 1998; Froemke and Dan, 2002). This temporal relation matches the postulate of Hebb (1949) that if the presynaptic neuron takes part in firing the postsynaptic neuron (i.e. the presynaptic spikes

precede a postsynaptic spike) this should lead to a strengthening of the synaptic connection between these neurons. These changes are thus also termed 'Hebbian', and are believed to be the basis of learning and memory (Martin et al., 2000).

Learning rules for such spike timing-dependent plasticity (STDP) have been formulated based on these findings, and the effects of such time-dependent 'learning windows' have been analyzed theoretically (Kempter et al., 1999; Song et al., 2000; Gütig et al., 2003). In modeling studies, salient features of cortical organization like orientation and direction selectivity, ocular dominance columns, and maps as well as remapping following 'injury' could be obtained in neural networks through STDP at excitatory synapses (Song and Abbott, 2001).

5.1.2 Inhibitory Synapses

LTP and LTD also occur at inhibitory synapses (Aizenmann et al., 1998; Kotak and Sanes, 2000; Gaiarsa et al., 2002). As for excitatory synapses, plasticity at inhibitory synapses is triggered by a rise in the intracellular calcium-concentration. Recently, it has been shown that also at inhibitory synapses the direction and strength of the change in synaptic efficacy can depend on the precise timing of spikes. The timing relation that was observed in inhibitory synapses in the entorhinal cortex was similar to excitatory synapses (Haas et al., 2006).

5.1.3 Synaptic Plasticity in the Auditory System

Much of the experimental work on synaptic plasticity has been done on neurons in the hippocampus or the visual and somatosensory cortex, but more recently also the auditory system has been examined. LTP (Kudoh and Shibuki, 1994, 1996) and LTD (Kudoh et al., 2002) have been observed in the auditory cortex. Activity-dependent changes in synaptic strength have also been found in the auditory midbrain and brainstem. In the central nucleus of the inferior colliculus, long-term potentiation of evoked field potential amplitude could be elicited by tetanic stimulation (Zhang and Wu, 2000). Moreover, long term depression was observed at inhibitory synapses in the medial superior olive (Kotak and Sanes, 2000), and plasticity at inhibitory synapses has been shown to be a salient feature for the development of sound localization mechanisms in the medial superior olive (MSO) of mammals (Seidl and Grothe, 2005). Even as early as in the DCN, LTP and LTD have been observed (Fujino and Oertel, 2003; Tzounopoulos et al., 2004). The synaptic connections of parallel fibers onto fusiform cells and cartwheel cells of the DCN were found to be modifiable. Stimulation of the parallel fibers prior to evoking a postsynaptic spike in a fusiform cell lead to long-term potentiation, and the reversed timing relation caused long-term depression. In contrast to that, activation of parallel fibers prior to a postsynaptic spike in a cartwheel cell caused long-term depression, and the opposite timing relation left synaptic strengths unchanged (Tzounopoulos et al., 2004). The purpose of this combination of Hebbian and anti-Hebbian plasticity in the circuit of the DCN has not been elucidated yet. Interestingly, the synapses of auditory nerve fibers on fusiform cells could not be modified by the short-term stimulation used in these studies (Fujino and Oertel, 2003).

Theoretical studies indicate that synaptic plasticity plays an important role in shaping the response properties of auditory brain stem structures. The sub-millisecond timing precision needed to accurately process binaural localization cues in the nucleus laminaris of barn owls (corresponding to the MSO in mammals) could be achieved by employing an unsupervised

spike-timing dependent Hebbian learning rule (Gerstner et al., 1996). Moreover, also the reorganization of tonotopic maps that is observed after hearing loss could be mediated by LTP and LTD of intracortical connections (Jenison, 1997).

5.2 Homeostatic Plasticity

The plasticity mechanisms described so far are local mechanisms that specifically affect the strength of individual synapses or small populations of synapses. There are, however, also global mechanisms that affect all synapses or change intrinsic properties of a neuron in an activity-dependent fashion.

5.2.1 Homeostatic Plasticity in Cell Culture

In cultured cortical neurons, chronic blockade of spiking activity through tetrodotoxin led to increased amplitudes of miniature excitatory postsynaptic currents, indicating that the strength of excitatory synapses was increased (Turrigiano et al., 1998). Moreover, the same protocol caused a reduction of the amplitude of miniature inhibitory postsynaptic currents, thus a reduction of the strength of inhibitory synapses occurred (Kilman et al., 2002). Finally, also the intrinsic excitability as measured by the number of spikes produced in response to a current injection was found to be increased after chronic activity blockade (Desai et al., 1999b). When activity was chronically increased through the application of the GABA-antagonist bicuculline, changes in the opposite direction were observed (Turrigiano et al., 1998). Changes in synaptic strength or excitability occurred on a very slow time-scale of hours to days. The data were consistent with changes in synaptic strength through multiplicative scaling of the efficacy of all synapses (Turrigiano et al., 1998).

The direction of the observed changes in synaptic strength and excitability was always such that they were suitable to counteract the changes in activity. When the excitability of single hippocampal neurons was decreased through overexpression of an inward rectifier potassium channel, excitatory synaptic strengths were increased the affected neurons, which restored the activity to control levels (Burrone et al., 2002). Similarly, when the activity of a culture of cortical neurons was persistently increased by blocking inhibition with bicuculline, excitatory synaptic strengths were reduced, which decreased the neuronal activity to a normal level (Turrigiano et al., 1998). This global plasticity mechanism is therefore called homeostatic plasticity, and it is believed to stabilize neuronal activity at a certain target level, ensuring stability of neural function (Turrigiano, 1999; Turrigiano and Nelson, 2000; Burrone and Murthy, 2003).

The molecular mechanisms of homeostatic plasticity are currently being investigated. On the postsynaptic side, activity-dependent scaling of synaptic strength was found to be caused by a change in the number of receptors that are accumulated at the synapses (Rao and Craig, 1997; O'Brien et al., 1998; Kilman et al., 2002). On the presynaptic side, the size of the readily releasable pool of vesicles and the release probability were increased after prolonged inactivity (Murthy et al., 2001).

Homeostatic plasticity works on long time-scales from hours to days. Intracellular Ca^{2+}-levels are believed to play an important role as activity sensors for monitoring activity over such long time scales (Marder and Prinz, 2002). However, the mechanisms and signaling pathways that are involved in sensing activity and controlling synaptic strengths and intrinsic excitability

are mostly unknown (Davis, 2006).

5.2.2 Homeostatic Plasticity In Vivo

Most of the findings on homeostatic plasticity have been obtained in experiments using cultured cortical neurons. However, recent studies have shown that homeostasis can also occur *in vivo*. When young rats (postnatal day 15) were subjected to visual deprivation for two days, excitatory synaptic strengths in the visual cortex were increased, and inhibitory synapses were weakened (Maffei et al., 2004). Interestingly, also the spontaneous firing rates of specific cortical neurons were increased, and restoring vision reversed the changes.

5.2.3 Homeostatic Plasticity in the Auditory System

Homeostatic plasticity or a similar mechanism could also be involved in plastic changes in the auditory system after sensory deprivation. In the IC of gerbils, for example, bilateral deafening leads to increased amplitudes of excitatory postsynaptic currents and an increased equilibrium potential of inhibitory postsynaptic currents (Vale and Sanes, 2002), suggesting that the balance between excitation and inhibition is shifted in a homeostatic fashion. Moreover, glutamatergic synaptic transmission in the CN of chinchillas was found to be temporarily increased after acoustic trauma (Muly et al., 2004). Increased amplitudes of excitatory postsynpatic currents were also observed in the anteroventral CN of congenitally deaf mice in response to electrical stimulation of the AN (Oleskevich and Walmsley, 2002). Furthermore, glycinergic inhibition in the DCN was persistently weakened following unilateral cochlear ablation (Suneja et al., 1998a,b) or age-related hearing loss (Caspary et al., 2005). Finally, in the auditory cortex of gerbils, increased excitability as well as increased excitatory and decreased inhibitory synaptic transmission were measured after bilateral cochlear ablation (Kotak et al., 2005). Homeostatic plasticity may thus be involved in activity-dependent regulatory processes throughout the auditory system.

Summary and Conclusions

Activity-dependent neuronal plasticity can modify the strength of synapses and adapt intrinsic properties of nerve cells. Thus, altered auditory nerve activity after hearing loss could trigger plastic changes in central auditory neurons. This could also give rise to tinnitus-related activity patterns like for example hyperactivity of neurons in the DCN. Which of the plasticity mechanism might be responsible for the observed changes remains to be revealed.

Spike-timing dependent plasticity could be involved in the reorganization of tonotopic maps in the auditory cortex that is believed to be involved in the development of tinnitus (Eggermont and Roberts, 2004). Moreover, cortical circuits are characterized by lateral connections forming recurrent neuronal networks. In principle, recurrent networks are capable of generating self-sustaining persistent activity (Hopfield, 1982). When the strength of cortical recurrent connections is altered due to changes in afferent activity patterns after hearing loss, persistent activity might arise, which could be perceived as tinnitus.

Plastic changes in the DCN after hearing loss might be mediated by different plasticity mechanisms, as the tonotopic map of the DCN does not show evidence of plastic reorgani-

zation (Kaltenbach et al., 1992). Moreover, acoustic trauma and administration of ototoxic drugs lead to similar patterns of hyperactivity. Both of these manipulations increase the response thresholds of the affected auditory nerve fibers, thus decreasing auditory nerve activity. Therefore, a decrease in activity is to be expected in the CN, possibly triggering homeostatic plasticity. The consequences of a homeostatic stabilization of neuronal activity in the CN after hearing loss will be evaluated using a computational model in Chapters 7 and 8.

Chapter 6

Course of Hearing Loss and Occurrence of Tinnitus

As we have presented in Section 4.1.2, tinnitus and hearing loss are related: The prevalence of tinnitus increases with hearing loss (Chung et al., 1984), and there is a correspondence between the characteristics of the tinnitus sensation and the amount and frequency range of hearing loss (Henry et al., 1999; Noreña et al., 2002). However, not all patients with hearing loss develop tinnitus, as demonstrated by the higher prevalence of hearing loss compared to tinnitus (Lockwood et al., 2002). It is therefore unclear which factors of hearing loss contribute to the occurrence of tinnitus.

Tinnitus is believed to arise from alterations in the spontaneous activity of neurons in the auditory system (see Chapter 4, pages 23 and 24). In animals, hearing loss through cochlear damage reduces the spontaneous firing rate in the affected auditory nerve fibers (Liberman and Dodds, 1984a). This reduction can cause discontinuities in the profile of spontaneous activity along the tonotopic axis in the auditory pathway. Modeling studies suggest that such discontinuities could be exaggerated by lateral inhibition (Gerken, 1996) and homeostatic changes (Schaette and Kempter, 2006), leading to activity patterns in the models that are consistent with tone-like tinnitus.

Such concepts suggest that the development of tinnitus depends on the course of the audiogram, in that some audiogram shapes are more likely to lead to tinnitus than others. To investigate this hypothesis, we analyzed a sample of patients that all had noise-induced hearing loss from chronic noise exposure in the workplace. This choice of subjects eliminates possible confounding factors that could arise from mixed etiologies of hearing loss[1].

6.1 Patient Data Acquisition and Analysis

We performed a retrospective analysis on patient data that had been collected in the group of Prof. Gross, Phoniatrics, Charité Berlin from 1993-2003. The patients were compensation claimants that had been sent to the clinic for evaluation of work-related noise-induced hearing loss. Audiological examination and tinnitus pitch matching were performed at the Phoniatrics Department of the Charité, Campus Benjamin Franklin.

[1]This chapter is based on König and Schaette et al. (2006). Both first authors contributed equally to this study. The patient data was acquired by O. König and analyzed by R. Schaette.

The patient sample consisted of 71 adults (mean age 56 years; range 38-69 years; all males). The subjects were in good general health and reported an unremarkable history of otological diseases or exposure to ototoxic drugs. All patients had moderate-to-severe noise-induced hearing loss caused by chronic noise exposure in the workplace. There were 30 subjects without tinnitus, 24 subjects with tone-like tinnitus, and 17 subjects with noise-like tinnitus. The three groups did not differ significantly in age (no tinnitus: 56.6 ± 1.1 years; tone-like tinnitus 55.0 ± 1.4 years; noise-like tinnitus 56.3 ± 1.6 years). For subjects with tinnitus, the mean reported duration of hearing loss was 10.2 ± 1.24 years, and for subjects without tinnitus 11.67 ± 1.86 years (difference not significant, $p = 0.50$, t-test). All tinnitus subjects had experienced their tinnitus for more than one year, with a mean reported duration of 8.83 ± 1.33 years. The duration of tinnitus experience was not significantly different from the duration of hearing loss ($p = 0.47$, t-test). We note that the duration of hearing loss and tinnitus could not always be reliably determined, as noise-induced hearing loss is slowly progressing, and tinnitus often develops from occasional episodes to a permanent sensation.

All tinnitus patients had chronic bilateral tinnitus, i.e., tinnitus was a permanent sensation, was perceived in both ears with similar pitch, and had persisted for at least one year. We chose to exclude patients with unilateral tinnitus to eliminate possible confounding factors that could arise from assigning the two ears of a single patient to two different groups in the analysis. Moreover, unilateral tinnitus might be different from bilateral tinnitus, as it is often associated with a difference in hearing level between the ears (Chung et al., 1984; Ochi et al., 2003). We also excluded patients using a hearing aid, as hearing aids can reduce tinnitus (Surr et al., 1999; Folmer and Carroll, 2006) and are used in tinnitus therapy (Jastreboff and Jastreboff, 2000).

6.1.1 Audiological Examination

A total of 142 ears (71 right, 71 left) were used in further analysis. Inclusion criteria were (1) no significant air-bone gap at seven test frequencies (0.25, 0.5, 1, 2, 4, 6 and 8 kHz); (2) normal middle ear status with type A tympanograms and a well-defined compliance maximum not less than -100 daPa; (3) normal otoscopic findings; and (4) not using a hearing aid. Pure-tone audiometry was performed with a clinical audiometer calibrated to accepted standards (American National Standards Institute. Specifications for audiometers, S3.6. New York; American National Standards Institute, 1969). Tympanometric measurements were obtained with a middle-ear analyzer calibrated daily according to the manufacturer's instructions.

6.1.2 Tinnitus Pitch Matching

For patients with tone-like tinnitus, the tinnitus frequency was determined with two different psychophysical procedures in the ear ipsilateral to the tinnitus: an adaptive method (bracketing) and the method of adjustment. Each procedure involved equating the pitch of a pure tone (0.125, 0.25, 0.5, 0.75, 1, 2, 3, 4, 6 and 8 kHz) to the most prominent tinnitus pitch. There was no statistically significant difference for the means and standard deviations among the different methods for the group data. Because some patients were unreliable in their pitch matching, we repeated the match up to seven times.

6.1.3 Characterization of the Shape of the Audiogram

To obtain a measure of the overall amount of hearing loss of a patient we used the area under the audiogram curve. Therefore, the audiogram frequencies were converted to a logarithmic scale, and the resulting audiogram was interpolated linearly between the measured points. Then we calculated the integral from 0.125 to 8 kHz to obtain the area under the audiogram curve.

Audiogram slopes were computed as follows: for each adjacent two frequencies in an audiogram, the difference in dB hearing level was calculated and then divided by the frequency difference measured in octaves. This procedure yields the steepness in dB/octave. The steepness value was then assigned to the geometric mean of the two frequencies to construct derivative audiograms.

Audiogram edges were detected in a two-step process. First we determined the frequency range where hearing levels had not dropped more than 20 dB below the best hearing level observed in the audiogram. In this range, we looked for a maximum of the second derivative of the audiogram (computed from the derivative audiogram using the method described above) to identify the audiogram edge. If no edge could be identified in that way, the highest frequency that still met the 20 dB hearing level criterion was said to be the audiogram edge. To compute the mean audiogram edge across individuals, edge frequencies were first converted to a logarithmic scale, and then averaged.

6.1.4 Significance Tests

Unpaired two-sample t-tests were used to determine whether differences were significant. We used a significance level of $\alpha = 0.05$. Whenever more than one test was carried out on a data set, a Bonferroni correction was applied to adjust the significance level ($\alpha = 0.05/n$ for n tests).

All data analysis was carried out using MATLAB 7 (The MathWorks Inc., Natick, Massachusetts).

6.2 Results

To reveal features of audiograms that promote the occurrence of tinnitus we analyzed data from 71 patients with noise-induced hearing loss. Thirty patients had no tinnitus, 24 patients had tone-like tinnitus, and 17 patients had noise-like tinnitus.

6.2.1 Tinnitus Pitch and Hearing Loss

When patients with tone-like tinnitus were asked to match pure tones (0.125, 0.25, 0.5, 0.75, 1, 2, 3, 4, 6, or 8 kHz) to the dominant pitch of their tinnitus sensation, tinnitus pitch was generally matched to frequencies above the audiogram edge (see Methods) where hearing is impaired (Figs. 6.1a,b). On average, tinnitus pitch was 1.48 ± 0.12 octaves above the audiogram edge, and there was a weak but significant correlation between edge frequency and tinnitus pitch ($r = 0.30$, $p = 0.04$).

To further examine the relation between tinnitus pitch and hearing loss, we grouped the patients by tinnitus pitch (≤ 3 kHz, 4 kHz, ≥ 6 kHz) and calculated the mean audiogram as well as the mean audiogram edge frequency for each group. We also determined the overall amount of hearing loss as quantified by the area under the audiogram curve for each ear (see Methods),

and then computed the mean overall hearing loss for each group. As can be seen in Figs. 6.1c and d, patients with a tinnitus pitch ≤ 3 kHz had the worst hearing and the lowest audiogram edge frequency, whereas those with a pitch ≥ 6 kHz had the best hearing and the highest audiogram edge frequency, and the 4 kHz group was intermediate. Significant differences were observed between the groups "≤ 3 kHz" and "≥ 6 kHz' for the average edge frequency ($p = 0.005$, t-test) and the overall amount of hearing loss ($p = 0.006$, t-test), whereas differences between the groups "≤ 3 kHz" and "4 kHz", as well as between the groups "4 kHz" and "≥ 6 kHz" failed to achieve significance.

6.2.2 Severity of Hearing Loss and Occurrence of Tinnitus

The observed relation between tinnitus pitch and the amount and frequency-range of hearing loss suggested that the occurrence of tinnitus could depend on the severity of hearing impairment. We therefore compared the overall amount of hearing loss of subjects with and without tinnitus. Surprisingly, we found that hearing-impaired patients with tinnitus (tone-like and noise-like) on average had less hearing loss than those without tinnitus (Fig. 6.2a), and the difference was highly significant ($p = 6 \cdot 10^{-4}$, t-test). The difference within the tinnitus group (tone-like tinnitus vs. noise-like tinnitus), on the other hand, was not significant ($p = 0.26$, t-test, Fig. 6.2b). Similarly, we found that tinnitus patients and subjects without tinnitus differed in the location of the mean audiogram edge. Patients with tinnitus had an average edge frequency of 1.31 kHz $\pm$ 0.09 octaves, whereas patients without tinnitus had a mean edge frequency of 0.82 kHz $\pm$ 0.12 octaves. This difference was highly significant, too ($p = 7 \cdot 10^{-6}$, t-test). When the tinnitus-group was subdivided into tone-like and noise-like tinnitus, we obtained a mean edge of 1.47 kHz $\pm$ 0.1 octaves for tone-like tinnitus, and 1.11 $\pm$ 0.12 octaves for noise-like tinnitus. The difference between the two groups just failed to achieve significance ($p = 0.03$, t-test).

6.2.3 Audiogram Steepness and Occurrence of Tinnitus

The mean audiograms in Fig. 6.2c show that, on average, subjects with and without tinnitus had similar hearing levels at the lowest and the highest frequencies, whereas the course of the audiograms at intermediate frequencies was different. To quantify the course of the audiograms at intermediate frequencies we determined the maximum steepness for each audiogram (see Methods). This analysis revealed that tinnitus patients tended to have steeper audiogram slopes than subjects without tinnitus. Subjects without tinnitus had a mean maximum steepness of -43.1 ± 2.4 dB/octave, whereas patients with tinnitus had a mean maximum steepness of -52.9 ± 1.9 dB/octave (Fig. 6.2d). The difference in mean maximum steepness between patients with and without tinnitus was significant ($p = 0.002$, t-test). After subdividing the tinnitus group, we obtained a mean maximum steepness of -53.4 ± 2.5 dB/octave for tone-like tinnitus, and -52.2 ± 3.1 dB/octave for noise-like tinnitus (Fig. 6.2e). This difference was not significant ($p = 0.91$, t-test). For tone-like tinnitus, the tinnitus pitch was on average 0.81 ± 0.1 octaves above the frequency of the steepest slope of the audiograms. Moreover, there was a significant correlation between tinnitus pitch and the frequency of the steepest slope of the audiogram ($r = 0.33$, $p = 0.022$).

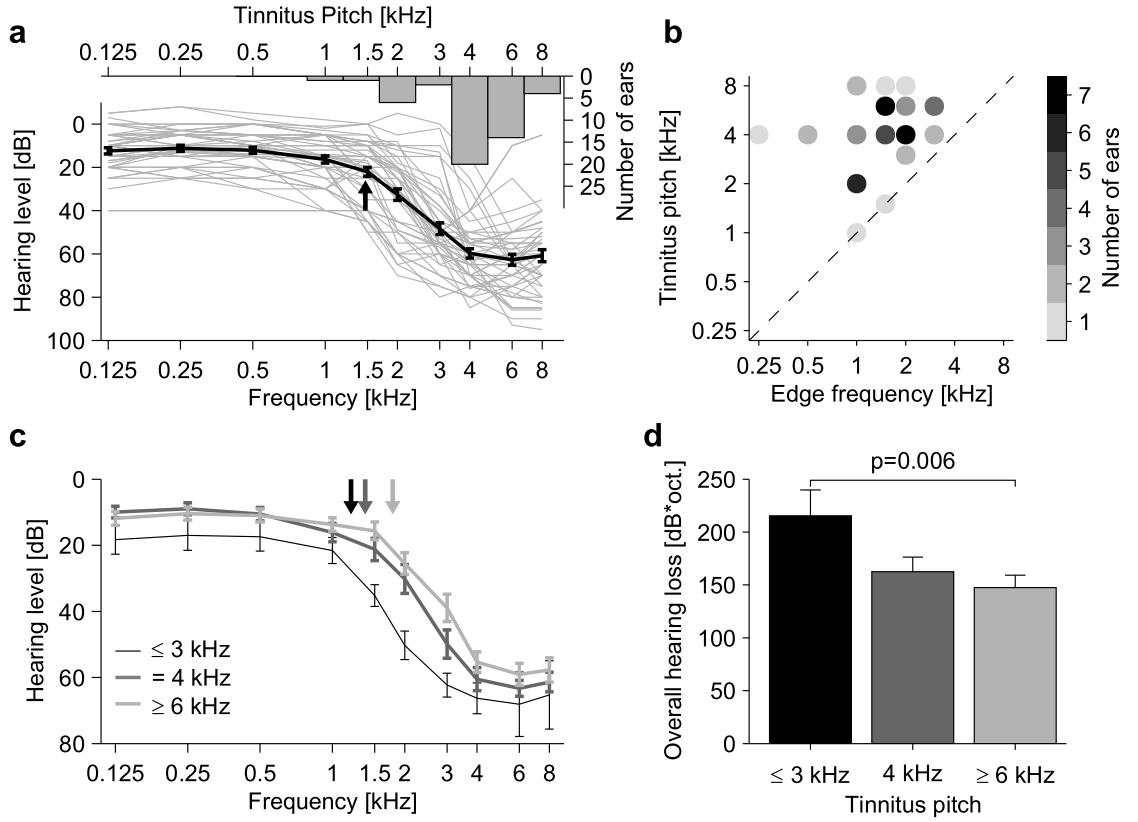

Figure 6.1: Association between tinnitus pitch, audiogram edge, and overall amount of hearing loss. **a)** Audiograms (thin lines) of 24 patients with tone-like tinnitus, mean audiogram (thick line), and distribution of tinnitus pitch (bars). Tinnitus pitch is located predominantly at frequencies above the mean audiogram edge (arrow) where hearing is impaired. **b)** Tinnitus pitch vs. audiogram edge frequency. The gray level of each point denotes the number of ears with the corresponding combination of edge frequency and tinnitus pitch. **c,d)** Mean audiograms (lines in c) and audiogram edges (arrows in c) and overall amount of hearing loss (d) of patients grouped by tinnitus pitch (≤ 3 kHz, 4 kHz, ≥ 6 kHz). The groups with a tinnitus pitch of ≤ 3 kHz (black) and ≥ 6 kHz (light gray) significantly differed in their their overall amount of hearing loss. Error bars denote $\pm$ 1 s.e.m.

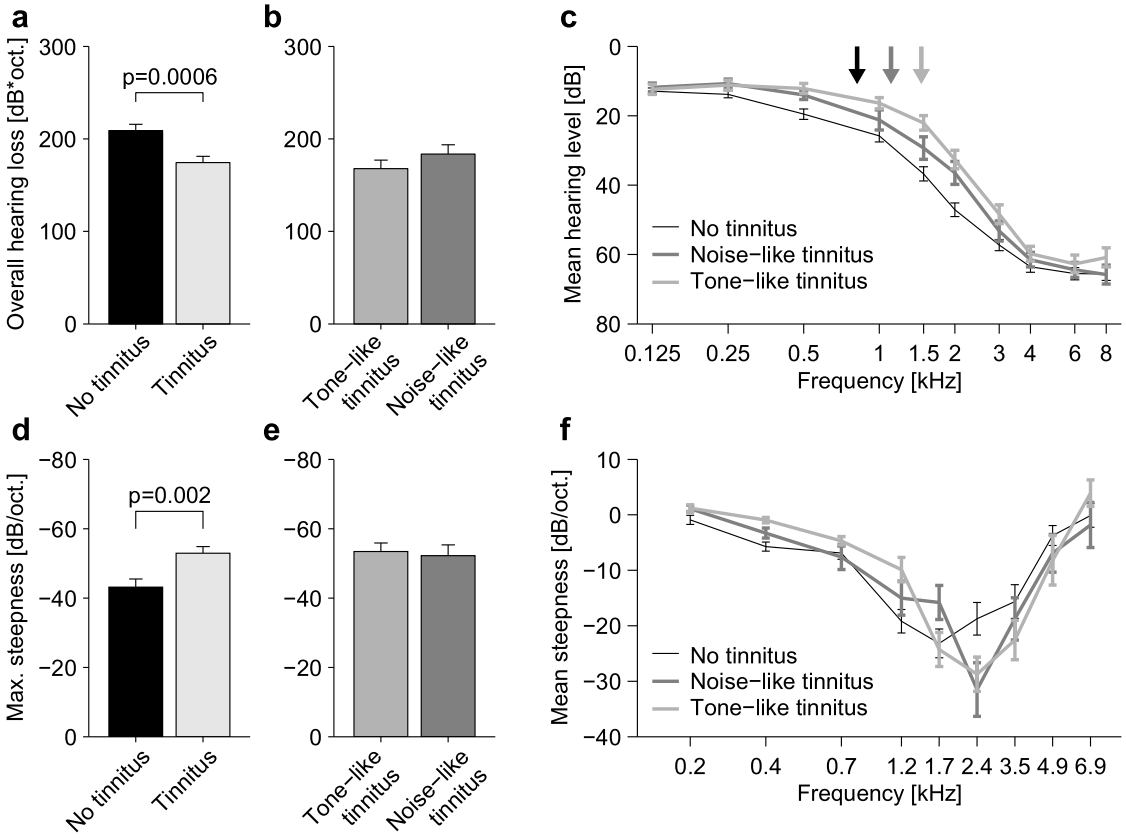

Figure 6.2: Audiometric differences between hearing-impaired patients with and without tinnitus. **a)** Patients without tinnitus ($n = 30$) had significantly more overall hearing loss than patients with tinnitus ($n = 41$). **b)** The mean overall hearing loss in patients with tone-like tinnitus ($n = 24$) and noise-like tinnitus ($n = 17$) was not significantly different. **c)** Mean audiograms (lines) and audiogram edge frequencies (arrows) of patients without tinnitus (black), with noise-like tinnitus (dark gray), and with tone-like tinnitus (light gray). **d)** Audiograms of patients with tinnitus had a significantly higher mean maximum steepness than those of patients without tinnitus. **e)** The mean maximum steepness of the audiograms of patients with tone-like and noise-like tinnitus was not significantly different. **f)** Mean derivative audiograms; color assignments as in c). Error bars denote $\pm$ 1 s.e.m.

6.3 Discussion

In this chapter, we analyzed a sample of patients with moderate to severe noise-induced hearing loss due to chronic noise-exposure in the workplace. We found that patients with and without tinnitus significantly differed in the course of their audiograms. On average, the patients with tinnitus had less hearing loss, steeper maximum slopes of their audiograms, and the edges of their audiograms were located at higher frequencies compared to the patients without tinnitus (Fig. 6.2). We did not find significant differences in these parameters between tone-like and noise-like tinnitus.

The relation in our patient sample between tinnitus pitch and the frequency-range of hearing loss (Fig. 6.1a,b) is consistent with results in earlier studies: tinnitus pitch is predominantly matched to frequencies above the audiogram edge (Henry et al., 1999), and tinnitus spectra as measured by Noreña et al. (2002) and Roberts et al. (2006) correspond to the frequency-range of hearing loss. A distributed spectrum of the tinnitus percept could also explain why some of our subjects were unreliable in matching the pitch of their tinnitus to pure tones, which has also been observed in other studies (Burns, 1984).

The prevalence of tinnitus has been reported to increase with increasing hearing loss in noise-exposed workers that were routinely screened (Chung et al., 1984), whereas in those claiming compensation for work-related hearing loss, the tinnitus prevalence was approximately constant over a wide range of hearing thresholds (McShane et al., 1988). Moreover, Phoon et al. (1993) found that noise-exposed workers with tinnitus had higher average hearing thresholds than those without tinnitus, whereas we found that subjects without tinnitus had more overall hearing loss than subjects with tinnitus. These discrepancies could be due to a different choice of subjects and a different inclusion criterion for tinnitus. We only analyzed subjects with chronic tinnitus experiencing a permanent tinnitus sensation, whereas other studies also included subjects with occasional episodes of tinnitus. However, the inconsistent results on the relation between tinnitus and hearing loss could also indicate that hearing thresholds alone might be insufficient to predict the occurrence of tinnitus. We therefore also analyzed the shape of the audiogram. To quantify the course of the audiogram, we chose the audiogram steepness, as it is largely independent of the overall amount of hearing loss. We could thus demonstrate that not only the amount of hearing loss, but also the shape of the audiogram might be an important factor for the occurrence of tinnitus. In our sample of patients, tinnitus was connected to audiograms with a steep slope, the maximum steepness of the audiograms of tinnitus subjects was significantly higher compared to subjects without tinnitus.

Psychophysical studies demonstrate that steeply sloping hearing loss is associated with local improvements in frequency discrimination thresholds (McDermott et al., 1998; Thai-Van et al., 2002, 2003), which has been interpreted as a correlate of cortical reorganization. Cortical reorganization is believed to play a role in the development of tinnitus (Rauschecker, 1999; Eggermont and Roberts, 2004). Interestingly, only subjects with a hearing loss slope of more than 50 dB/octave displayed a significant improvement in frequency discrimination (Thai-Van et al., 2002). This value is close to the mean maximum steepness in our tinnitus patients (-52.9 ± 1.9 dB/octave), and greater than the mean maximum steepness of our subjects without tinnitus (-43.1 ± 2.4 dB/octave, Fig. 6.2d).

Animal studies have found substantial cortical reorganization (Rajan and Irvine, 1998b; Komiya and Eggermont, 2000; Seki and Eggermont, 2002; Noreña et al., 2003; Noreña and Eggermont, 2005) and increased spontaneous firing rates of cortical neurons (Seki and Egger-

mont, 2002; Noreña and Eggermont, 2006) after hearing loss. The earliest stage in the auditory pathway where increases in spontaneous activity after hearing loss have been observed is the dorsal cochlear nucleus (Kaltenbach and McCaslin, 1996). These increases in spontaneous firing rate were correlated to behavioral evidence for tinnitus (Brozoski et al., 2002; Kaltenbach et al., 2004). Increased spontaneous firing rates developed in those parts of the dorsal cochlear nucleus that received input from damaged parts of the cochlea (Kaltenbach et al., 2002). Modeling studies indicate that the type and severity of cochlear damage determine how strongly the spontaneous firing rates are increased (Schaette and Kempter, 2006, see also Chapter 7). The profile of the spontaneous firing rates along the tonotopic axis thus depends on the shape of the audiogram. For steep audiogram slopes, induced for example by damage to hair cell stereocilia in the high-frequency range, this model predicts steep, abrupt transitions in the spontaneous firing rate of neurons, with spontaneous firing rates peaking in the region of hearing loss (see Fig. 7.7e on page 55). This peak could be misinterpreted by central auditory structures as a sound-evoked pattern, leading to the perception of a sound. Whether the resulting 'model tinnitus' is consistent with patient data will be addressed in detail in Chapter 9. Moreover, in this model, only steep audiogram slopes lead to pronounced structures in the profile of spontaneous activity along the tonotopic axis. Distinct structures in the spontaneous activity could be perceived as sound, thus offering an explanation for the association of tinnitus with steep audiogram slopes. In a recent modeling study, it was also proposed that gain adaptation and lateral inhibition in the auditory system could be involved in the generation of tinnitus-related activity patterns for audiograms with steep slopes (Parra and Pearlmutter, 2007). These concepts also suggest that it should be possible to predict the occurrence of tinnitus from the audiogram. However, clinical audiograms as used in this study are too coarse for this purpose.

As a future perspective, studies combining high-resolution audiometry, psychophysical procedures identifying cochlear dead regions (Moore et al., 2000) and precise characterization of the tinnitus percept would be desirable to further elucidate the relation between tinnitus and hearing loss.

Chapter 7

A Computational Model for the Development of Tinnitus-Related Hyperactivity

The earliest processing stage in the auditory pathway where tinnitus-related changes have been observed is the dorsal cochlear nucleus (DCN). Acoustic trauma leads to increased spontaneous firing rates of DCN neurons (see Chapter 4, page 24), and the degree to which the spontaneous rates are elevated is related to the strength of the behavioral evidence for tinnitus (Kaltenbach et al., 2004). Such hyperactivity occurs only in those regions of the DCN that are innervated by the lesioned parts of the cochlea (Kaltenbach et al., 2002). These experimental results present a paradoxical situation: cochlear damage leads to an overall decrease of auditory nerve (AN) activity, but the spontaneous firing rates in the DCN are increased.

Interestingly, hyperactivity in the DCN develops within days after hearing loss (Kaltenbach et al., 1998; Kaltenbach et al., 2000). Mechanisms of homeostatic plasticity (see Chapter 5, page 31) also operate on this time scale (see e.g. Turrigiano et al., 1998). Homeostatic plasticity is a response of neurons to sustained changes in their mean activity caused, for example, by changed mean synaptic drive. Homeostasis aims at stabilizing the mean firing rate of a neuron (Turrigiano, 1999; Burrone and Murthy, 2003) by scaling the strength of synapses and altering the intrinsic neuronal excitability (Turrigiano et al., 1998; Desai et al., 1999b; Kilman et al., 2002). Such changes have been observed in the auditory cortex and in various regions of the auditory brainstem in response to sensory deprivation by means of cochlear ablation or cochlear damage through acoustic trauma (see Chapter 5, page 32): Excitatory synaptic transmission was strengthened (Vale and Sanes, 2002; Muly et al., 2004; Kotak et al., 2005), inhibitory transmission was weakened (Suneja et al., 1998a,b; Vale and Sanes, 2002; Kotak et al., 2005), and excitability was increased (Kotak et al., 2005).

To address the question of how peripheral hearing loss may lead to tinnitus-related hyperactivity of neurons in the auditory brainstem, we utilize a phenomenological model of the responses of AN fibers and downstream auditory neurons, for example in the cochlear nucleus. The computational model is not intended to capture all known physiological details of the AN and the cochlear nucleus in detail. Instead we use a minimal model to demonstrate the basic mechanism of how homeostatic plasticity could contribute to the development of hyperactivity in response to altered input statistics[1].

[1]This chapter is based on Schaette and Kempter (2006)

7.1 Hyperactivity through Homeostatic Plasticity

The aim of this chapter is to demonstrate how a stabilization of neuronal activity through homeostatic plasticity could contribute to the development of hyperactivity in the auditory system after hearing loss. Figure 7.1 illustrates how homeostasis stabilizes a neuron's mean activity. We assume that, initially, some input drives the neuron to fire within a range between its spontaneous and maximum firing rates. The mean firing rate is determined by the statistics of the input signal. Let us focus on a case where after a lesion the statistics of the input change such that the mean firing rate of the neuron is decreased without affecting the range of firing rates, a scenario which is reminiscent of the loss of outer hair cells in the cochlea. If homeostatic plasticity then restores the mean rate to its target value, for example by increasing synaptic efficacies, this can also increase the neuron's spontaneous firing rate, thus causing hyperactivity. Hyperactivity typically develops when the activity of the neuron is changed such that the ratio between mean and spontaneous firing rate is reduced; further details of the activity statistics are not overly important. We now apply this concept to the first stages of the auditory pathway, using a phenomenological model of the responses of auditory nerve (AN) fibers and downstream auditory neurons in the cochlear nucleus (CN).

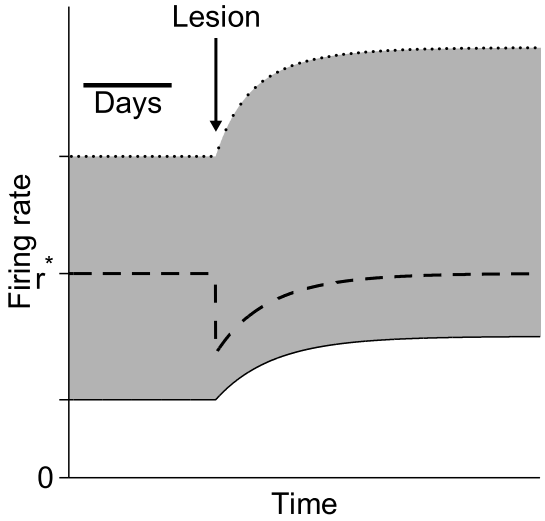

Figure 7.1: Homeostatic stabilization of the mean firing rate of a neuron and hyperactivity. The gray area illustrates the range of firing rates from spontaneous (solid line) to maximum rate (dotted line) as a function of time. If for example a lesion suddenly decreases the mean firing rate (dashed line) without affecting the dynamic range of rates, a subsequent restoring of the mean rate to a target value r^* can lead to an increased spontaneous firing rate, or hyperactivity. Such a homeostatic stabilization could occur at many different levels in the auditory pathway as well as in other areas of the central nervous system.

7.2 Phenomenological Auditory Nerve Model

We start by setting up a phenomenological model of the responses of auditory nerve fibers to acoustic stimulation. Then we consider how the response properties are changed by hearing

loss through various kinds and degrees of cochlear damage.

7.2.1 Population Firing Rate of the Auditory Nerve

Based on various experimental studies, we describe auditory nerve activity by a population firing rate (black lines in Fig. 7.2), which is an average over several type-I AN fibers with similar characteristic frequencies. Being a population average, it comprises AN fibers with different spontaneous rates, thresholds, and dynamic ranges. We regard this as a reasonable approximation of the input of a downstream neuron that has synaptic contacts to many different AN fibers. The population response threshold is set to 0 dB SPL, which corresponds to the threshold of the most sensitive fibers. Below threshold there is spontaneous activity of 50 Hz, corresponding to an average over AN fibers with low and high spontaneous rates. For supra-threshold stimuli, the average population discharge rate grows with the stimulus intensity and saturates at 250 Hz. The dynamic range (20 to 80% rise) of the population response is 40 dB (Sachs and Abbas, 1974; Dallos and Harris, 1978; Liberman, 1978; Wang et al., 1997).

7.2.2 Damage to Cochlear Hair Cells Alters AN Rate-Intensity Functions

Sensorineural hearing loss changes the response properties of the AN. We distinguish between hearing loss caused by loss of inner hair cells (IHCs), loss of outer hair cells (OHCs), and stereocilia damage (SD).

IHCs provide the main input to AN fibers. Each IHC is innervated by 10-30 AN fibers, but each AN fiber contacts only one IHC (Ryugo, 1992). Loss of IHCs therefore deprives associated AN fibers of their input, whereas the response properties of AN fibers associated with the remaining healthy IHCs seem largely unaffected (Wang et al., 1997). The degree of IHC loss is proportional to the decrease of the amplitude of the AN's compound action potential, i.e. the summed discharge of all AN fibers (Wang et al., 1997). We therefore model IHC loss by scaling down the rate-intensity function of the AN fiber population in proportion to the amount of IHC loss. This simplification of the effects of IHC loss implies that spontaneous as well as maximum rates of the population response are reduced, but the response threshold remains unchanged (Fig. 7.2a and Methods before Eq. 5).

OHCs are thought to act as active amplifiers inside the cochlea; see Geisler (1998) for a review. Pure loss of OHCs, for example induced by ototoxic agents, typically increases the threshold of AN fibers, while spontaneous and maximum discharge rate remain mostly unaffected (Dallos and Harris, 1978; Schmiedt and Zwislocki, 1980). We therefore model OHC loss by an increase in the response threshold of the fiber population, where the increase is proportional to the amount of OHC loss. Based on experimental studies, the loss of all OHCs is assumed to elevate the threshold by 60 dB. Moreover, OHC loss steepens the rate-intensity function of the AN fiber population and reduces its dynamic range (Fig. 7.2b and Methods before Eq. 6).

Stereocilia couple inner and outer hair cells to the tectorial membrane. They are damaged by noise overexposure (see e.g. Wang et al., 2002b), which can also cause a loss of hair cells. SD elevates the response threshold (Liberman, 1984; Heinz and Young, 2004) and decreases the spontaneous firing rate of AN fibers (Liberman and Dodds, 1984a), but SD does not change the maximum discharge rate (Liberman and Kiang, 1984). We therefore model SD caused by noise overexposure by an increase of the response threshold and a decrease in the spontaneous

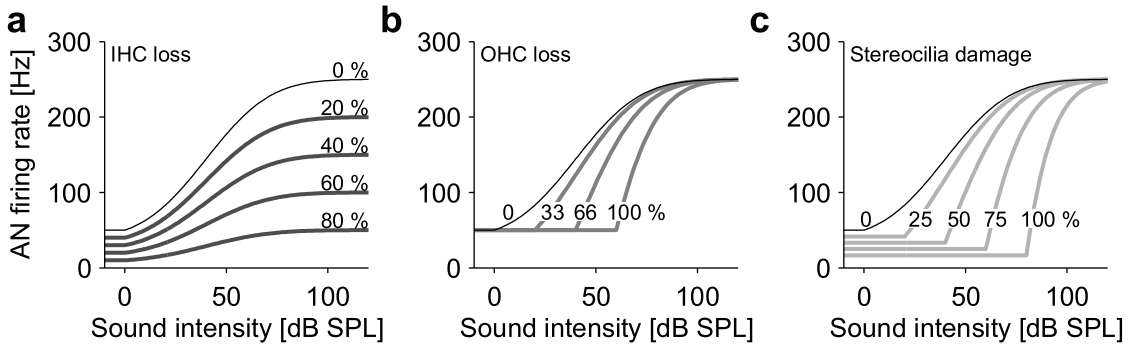

Figure 7.2: Firing-rate model for a small population of auditory nerve (AN) fibers with similar characteristic frequencies. The population firing rate increases with increasing sound intensity. We model hearing loss caused by damage to or loss of cochlear hair cells. **(a)** Loss of inner hair cells (IHCs) scales down the AN population response (0% IHC loss: black line; 20, 40, 60, 80% loss: dark gray lines). **(b)** Loss of outer hair cells (OHCs) increases the response threshold (0% loss: black line; 33, 66, 100% loss: medium gray lines). **(c)** Damage to stereocilia of inner and outer hair cells increases the response threshold and decreases the spontaneous firing rate of AN fibers (0% damage: black line; 25, 50, 75, 100% damage: light gray lines).

firing rate of the rate-intensity function of the AN fiber population. Changes are assumed to be proportional to the degree of SD. From the experimental literature, we estimate that the threshold is elevated by 80 dB for severe loss of stereocilia (100% SD), and that the spontaneous rate is reduced by a factor of two thirds (Fig. 7.2c and Methods before Eq. 7). Similar to pure OHC loss, we assume a steepening of the rate-intensity functions also for SD, which might not always be the case (Heinz and Young, 2004, see Discussion). Our description of the effects of SD comprises damage to or loss of the stereocilia of IHCs and OHCs, and it also includes the effects of the loss of OHCs, because we assume that the total loss of an OHC's stereocilia has the same effect as the complete loss of an OHC. Moreover, for simplicity, we only consider the common case where stereocilia of IHCs and OHCs are affected to a similar degree (see, e.g. Kaltenbach et al., 1992; Wang et al., 2002b), and thus do not differentiate between SD at IHCs and SD at OHCs.

In summary, each type of damage to the cochlea characteristically alters the rate-intensity function of the AN, which may trigger further changes along the auditory pathway.

7.2.3 Sensorineural Hearing Loss Changes the Distribution of AN Firing Rates

Before we can investigate the effects of homeostatic plasticity in downstream auditory neurons in response to sensorineural hearing loss, we first have to establish how the distribution of AN population firing rates is altered by cochlear damage. The fraction of time the AN population fires at some specific rate is determined by its rate-intensity function in conjunction with the distribution of sound intensities in an animal's environment. Let us assume that the sound intensity levels of acoustic stimuli obey a Gaussian distribution with 40 dB mean and 25 dB standard deviation, so that most of the intensities are within the dynamic range of AN responses (Fig. 7.3a, see also Methods). We note that the Gaussian distribution of sound

levels corresponds to a long-tailed distribution of the linear amplitudes of acoustic stimuli, as found for natural sounds (see e.g. Escabi et al., 2003). Moreover, we assume that AN rate-intensity functions are tuned to the distribution of sound intensities so that the firing rates of the AN have maximum information on the sound intensity (infomax principle, compare Laughlin, 1981). This assumption is made in order to simplify further arguments and to allow an analytical approach (see Methods). However, the detailed choice of the forms of both the rate-intensity function and the distribution of sound intensities are not critical for the main conclusions that can be drawn form our model; all unimodal distributions where the majority of sound intensity levels is within the dynamic range of the AN fibers yield similar results.

The probability density function of AN population rates for a healthy cochlea is shown in Fig. 7.3b (right panel). The probability of spontaneous AN activity is given by the fraction of time the sound intensity is below the response threshold of 0 dB. Therefore, the spontaneous firing rate of 50 Hz occurs with probability 0.05 (Fig. 7.3b, right panel, horizontal peak). For supra-threshold intensities, the probability density for firing at a given rate is constant in the interval between 50 and 250 Hz, due to our infomax tuning assumption. In the following, we are going to evaluate three examples of cochlear damage, 30% IHC loss, 66% OHC loss, and 50% SD. The amounts of damage were chosen for similar threshold elevation (OHC loss and SD), similar reduction of the mean AN rate (IHC and OHC loss), and similar reduction of the spontaneous AN firing rate (IHC loss and SD).

The effect of 30% IHC loss is illustrated in Fig. 7.3c. As IHC loss was assumed to scale down the whole AN population response, the range of firing rates is reduced and the mean firing rate is decreased in proportion to the amount of IHC loss. Furthermore, the spontaneous firing rate is lowered. However, as IHC loss does not chage the response threshold of the AN fibers, the probability of occurence of spontaneous activity is unchanged compared to the healthy case. The result of 66% OHC loss is shown in Fig. 7.3d. OHC loss elevates the response threshold of AN fibers, while the spontaneous and the maximum firing rate remain unchanged. As an elevated threshold renders more stimuli sub-threshold, the probability of occurrence of spontaneous activity is increased from 0.05 to 0.5, which simply means that epochs of spontaneous firing occur more often. Consequently, driven activity occurs less frequently, and this is why OHC loss decreases the mean firing rate of the AN. Finally, an example for 50% SD is given in Fig. 7.3e. The response threshold is elevated by SD, and therefore the probability of occurrence of spontaneous activity is increased, similar to OHC loss. However, SD also decreases the spontaneous firing rate of the AN, while the maximum firing rate remains constant. Thus, epochs of spontaneous firing occur more often, but the firing rate within such an epoch is decreased. As a consequence, the mean AN population firing rate is decreased more strongly than for the same threshold shift caused by OHC loss.

To summarize, the loss of IHCs, loss of OHCs, and SD all decrease the mean population firing rate of the AN. This is achieved, however, in different ways. Most relevant for a development of hyperactivity in our model is that OHC loss and SD mainly increase the probability of occurrence of spontaneous activity, whereas a loss of IHCs scales down the AN population response.

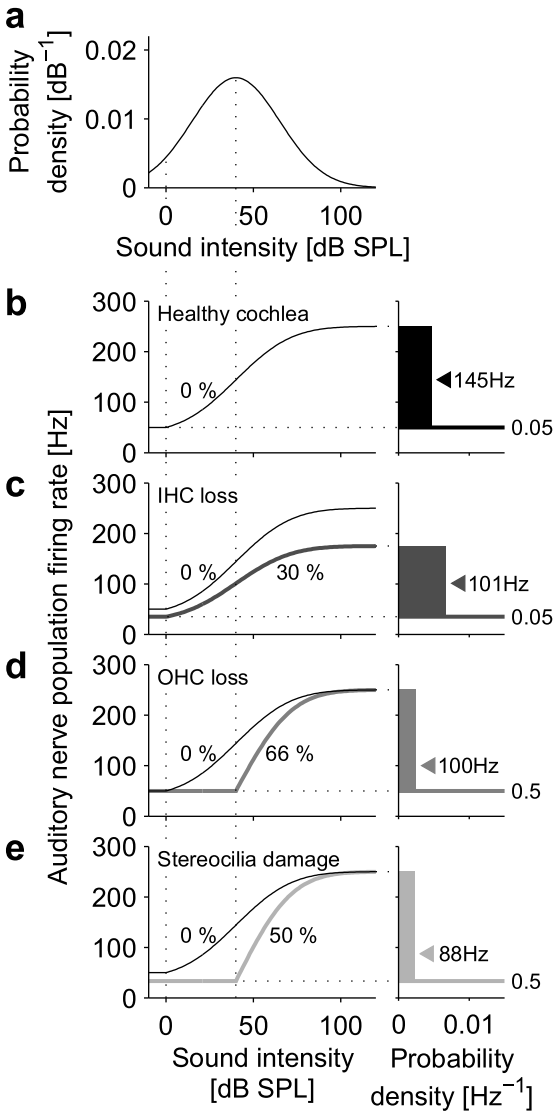

Figure 7.3: Firing statistics of the AN model. **(a)** The distribution of sound intensity levels in units of dB is assumed to be Gaussian (40 dB mean, 25 dB standard deviation). **(b-e)** *(Left panels)* Rate-intensity functions of the AN population firing rate (b: healthy cochlea, c: 30% IHC loss, d: 66% OHC loss, and e: 50% SD). *(Right panels)* Firing-rate probability distributions of AN responses corresponding to the rate-intensity functions on the left and for the distribution of sound intensities in (a). Probability densities are on the abscissa, firing rates on the ordinate. The numbers at the horizontal 'delta' peaks of the distributions, e.g. 0.05 and 0.5, indicate the probability of occurrence of spontaneous activity for subthreshold stimuli. Shaded areas depict the distributions of firing-rate responses to suprathreshold stimuli. Arrowheads denote mean firing rates. **(b)** Healthy cochlea (0% damage). Spontaneous activity is rare (probability 0.05). The range of firing rates is between 50 and 250 Hz. The mean activity is 145 Hz (arrowhead). **(c)** IHC loss (example: 30%, dark gray) reduces spontaneous, mean (101 Hz) and maximum firing rates, while the probability of occurrence of spontaneous activity remains at 0.05. **(d)** 66% OHC loss (medium gray) increases the AN response threshold by 40 dB without affecting the range of firing rates. Due to the threshold increase, the probability of occurrence of spontaneous activity is increased to 0.5, and the mean firing rate is decreased to 100 Hz. **(e)** 50% stereocilia damage (light gray) increases the AN response threshold by 40 dB and decreases the AN's spontaneous (33 Hz) and mean firing rate (88 Hz). The probability of occurrence of spontaneous activity is increased to 0.5.

7.3 Model for a Downstream Auditory Neuron

Let us now evaluate how the responses of a model neuron are changed through hearing loss. The model neuron could represent a downstream auditory neuron in the cochlear nucleus (CN) that receives excitatory input from the AN. We assume that the model neuron is innervated by AN fibers with similar characteristic frequencies that are described by the mean population firing rate. The neuron is modeled as a firing rate unit with a nonlinear response function R that includes a gain factor g, which determines the impact of AN input on the model neuron's firing rates. The firing rate r of a model neuron in response to AN input at rate f is then given by $r = R(f) = r_{\text{high}} \tanh(g \cdot f / r_{\text{high}})$, with r_{high} being the maximum firing rate of the model neuron (see also Fig. 7.4a,b and Methods, Eqs. 10–12).

7.3.1 Homeostatic Plasticity After Hearing Loss Can Lead to Hyperactivity

We propose that a CN neuron has some target mean firing rate r^* (when averaged over days) that is stabilized by homeostatic plasticity. In the model, this rate stabilization is implemented through an adjustment of the gain factor g. This adjustment is in accordance with homeostasis through synaptic scaling (Turrigiano et al., 1998; Kilman et al., 2002) and neuronal excitability changes (Desai et al., 1999b). Here, we do not model the dynamics of homeostatic plasticity, i.e. the time-course of g, but simply focus on the equilibrium state that is reached as a result of homeostasis. Let us now illustrate the consequences of homeostatic stabilization of the model neuron's mean firing rate for the three examples of cochlear damage that we have introduced in Fig. 7.3:

IHC loss (30% in Fig. 7.4c) was argued to decrease mean, spontaneous and maximum firing rate of the AN, which, initially, also decreases the firing rate in the model neuron (Fig. 7.4c, panel $g = 1$). In order to counteract this decrease, homeostatic plasticity increases the model neuron's gain factor from $g = 1$ to some value $g > 1$. This restores the neuron's mean firing rate to its reference value r^*. Moreover, the neuron's reconstituted response distribution (Fig. 7.4c, panel $g = 1.43$) matches the one for 0% IHC loss (Fig. 7.4b, panel $g = 1$). Thus, moderate loss of IHCs can be fully compensated by homeostasis in the framework of our model.

OHC loss (66% in Fig. 7.4d), on the other hand, was argued to increase the probability of occurrence of spontaneous activity in both the AN and the model neuron without changing the spontaneous firing rate. When homeostatic plasticity increases the gain factor g to counteract the decreased mean firing rate, the distribution of the model neuron's responses is drastically altered as compared to the healthy case: the maximum firing rate in the model neuron is elevated and, most importantly, also the spontaneous firing rate is increased (Fig. 7.4d, panel $g = 1.54$, see also Fig. 7.7.5).

SD (50% in Fig. 7.4e) was argued to increase the probability of occurrence of spontaneous activity and to decrease the spontaneous firing rate in both the AN and the model neuron. Similar to OHC loss, homeostatic plasticity may recover the mean rate in the model neuron, but then the spontaneous rate is elevated as well (Fig. 7.4e, panel $g = 1.89$).

Thus, homeostatic compensation of OHC loss, for example after administration of ototoxic drugs, or SD as induced by noise overexposure can lead to increased spontaneous firing rates or *hyperactivity* of auditory neurons downstream of the AN.

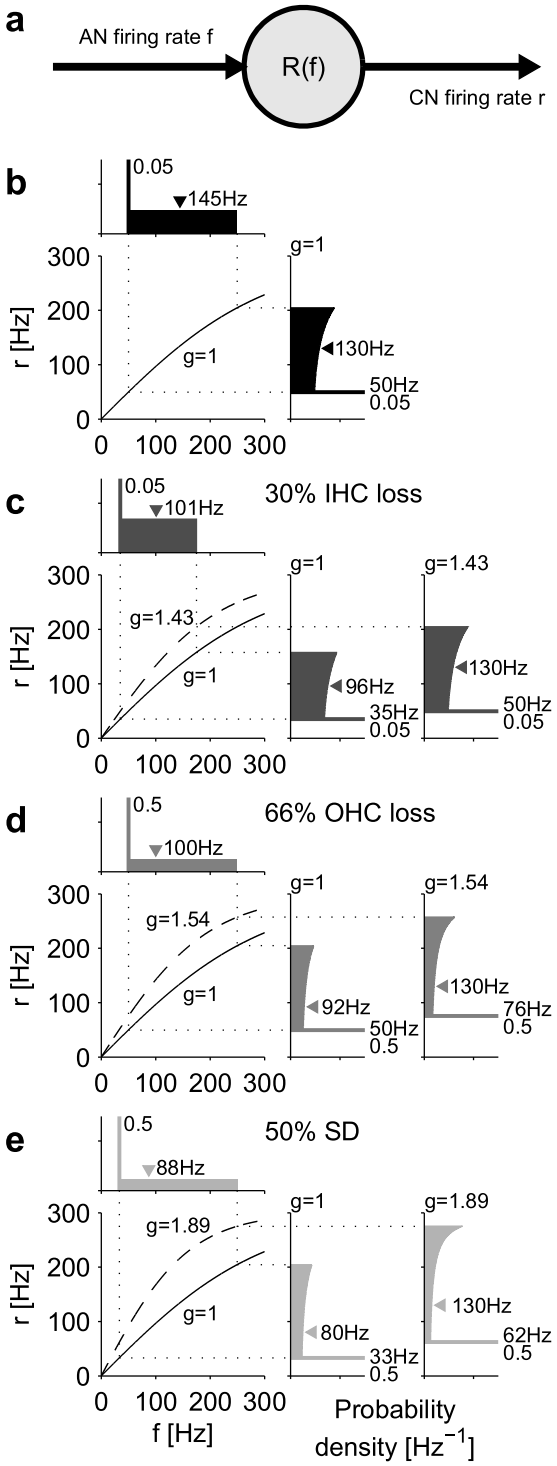

Figure 7.4: Model for a downstream auditory neuron in the cochlear nucleus (CN) and illustration of the result of homeostatic plasticity. **(a)** The model neuron receives excitatory input at rate f from a population of auditory nerve (AN) fibers. The model neuron's output firing rate $r = R(f) = r_{\text{high}} \tanh(g \cdot f / r_{\text{high}})$ is determined by the response function R with its adjustable gain factor g and constant maximum firing rate $r_{\text{high}} = 300\,\text{Hz}$. Homeostatic plasticity adjusts the mean of the output rate r by changing the gain factor g. **(b)** Healthy cochlea (no damage). The probability of AN fibers to fire at a given rate (*top*; identical to Fig. 3b) is mapped by the response function (*bottom left*) to the firing probability of the model neuron (*right panel*). The neuron's mean firing rate is 130 Hz (arrowhead), the spontaneous firing rate is 50 Hz, and the maximum firing rate is 205 Hz (horizontal dotted lines). The probability 0.05 of spontaneous firing in the model neuron is the same as in the AN. All probability distributions are at identical scales. **(c,d,e)** Same as in (b), but for different types of damage to the cochlea (gray), both before ($g = 1$) and after homeostasis ($g > 1$). **(c)** 30% IHC loss (dark gray) decreases the mean firing rate of the model neuron to 96 Hz and the spontaneous firing rate to 35 Hz (*panel* $g = 1$). Homeostatic plasticity increases the gain to $g = 1.43$ (dashed line in bottom left panel), which fully restores the neuron's response distribution; see (b). **(d)** 66% OHC loss (medium gray) increases the probability of occurrence of spontaneous activity to 0.5 without affecting the range of firing rates. The mean firing rate of the model neuron is decreased to 92 Hz (*panel* $g = 1$). Homeostasis increases the gain to $g = 1.54$ (dashed line in bottom left panel), but this substantially alters the neuron's response distribution (*panel* $g = 1.54$). Especially, the spontaneous firing rate is increased from 50 to 76 Hz. **(e)** 50% SD (light gray) decreases the mean firing rate in the model neuron to 80 Hz and the spontaneous firing rate to 33 Hz (*panel* $g = 1$). After homeostasis (*panel* $g = 1.89$), the spontaneous firing rate is increased to 62 Hz.

7.3.2 Saturation of Homeostasis Decreases Hyperactivity

In Figs. 7.2 & 7.3 we have indicated that severe cochlear damage leads to low AN activity. If this is to be compensated by homeostasis in the model neuron, large increases in response gain g would be needed. However, in a biological system, physiological constraints are likely to impose an upper limit on homeostatic scaling. We therefore explore the influence of an upper limit on the gain factor g, which is estimated to be $g_{max} = 3$ (based on results in Turrigiano et al., 1998). If this saturation limit is reached, homeostatic plasticity is not able to restore the mean firing rate of the model neuron.

Figure 7.5 summarizes the effect of homeostasis and its saturation on the model neuron's activity for all degrees (0 to 100%) of hair cell loss or stereocilia damage. For IHC loss (Fig. 7.5a), homeostasis saturates at 67% loss. Below this limit, the spontaneous firing rate is restored to its normal value after homeostasis. Degrees of damage beyond the saturation limit lead to spontaneous firing rates of the model neuron that are even lower than normal. On the other hand, if AN activity is decreased by OHC loss (Fig. 7.5b), the saturation limit of homeostasis is never reached, at least not for the set of parameter values we found feasible to describe OHC loss. The neuron's spontaneous firing rate after homeostasis is thus a monotonically increasing function of the degree of OHC loss. Finally, SD can lead to saturation of homeostasis in the model neuron (Fig. 7.5c). Below the saturation limit of 67% SD, the neuron's spontaneous firing rate increases with increasing SD. If SD is larger than the saturation limit, the spontaneous firing rate decreases again. The maximum, or kink, of the neuron's spontaneous rate occurs at the saturation limit of homeostasis.

7.3.3 Non-AN Input Boosts the Development of Hyperactivity

Homeostatic plasticity is a mechanism that can scale all synapses of a neuron (Turrigiano, 1999). Therefore, a homeostatic increase in response gain to compensate for decreased AN activity could also influence non-auditory inputs. The CN receives input from a variety of other brain regions in addition to feedforward input from the AN. The most diverse set of such additional inputs is found in the dorsal cochlear nucleus (DCN). There are projections from the contralateral CN (Cant and Gaston, 1982; Shore et al., 1992), top-down connections from the cortex (Weedman and Ryugo, 1996; Jacomme et al., 2003), and inputs from the somatosensory system (Kanold and Young, 2001; Zhou and Shore, 2004).

To evaluate the consequences of non-auditory input to the model neuron, we simply consider a constant excitatory input f_{add} in addition to the variable input f from the AN (Fig. 7.6a). Both inputs are scaled by the gain factor g, so that the model neuron's rate reads $r = R(f + f_{\text{add}}) = r_{\text{high}} \tanh([g \cdot (f + f_{\text{add}}) - \theta]/r_{\text{high}})$, where we have introduced a response threshold θ. We set this threshold to $\theta = f_{\text{add}}$ so that the previous scenario without additional input in Figures 7.4–7.5 can be directly compared to the scenario with additional input in Fig. 7.6. For the healthy case with $g = 1$, both scenarios are identical (Fig. 7.6b). For homeostatic scaling that leads to $g > 1$, however, additional excitatory input to the model neuron gives rise to marked differences that depend on the type of cochlear damage.

We found that IHC loss can also lead to hyperactivity if there is additional excitatory input to the model neuron (Fig. 7.6c). The higher the firing rate of the additional input the more hyperactivity. Moreover, the saturation point of homeostasis is shifted towards greater damage. The situation is different for OHC loss: the results obtained with additional input are very

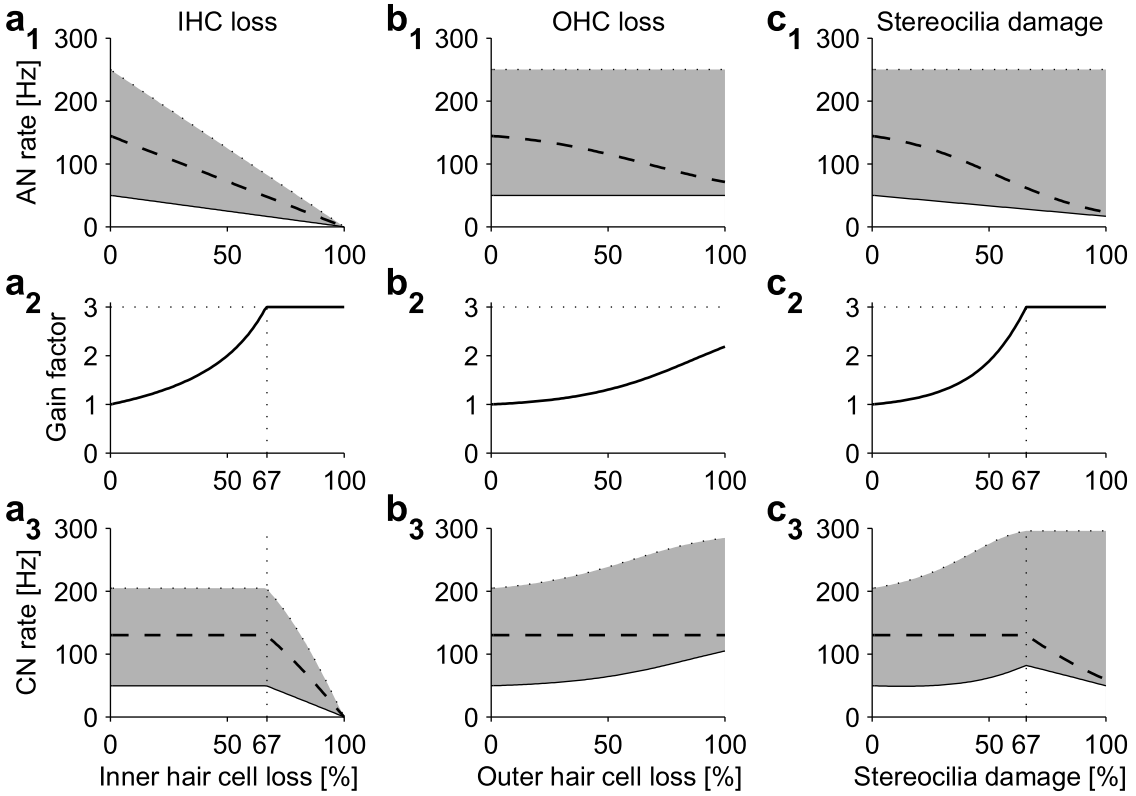

Figure 7.5: AN activity, gain factor, and CN activity after homeostasis in dependence upon the degree of IHC loss, OHC loss, and stereocilia damage (SD). **($\mathbf{a}_1$-$\mathbf{a}_3$)** IHC loss. **($\mathbf{a}_1$)** AN firing rates. Spontaneous (solid line), mean (dashed line), and maximum (dotted line) firing rate are reduced in proportion to the amount of IHC loss. The shaded area illustrates the range of firing rates. **($\mathbf{a}_2$)** Gain factor after homeostasis. Homeostatic scaling saturates because we have imposed an upper bound on the gain factor (here: $g_{\max} = 3$). **($\mathbf{a}_3$)** CN model neuron firing rates after homeostasis. The mean firing rate (dashed line) is restored to its healthy value for up to 67% IHC loss. Beyond this limit, when homeostasis is saturated, the neuron's rates decrease with increasing loss of IHCs. **($\mathbf{b}_1$-$\mathbf{b}_3$)** OHC loss. **($\mathbf{b}_1$)** The mean activity of the AN decreases with increasing OHC loss, but the range of firing rates, from spontaneous to maximum rate, remains constant. **($\mathbf{b}_2$)** The gain factor after homeostasis increases with increasing OHC loss. **($\mathbf{b}_3$)** The model neuron's mean rate is restored to its target value for all degrees of OHC loss, but the spontaneous firing rate is increased. **($\mathbf{c}_1$-$\mathbf{c}_3$)** Stereocilia damage (SD). **($\mathbf{c}_1$)** Mean and spontaneous AN firing rates are decreased by SD. **($\mathbf{c}_2$)** The gain factor saturates for more than 67% SD. **($\mathbf{c}_3$)** The mean firing rate in the model neuron is restored to its target value for up to 67% SD, and the spontaneous activity is increased. For larger amounts of SD, the mean and spontaneous rate decline; the maximum rate stays constant.

similar to those obtained without (Fig. 7.6d). For SD, the model with additional input exhibits higher spontaneous firing rates after homeostasis than the model without. Also, the saturation point of homeostasis is shifted towards greater damage (Fig. 7.6e).

In conclusion, when the activity of the AN, which provides excitatory input to the CN, is reduced because of cochlear damage, homeostatic plasticity increases the effective response gain that affects all inputs. Therefore, additional non-auditory inputs are also amplified and then contribute to hyperactivity. This mechanism suggests how, for example, somatosensory input could be involved in the generation of tinnitus.

7.4 Model Results for Cochlear Pathologies Associated with Tinnitus

In humans, acoustic trauma and cisplatin treatment (used in cancer therapy) are often associated with tinnitus. Animal studies demonstrate that both acoustic trauma and cisplatin administration damage cochlear hair cells and lead to hyperactivity of DCN neurons (Kaltenbach et al., 1998, 2000; Brozoski et al., 2002; Kaltenbach et al., 2002, 2004). We are now going to present results of our model for the corresponding characteristic patterns of cochlear damage, where combinations of OHC and IHC loss, or SD and IHC loss, concurrently influence the AN population response (see Methods, Eqs. 8 and 9). We therefore consider a tonotopic array of CN neurons receiving input from the corresponding tonotopic loci of the cochlea via the AN (Fig. 7.7a).

Systemic cisplatin administration can cause severe OHC loss in the basal segment of the cochlea that responds to high frequencies, whereas IHCs are typically only affected to a limited degree (Kaltenbach et al., 2002; van Ruijven et al., 2004). Additionally, cisplatin can lead to a demyelination of AN fibers innervating the basal turn of the cochlea (van Ruijven et al., 2004, 2005). Therefore, in our framework we approximate the effects of cisplatin-induced combined damage to IHCs and AN fibers by moderate IHC loss. As for the spatial pattern of cochlear damage, we consider severe OHC loss and moderate IHC loss in the basal parts of the cochlea (Fig. 7.7b). In the model, homeostasis then leads to hyperactivity in those neurons that receive input from the damaged parts of the cochlea (Fig. 7c). Moderate IHC loss (i.e. cisplatin-induced damage to inner hair cells) in addition to severe OHC loss lowers the spontaneous firing rates, but only in the model without additional input. Similar observations have been made in the DCN of animals after cisplatin administration, where strong increases in spontaneous activity were observed for pure OHC loss, and smaller increases when additional IHC damage occurred (Kaltenbach et al., 2002).

Noise overexposure or other forms of acoustic trauma induce severe damage to the stereocilia of inner and outer hair cells that extends over large parts of the cochlea up to the basal end. Acoustic trauma also causes OHC and IHC loss. The spatial extent of OHC loss is generally similar to that of SD, whereas IHC loss is typically less severe and restricted to smaller parts of the cochlea (Meleca et al., 1997; Chen and Fechter, 2003). In our model, we therefore evaluate a pattern of cochlear damage with severe SD (note that our description of SD also includes the effects of OHC loss), and moderate IHC loss (see Fig. 7.7d). The observed pattern of hyperactivity after homeostatic plasticity heavily depends on the amount of non-auditory additional input to the model neurons. Without additional input, the spontaneous firing rate is only elevated at a single peak that is associated with the edge of the stereocilia lesion (Fig. 7.7e,

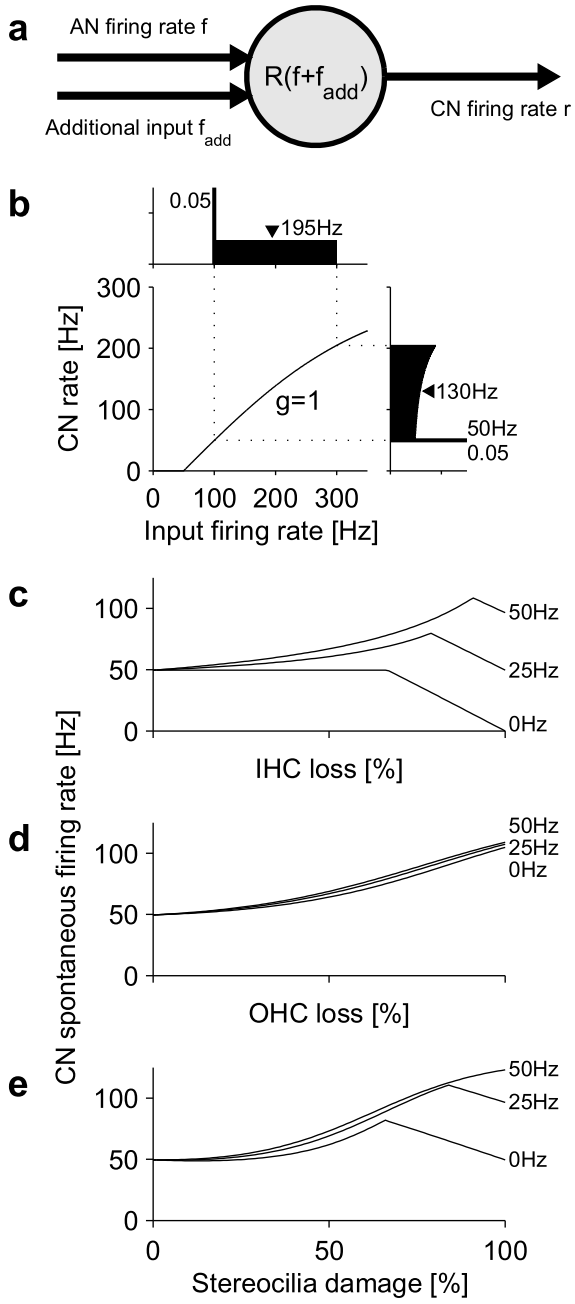

Figure 7.6: Effects of additional input on hyperactivity. **(a)** The model neuron receives excitatory input from a population of auditory nerve (AN) fibers at variable rate f and from additional, non-auditory input fibers at constant rate f_{add}. The model neuron's output firing rate is $r = R(f + f_{\mathrm{add}}) = r_{\mathrm{high}} \tanh\left([g \cdot (f + f_{\mathrm{add}}) - \theta]/r_{\mathrm{high}}\right)$, with $\theta = f_{\mathrm{add}}$ being the response threshold. **(b)** Healthy cochlea, $g = 1$. (*Top*) Distribution of the input $f + f_{\mathrm{add}}$, with $f_{\mathrm{add}} = 50\,\mathrm{Hz}$. (*Bottom left*) Response function R and (*bottom right*) response distribution of the DCN neuron for $g = 1$ (identical to the one without additional input in Fig. 4b). **(c)** Spontaneous firing rate of the model neuron after IHC loss and homeostasis for different values of f_{add} (0, 25, and 50 Hz). With additional input, hyperactivity also occurs after IHC loss, and the saturation point of homeostasis (kink in the curve) is shifted towards greater IHC loss. **(d)** For OHC loss, hyperactivity only weakly depends on f_{add}. **(e)** For SD, the maximum increase in spontaneous firing rate depends on the value of f_{add}, and the saturation point of homeostasis is shifted towards greater damage.

upper panel, $f_{\text{add}} = 0$ Hz). The peak structure is caused by the saturation of homeostasis (compare Fig. 7.7c). At frequencies where IHCs are lost in addition to severe SD, spontaneous firing rates can be even lower than before. With increasing additional input (25 and 50 Hz in Fig. 7e, upper panel), the peak in the spontaneous firing rate profile is shifted towards higher frequencies because homeostasis saturates at greater damage. Moreover, the peak becomes broader for 25 Hz additional input to finally extend over large parts of the tonotopic array for 50 Hz, at which the spontaneous firing rate is strongly elevated for all neurons that receive input from the damaged regions of the cochlea. The latter hyperactivity profile for 50 Hz additional input is similar to those observed experimentally in the DCN after severe unilateral acoustic trauma (Kaltenbach et al., 1998, 2000, 2004).

Hyperactivity caused by unilateral acoustic trauma was shown to persist even after cochlear ablation (Zacharek et al., 2002). Spontaneous firing rates were decreased by the ablation, but remained increased compared to the healthy case. To capture this experiment in the model, we first let homeostasis increase the model neuron's gain to compensate for the effects of acoustic trauma. Then we remove all AN activity, leaving only the additional input (50 Hz in our example). As homeostasis is a slow process, the gain remains adjusted to acoustic trauma for at least several hours after the ablation. The additional input is thus amplified, leading to spontaneous firing rates in the model that are reduced compared to the situation before the ablation (Fig. 7.7e, lower panel, 'ablated'), but still elevated, and the distribution of spontaneous rates reflects the pattern of cochlear damage. After longer waiting times on the order of days, homeostatic plasticity adapts the neuron's gain to the only remaining input f_{add}. In the model, f_{add} is constant across frequencies, leading to a flat profile of elevated spontaneous firing rates (dotted line in Fig. 7.7e, lower panel) when homeostasis is saturated at its upper bound. In experiments, the equilibrium distribution of spontaneous firing rates after AN section will depend on the distribution and activity of additional inputs across frequency channels in the auditory system.

7.5 Reversing Hyperactivity through Additional Acoustic Stimulation

Having established how hyperactivity and possibly tinnitus could develop through homeostatic plasticity after hearing loss, we are now able to evaluate how the pathologic changes could be reversed through additional sensory stimulation. It is obvious that hyperactivity could be reversed in our model by restoring the regular distribution of AN firing rates, which corresponds to a perfect "hearing aid". A simpler and feasible way, however, would be permanent additional stimulation through specially adjusted noise devices. Let us now discuss the effects of different stimulation strategies on hyperactivity in our model. We evaluate a white-noise stimulus, as often used in tinnitus therapy (Hazell, 1999), and a specially designed matched-noise stimulus for an example of noise-induced hearing loss with severe stereocilia damage that strongly elevates hearing thresholds in the high-frequency range (Fig. 7.8a, upper panel). We employ the model variant without additional input, as it exhibits a distinct peak in the spontaneous firing-rate profile after homeostatic plasticity, which could be interpreted as the basis for a tone-like tinnitus sensation (Fig. 7.8a, lower panel). The peak is caused by the saturation of homeostasis, see also Figs. 7.6e and 7.7e.

We first explore white-noise stimulation at 40 dB (Fig. 7.8b). Above ca. 3 kHz it is below

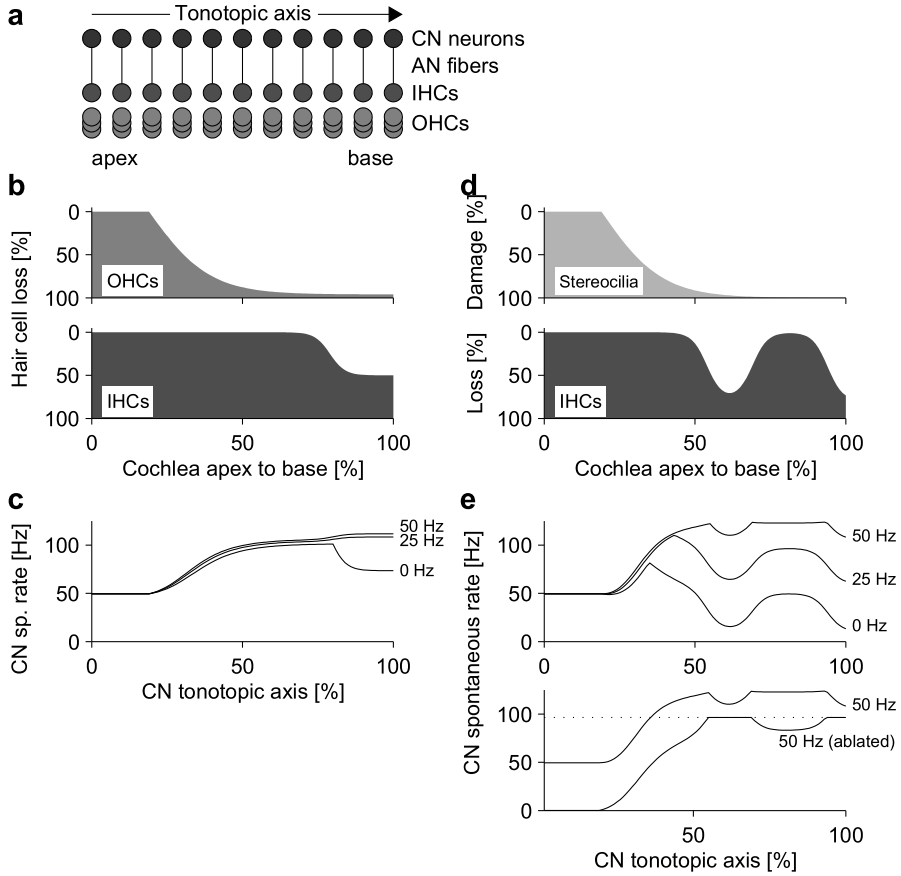

Figure 7.7: Two examples of model results for cochlear pathologies that can lead to tinnitus in humans. **(a)** Illustration of the tonotopic connection between cochlea and CN. **(b)** Cochleograms indicate damage induced by systemic cisplatin administration. OHC loss extends over large parts of the cochlea (*top panel*). Additional damage to IHCs and AN fibers is approximated in our model by moderate IHC loss (*bottom panel*). **(c)** Spontaneous activity of CN model neurons after homeostasis as a function of a neuron's location along the tonotopic axis for three different rates (0, 25, and 50 Hz) of the additional input. Hyperactivity is observed in those model neurons that receive input from regions of the cochlea where OHCs are lost. Without additional input, extra IHC loss leads to lower spontaneous firing rates than the same amount of OHC loss alone. **(d)** Cochlear damage through noise-induced hearing loss. Stereocilia are severely damaged over large parts of the cochlea (*top panel*). IHC loss is less pronounced (*bottom panel*). **(e)** CN spontaneous rate after homeostasis. (*Top panel*) The amount and extent of hyperactivity heavily depends on the strength of the additional input, ranging from a single peak associated with the edge of the cochlear lesion for $f_{\text{add}} = 0\,\text{Hz}$ to strongly elevated spontaneous firing rates over large parts of the tonotopic axis for $f_{\text{add}} = 50\,\text{Hz}$. Peak-like structures are caused by the saturation of homeostasis. (*Bottom panel*) For strong additional input (here: 50 Hz), hyperactivity can persist after cochlear ablation. Immediately after the ablation, the profile still reflects cochlear damage (lower solid line), but later turns into a flat profile for the chronic case (dotted line).

the hearing threshold. The mean AN firing rate is increased by the additional stimulation only in the low-frequency range (not shown), where homeostatic plasticity then decreases the gain in the model neurons to compensate for the increased AN input (Fig. 8b, middle panel). Neurons in the high-frequency range are not affected, and the hyperactivity peak is unchanged. During stimulation, the white-noise stimulus evokes firing rates in the model neurons that are higher than those at the hyperactivity peak, possibly masking the tone-like tinnitus (Fig. 7.8b, lower panel, dashed line). Immediately after the white-noise stimulus is turned off, however, the hyperactivity peak is even more pronounced (Fig. 7.8b, lower panel, thick gray line) than before the additional stimulation (see Fig. 7.8a), as the homeostatic adaptation has lowered the gain in the low-frequency range and thus has decreased the spontaneous firing rates there. An unspecific white-noise stimulus therefore masks a hyperactivity peak in the the model, but even exaggerates it after the stimulus is turned off.

In a second scenario, we derive a matched-noise stimulus (see Methods) that reverses hyperactivity and leads to a flat profile of the spontaneous firing rate across the tonotopic axis of the model neurons after homeostasis, as in the healthy situation (Fig. 7.8c, upper panel). This stimulus is 1.5-4 dB above the hearing threshold only in the high-frequency range, where hearing is impaired, and therefore increases the mean firing rate of AN fibers in this frequency range. As a consequence, homeostatic plasticity is triggered in those model neurons receiving input from the additionally stimulated AN fibers, where it lowers the pathologically increased gain factors. After homeostasis, the matched-noise stimulus evokes low to medium firing rates in the model (Fig. 7.8c, lower panel, dashed line), thus homeostasis does not suppress the response to the stimulus. Once stimulation is turned off, the spontaneous firing rate profile across the tonotopic axis is flat (Fig. 7.8c, lower panel, thick gray line). Hyperactivity would only slowly reemerge after prolonged periods without stimulation, and the time-course of reemergence is governed by the time-scale of days of homeostatic plasticity. It may therefore be possible to find a stimulation paradigm where intervals with and without stimulation are interleaved, which provides an efficient suppression of hyperactivity without the necessity of constant stimulation.

The observation that in our model additional acoustic stimulation can reverse hyperactivity is matched by the findings that hearing aids (Surr et al., 1999), noise devices (Schneider et al., 1999), and cochlear implants (Ito and Sakakihara, 1994; Quaranta et al., 2004) can reduce perceived tinnitus severity. Our matched-noise stimulus, however, is different from common masking approaches with unspecific broad-band stimuli as it is designed not solely to mask tinnitus, but to decrease elevated spontaneous activity that constitutes the basis for the tinnitus sensation.

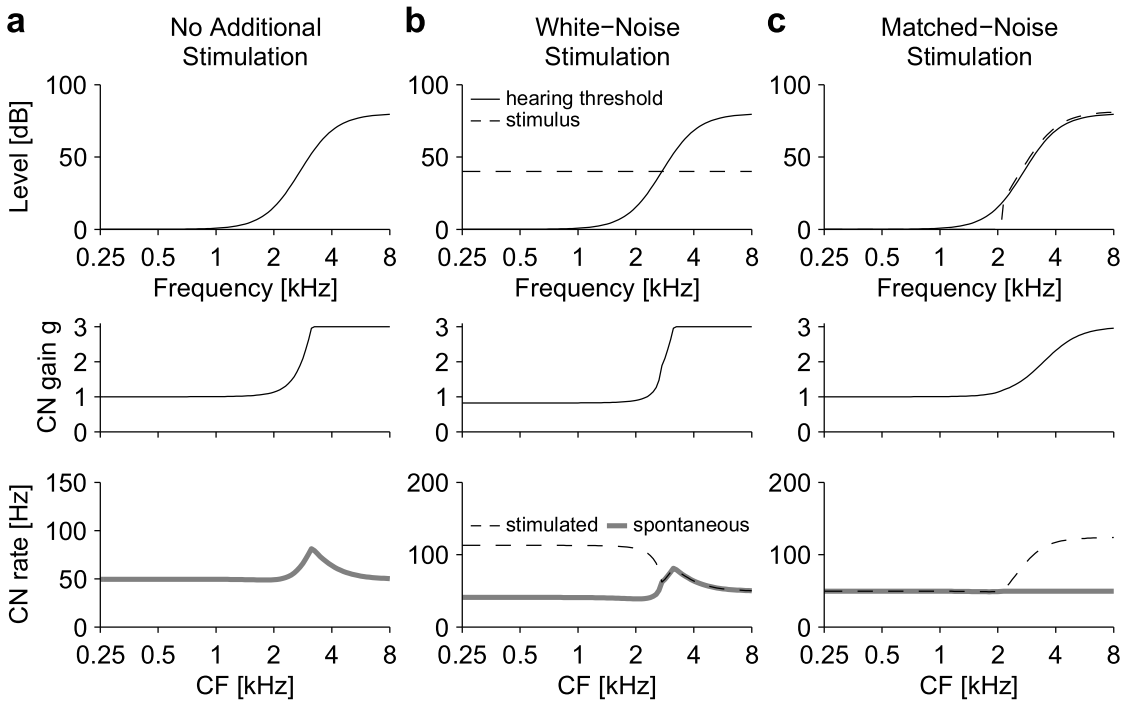

Figure 7.8: Effects of sound stimulation on hyperactivity of CN model neurons. Each of the three top panels shows the hearing threshold curve for a case of severe noise-induced high-frequency hearing loss (solid lines) modeled through SD. We also depict levels of different acoustic stimuli (dashed lines). Let us consider the case when homeostatic plasticity has adapted the CN neurons to AN input evoked by a mixture of an additional sound stimulus (if applied) and ambient sounds. The resulting gain factors of CN model neurons in dependence upon the neurons' characteristic frequency (CF) are shown in the middle panels. The bottom panels show the corresponding spontaneous (thick gray lines) and stimulation-evoked (dashed lines) firing rates of the model neurons. **(a)** No additional stimulation. After homeostasis, there is a peak in the spontaneous firing rate profile of the CN where the gain g is saturated, reminiscent of a tone-like tinnitus. **(b)** 40 dB white-noise stimulation as often used for tinnitus masking. The stimulus is below the hearing threshold above ca. 3 kHz. During stimulation, evoked firing rates in the low-CF neurons are higher than those at the 'tinnitus frequency', possibly masking the percept. Immediately after switching off the white-noise stimulation, the hyperactivity peak in the firing rate profile is even more pronounced than without stimulation, see (a). **(c)** Matched-noise stimulation. The stimulus is slightly above (1.5-4 dB) the hearing threshold in the severely impaired high-frequency range. After homeostasis, the stimulus evokes moderate firing rates in the high-CF neurons. Immediately after switching off the matched-noise stimulation, the profile of spontaneous firing rates across the tonotopic axis is flat, the hyperactivity peak is gone.

7.6 Discussion

We have presented a phenomenological model of the early auditory pathway to assess the question of how sensorineural hearing loss could lead to pathologically increased spontaneous firing rates (hyperactivity) in the auditory brainstem, which may be perceived as tinnitus. Our model is based on a simplified description of the firing-rate response of auditory nerve (AN) fibers to acoustic stimuli, the effects of hearing loss through damage to cochlear hair cells, the responses of downstream auditory neurons in the cochlear nucleus (CN) to input from the AN and other sources, and the effect of a homeostatic plasticity mechanism that stabilizes the mean firing rate of CN neurons at a constant level.

In the healthy auditory system, homeostatic plasticity could help to ensure that auditory neurons are active within the right range of firing rates independent of the prevailing acoustic environment. Homeostatic plasticity in auditory neurons might also prevent us from perceiving spontaneous neuronal activity as sound. For pathologically altered processing in the cochlea, however, this plasticity mechanism could also have detrimental effects. We propose that homeostatic plasticity can lead to hyperactivity in cochlear nucleus neurons when the ratio between the mean and the spontaneous firing rate in the AN is decreased. Since sensorineural hearing loss always lowers the mean firing rate in the AN, the relative change of the spontaneous rate is crucial. We found that in a generic model of inner hair cell (IHC) loss that preserves the ratio of mean and spontaneous activity in the AN, restoring of the activity statistics of second-order neurons is possible. Because both outer hair cell (OHC) loss and stereocilia damage (SD) decrease the ratio between the mean and the spontaneous firing rate of the AN, homeostatic scaling leads to elevated spontaneous firing rates in CN neurons. Constant additional (non-auditory) input to a CN neuron can boost the development of hyperactivity because this input is also amplified after hearing loss, as homeostasis is a global mechanism affecting all synapses that provide input to the neuron.

The model is in agreement with several animal studies demonstrating that acoustic trauma can lead to increased spontaneous firing rates in the dorsal cochlear nucleus (DCN) (Brozoski et al., 2002; Kaltenbach et al., 2004) and to behavioral signs of tinnitus (Brozoski et al., 2002; Heffner and Harrington, 2002; Kaltenbach et al., 2004). Interestingly, the strength of the behavioral evidence for tinnitus is correlated to the amount of hyperactivity in the DCN (Kaltenbach et al., 2004). The DCN, however, need not be the sole generator of tinnitus-related activity in the auditory system, as DCN ablation does not seem to abolish behavioral signs of tinnitus (Brozoski and Bauer, 2005). If the proposed mechanism of activity stabilization is relevant for various types of neurons along a sensory pathway, hyperactivity could arise at any stage that is confronted with decreased excitatory input. Ablation of the DCN, for example, removes excitatory input to subsequent stages such as the inferior colliculus. It is thus conceivable that homeostasis triggers hyperactivity there.

In our model, homeostatic plasticity restores the mean firing rate of a second-order auditory neuron after hearing loss. The fraction of time the neuron spends firing at its spontaneous rate, however, cannot be decreased by homeostasis or other plasticity mechanisms, because this fraction is fixed by the response threshold of AN fibers. This fact applies to all neurons along the auditory pathway. Therefore, even if homeostatic plasticity simultaneously occurs at several stages of the auditory system, pathological neuronal activity generated at one processing stage cannot be reverted to healthy activity distributions by homeostasis in subsequent stages. As spontaneous firing after hearing loss typically has a higher probability than before, its con-

tribution to the mean activity is increased at all stages. Restoring the mean rate is therefore to be expected to increase the spontaneous rate throughout the auditory system.

Following sensory deprivation, indications of a homeostatic mechanism have indeed been seen at various stages of the auditory pathway. In the inferior colliculus of gerbils, for example, bilateral deafening leads to increased EPSC amplitudes and increased IPSC equilibrium potentials (Vale and Sanes, 2002), suggesting that the balance between excitation and inhibition is shifted in a homeostatic fashion. Moreover, in the cochlear nucleus of chinchillas, acoustic trauma temporarily increased glutamatergic synaptic transmission (Muly et al., 2004). Increased EPSC amplitudes were also observed in the anteroventral cochlear nucleus of congenitally deaf mice in response to electrical stimulation of the AN (Oleskevich and Walmsley, 2002). Furthermore, glycinergic inhibition in the DCN was persistently weakened following unilateral cochlear ablation (Suneja et al., 1998a,b) or age-related hearing loss (Caspary et al., 2005). Finally, in the auditory cortex of gerbils, increased excitability as well as increased excitatory and decreased inhibitory synaptic transmission were measured after bilateral cochlear ablation (Kotak et al., 2005). Homeostatic plasticity may thus be involved in activity-dependent regulatory processes throughout the auditory system. In addition to homeostasis, there may also be mechanisms that regulate activity of auditory neurons on faster time scales of seconds to minutes. The firing properties of neuronal populations in the inferior colliculus, for example, have been shown to adapt to the statistics of auditory stimuli on a time-scale of several seconds (Dean et al., 2005).

Further evidence for homeostasis-like mechanisms in the auditory pathway comes from the observed time scale of changes after sensory deprivation. Hyperactivity in the DCN develops within days after hearing loss. Although cochlear damage and thus the auditory threshold shift is already present two days after acoustic trauma, no increase in DCN spontaneous firing rates is observed at that time (Kaltenbach et al., 1998). Five days after acoustic trauma, however, hyperactivity is fully developed (Kaltenbach et al., 2000). This indicates that homeostatic plasticity could be involved, as changes through homeostasis also occur on a time-scale of days (Turrigiano et al., 1998). Reminiscent of homeostatic plasticity, Formby et al. (2003) found a gain control mechanism that regulates loudness perception depending on the overall amount of sensory input to the human auditory system. The gain control operated, again, on a time-scale of days.

Homeostatic regulation of neuronal activity levels might be a general principle in sensory pathways. In the visual system of rats (postnatal day 15), hyperactivity of cortical neurons has been observed after two days of visual deprivation (Maffei et al., 2004): Excitatory synaptic connections were strengthened, inhibitory synapses were weakened, and the spontaneous firing rates of specific cortical neurons were increased; restoring vision reversed the changes. In the somatosensory system, our findings might also be applicable to the phenomenon of phantom limb sensations that can arise after amputations. Another modeling study indicates that homeostatic plasticity after deafferentiation could be involved in post-traumatic epileptogenesis (Houweling et al., 2005).

To demonstrate that homeostatic plasticity after hearing loss can lead to increased spontaneous firing rates in second-order neurons, we deliberately chose a phenomenological modeling approach that is based on several simplifying assumptions. In our model of the AN population rate, for example, the shape of the rate-intensity function is coupled to the shape of the intensity distribution by the infomax tuning assumption. This results in a steepening of rate-intensity functions for elevated thresholds, which matches observations for isolated OHC loss (Harrison,

1981). SD also elevates thresholds, but single AN fibers can display rate-intensity functions that are even shallower than normal (Heinz and Young, 2004). Shallower rate-intensity functions, however, would lead to a greater reduction of the mean AN rate. In our model, more homeostatic compensation would then be needed in second-order neurons, resulting in more hyperactivity. Thus, for the development of hyperactivity, steepening of the rate-intensity functions is the more conservative assumption. Another simplifying assumption in our model is that we consider only excitatory input, whereas neurons in the cochlear nucleus are part of an elaborate circuitry containing a variety of inhibitory interneurons (Rhode and Greenberg, 1992; Young and Davis, 2002). This is most evident, for example, in the responses of type IV neurons of the DCN, which are characterized by inhibitory sidebands and strongly non-monotonic rate-intensity functions (Spirou and Young, 1991; Young and Davis, 2002). For such strong inhibition, the mean rate of these neurons could be close to the spontaneous rate, thus limiting the development of hyperactivity. In the following chapter, we will therefore set up a model of the basic DCN circuit to analyze the effect of inhibition on the mean rate of DCN projection neurons and on the development of hyperactivity after hearing loss.

The presented model is as simple as possible to exhibit the consequences of homeostatic plasticity in the auditory system. The model therefore has no free parameters, that is parameters do not need to be fitted. Several extensions of the model are possible in order to test whether its features are robust with respect to more biophysical details: A more detailed model of the basilar membrane, hair cells and the auditory nerve could be used (Zhang et al., 2001; Sumner et al., 2003). The second-order neuron could be described through a conduction-based unit (Kanold and Manis, 2001), and inserted into a neuronal network with inhibition (Reed and Blum, 1995; Blum et al., 1995; Franosch et al., 2003; Zheng and Voigt, 2006a). Finally, feedback through the efferent auditory system could be considered, and other damage and plasticity mechanism could be incorporated, like excitotoxicity and subsequent sprouting of new synapses, or long-term potentiation and depression at individual synapses. Also the time-course of homeostatic plasticity could be investigated. Most of these extensions are, however, beyond the scope of this study, as they would lead to a large amount of additional parameters that would add many degrees of freedom to the model, which need to be reasonably constrained to reach viable predictions. That is why we chose to utilize a minimal model that emphasizes the most important features of this complex system.

Even though our model is extremely simple, the relation between the pattern of cochlear damage and the resulting profile of hyperactivity in a tonotopic array of model neurons matches observations in the DCN of animals (see e.g. Kaltenbach et al., 2002). We note that for stereocilia damage resembling noise-induced hearing loss, the model generates activity peaks in neurons with best frequencies above the edge of the cochlear lesion. These peaks could be interpreted as a basis for tinnitus sensations with tonal characteristics and a pitch at a frequency where cochlear damage/hearing loss exceeds a certain degree. A similar association between tinnitus pitch (Henry et al., 1999) or tinnitus spectrum (Noreña et al., 2002) and the extent of hearing loss has been observed in humans. In Chapter 9 we will evaluate whether predictions of tinnitus pitch based on spontaneous activity patterns in an extended version of our model are consistent with patient data.

The proposed model for the development of hyperactivity complements the so-called 'Neurophysiological Model', which assumes that a tinnitus percept is generated by abnormal neuronal activity in the auditory periphery that is amplified through attentional and emotional processes (Jastreboff, 1999). From the 'Neurophysiological Model', the Tinnitus Retraining

Therapy has been derived (Jastreboff and Jastreboff, 1999), which uses a combination of psychological counseling with masking devices and hearing aids. Our model explains why hearing loss can induce increased spontaneous firing rates in the early auditory pathway that may constitute the basis of a tinnitus sensation, and it also provides a biologically plausible and consistent framework for understanding how tinnitus-related hyperactivity might be reduced through appropriate external stimulation. We hope that this understanding will lead to improved strategies for a treatment of tinnitus.

7.7 Methods

7.7.1 Distribution of Sound Intensities

We assume that the probability density function $p_\mathrm{I}(I)$ of the sound intensity levels I (in units of dB) of a mixture of acoustic stimuli, like speech or other communication signals, environmental sounds, and background noise, is Gaussian, on average over hours to days:

$$p_\mathrm{I}(I) = \frac{1}{\sqrt{2\pi\sigma_\mathrm{I}^2}} \exp\left(-\frac{(I-\mu_\mathrm{I})^2}{2\sigma_\mathrm{I}^2}\right). \tag{7.1}$$

We set the mean value μ_I of the intensity distribution to 40 dB. Standard deviations of 15 dB were reported for speech, 13 dB for vocalizations and 9 dB for environmental sounds (Escabi et al., 2003). To capture the resulting, broader, intensity distribution of a mixture of these classes of sound events that may have different mean values, we choose the standard deviation σ_I of the intensity distribution to be 25 dB (Fig. 7.3a). Moreover, for simplicity we assume the same intensity distribution for all frequencies. This Gaussian distribution of sound intensity levels in dB corresponds to a long-tailed distribution of the linear amplitudes of the sound stimuli (see e.g. Escabi et al., 2003). The exact shape of the distribution, however, is not critical. All unimodal distributions where the majority of sound intensity levels is within the dynamic range of AN fibers yield similar results.

7.7.2 Auditory Nerve Responses

The population firing rate $f(I)$ of the AN at a sound intensity I is the average over a small population of AN fibers with different thresholds and spontaneous rates, but tuned to similar frequencies. In other words, we average over AN fibers with high spontaneous rates and low thresholds as well as AN fibers with low spontaneous rates and high thresholds. Such a population firing rate approximates the input of a downstream neuron that has synapses with a large number of AN fibers. We assume the same response function $f(I)$ for all frequencies. For simplification of the arguments, we choose $f(I)$ to be adapted to $p_I(I)$ so that $f(I)$ has maximum information on I, if I is larger than some threshold I_th. For $I > I_\mathrm{th}$, $f(I)$ then is proportional to the normalized cumulative distribution function $\int_{I_\mathrm{th}}^{I} \mathrm{d}I'\, p_\mathrm{I}(I')$ of $p_\mathrm{I}(I)$ (infomax principle, compare Laughlin, 1981). For high I, $f(I)$ saturates at rate f_max. For $I < I_\mathrm{th}$ there is spontaneous activity $f(I < I_\mathrm{th}) = f_\mathrm{sp}$, which occurs with probability $P_\mathrm{sp} = \int_{-\infty}^{I_\mathrm{th}} \mathrm{d}I\, p_\mathrm{I}(I)$ (see also Fig. 7.2). To

summarize, we have

$$f(I) = \begin{cases} f_{\mathrm{sp}} & \text{for} \quad I < I_{\mathrm{th}}, \\ f_{\mathrm{sp}} + (f_{\mathrm{max}} - f_{\mathrm{sp}}) \dfrac{\int_{I_{\mathrm{th}}}^{I} \mathrm{d}I' \; p_{\mathrm{I}}(I')}{1 - P_{\mathrm{sp}}} & \text{for} \quad I \geq I_{\mathrm{th}}. \end{cases} \tag{7.2}$$

Due to our infomax assumption, the distribution $p_{\mathrm{f}}(f)$ of AN firing rates is flat for $f_{\mathrm{sp}} < f \leq f_{\mathrm{max}}$ and has a delta peak at frequency $f = f_{\mathrm{sp}}$ (see Fig. 7.3b),

$$p_{\mathrm{f}}(f) = P_{\mathrm{sp}} \; \delta(f - f_{\mathrm{sp}}) + \begin{cases} p_{\mathrm{d}} & \text{for} \quad f_{\mathrm{sp}} < f \leq f_{\mathrm{max}}, \\ 0 & \text{otherwise} \end{cases} \tag{7.3}$$

where $p_{\mathrm{d}} = \dfrac{1 - P_{\mathrm{sp}}}{f_{\mathrm{max}} - f_{\mathrm{sp}}}$ is the probability density of driven activity. The mean AN firing rate is $\langle f \rangle := \int \mathrm{d}f' \; f' \cdot p_{\,\mathrm{f}}(f')$. Using equation (7.3) we have

$$\begin{aligned} \langle f \rangle &= P_{\mathrm{sp}} f_{\mathrm{sp}} + \int_{f_{\mathrm{sp}}}^{f_{\mathrm{max}}} \mathrm{d}f \; f \cdot p_{\mathrm{d}} \\ &= P_{\mathrm{sp}} f_{\mathrm{sp}} + \frac{1}{2}(1 - P_{\mathrm{sp}}) \left(f_{\mathrm{max}} + f_{\mathrm{sp}} \right). \end{aligned} \tag{7.4}$$

7.7.3 Effects of Cochlear Damage on Auditory Nerve Activity

The main parameters that influence AN responses in our model equations (7.2), (7.3), and (7.4) are the threshold I_{th}, which determines the probability of spontaneous activity, the spontaneous rate f_{sp}, and the maximum rate f_{max}. They are changed by cochlear damage.

We consider the effects of loss of inner & outer hair cells and of damage to the stereocilia of inner & outer hair cells. We denote the fraction of remaining inner hair cells (IHCs) by H_{i}, the fraction of remaining outer hair cells (OHCs) by H_{o}, and the fraction of undamaged stereocilia by S. The three parameters $H_{\mathrm{i}}, H_{\mathrm{o}}$, and S vary between 1 (healthy) and 0 (loss of all hair cells or damage of all stereocilia). For simplification, we assume that our infomax assumption for the AN population response (see above) also holds in the case of cochlear damage.

The death of an IHC deprives the corresponding AN fibers of their input, because each AN fiber only contacts one IHC, and each IHC is contacted by 10-30 AN fibers (Ryugo, 1992). Moreover, the amplitude of the AN's compound action potential is reduced approximately proportional to the amount of IHC loss (Wang et al., 1997; Salvi et al., 2000). We therefore model the effect of IHC loss by a multiplicative reduction of the AN population firing rate. IHC loss then affects the spontaneous firing rate, $f_{\mathrm{sp}}(H_{\,\mathrm{i}}) = H_{\mathrm{i}} \cdot f_{\mathrm{sp}}$, and the maximum firing rate of the AN, $f_{\mathrm{max}}(H_{\mathrm{i}}) = H_{\mathrm{i}} \cdot f_{\mathrm{max}}$ (see Fig. 2a). From equation (4), we find the mean AN firing rate after IHC loss,

$$\langle f(H_{\mathrm{i}}) \rangle = H_{\mathrm{i}} \cdot \langle f \rangle. \tag{7.5}$$

OHC loss is approximated by an increase in the AN threshold $I_{\,\mathrm{th}}$ in proportion to the amount of OHC loss, $I_{\mathrm{th}}(H_{\mathrm{o}}) = I_{\mathrm{th}} + \Delta_{\mathrm{o}} \cdot (1 - H_{\mathrm{o}})$, where $\Delta_{\mathrm{o}} = 60\,\mathrm{dB}$ is the threshold shift for the loss of all outer hair cells at $H_{\mathrm{o}} = 0$ (Dallos and Harris, 1978; Harrison, 1981). Therefore, the probability of spontaneous firing is increased, $P_{\mathrm{sp}}(H_{\mathrm{o}}) \geq P_{\mathrm{sp}}(1) = P_{\mathrm{sp}}$ where $P_{\,\mathrm{sp}}(H_{\mathrm{o}}) =$

$\int_{-\infty}^{I_{\rm th}(H_{\rm o})} {\rm d}I\, p_{\rm I}(I)$, and the probability density of driven activity is reduced to $p_{\rm d}(H_{\rm o}) = \dfrac{1-P_{\rm sp}(H_{\rm o})}{f_{\rm max}-f_{\rm sp}}$. The spontaneous and the maximum discharge rates are not affected (Dallos and Harris, 1978; Schmiedt and Zwislocki, 1980). The resulting response curves for the population firing rate of the AN are steeper, as observed experimentally for single fibers (Harrison, 1981); see also Fig. 7.2b. The mean firing rate is then given by

$$\langle f(H_{\rm o})\rangle = P_{\rm sp}(H_{\rm o}) f_{\rm sp} + \frac{1}{2}\left(1-P_{\rm sp}(H_{\rm o})\right)\left(f_{\rm max}+f_{\rm sp}\right). \tag{7.6}$$

Noise-induced damage to the stereocilia of inner and outer hair cells increases the response threshold of AN fibers and decreases their spontaneous firing rate (Liberman, 1984; Liberman and Dodds, 1984a). For a complete loss of all stereocilia ($S=0$) the threshold is increased by $\Delta_{\rm S} = 80\,{\rm dB}$, and the spontaneous rate is decreased by a factor of two-thirds (estimates based on Liberman, 1984; Liberman and Dodds, 1984a). For intermediate degrees of stereocilia damage (SD) where $0 \le S \le 1$, we have $I_{\rm th}(S) = I_{\rm th} + \Delta_{\rm S}\cdot(1-S)$, and $f_{\rm sp}(S) = f_{\rm sp} - \frac{2}{3}\cdot(1-S)\cdot f_{\rm sp}$ (see Fig. 2c). As for OHC loss, the probability of spontaneous activity depends on the amount of threshold shift, $P_{\rm sp}(S) = \int_{-\infty}^{I_{\rm th}(S)} {\rm d}I\, p_{\rm I}(I)$, and the probability density of driven activity is then given by $p_{\,\rm d}(S) = \dfrac{1-P_{\rm sp}(S)}{f_{\rm max}-f_{\rm sp}(S)}$. Together with the decrease in spontaneous firing rate, we obtain

$$\langle f(S)\rangle = P_{\rm sp}(S) f_{\rm sp}(S) + \frac{1}{2}\left(1-P_{\rm sp}(S)\right)\left(f_{\rm max}+f_{\rm sp}(S)\right). \tag{7.7}$$

for the mean firing rate of the AN after SD.

If IHC and OHC loss, or SD and IHC loss, occur together, we assume that the different types of cochlear damage independently influence the parameters of the AN response function. For IHC and OHC loss, we then get the spontaneous rate $f_{\rm sp}(H_{\rm i},H_{\rm o}) = H_{\rm i}\cdot f_{\rm sp}$, the maximum rate $f_{\rm max}(H_{\rm i},H_{\rm o}) = H_{\rm i}\cdot f_{\rm max}$, and the threshold $I_{\rm th}(H_{\rm i},H_{\rm o}) = I_{\rm th} + \Delta_{\rm o}\cdot(1-H_{\rm o})$. The mean firing rate of the AN population is

$$\langle f(H_{\rm i},H_{\rm o})\rangle = H_{\rm i}\cdot\langle f(H_{\rm o})\rangle, \tag{7.8}$$

where $\langle f(H_{\rm o})\rangle$ is given in equation (6). Similarly, for IHC loss and SD, we have the spontaneous firing rate $f_{\rm sp}(H_{\rm i},S) = H_{\rm i}\cdot\left(f_{\rm sp} - \frac{2}{3}\cdot(1-S)\cdot f_{\rm sp}\right)$, the maximum firing rate $f_{\rm max}(H_{\rm i},S) = H_{\rm i}\cdot f_{\rm max}$, and the threshold $I_{\rm th}(H_{\rm i},S) = I_{\rm th} + \Delta_{\rm S}\cdot(1-S)$. The mean AN population rate is

$$\langle f(H_{\rm i},S)\rangle = H_{\rm i}\cdot\langle f(S)\rangle, \tag{7.9}$$

where $\langle f(S)\rangle$ is given in equation (7).

7.7.4 Model for a Downstream Auditory Neuron

Downstream auditory neurons, for example in the cochlear nucleus, are modeled as firing rate units with some nonlinear response function. Each model neuron receives excitatory input from the AN at variable rate f and a constant additional input from other sources at rate $f_{\rm add}$. The sum of the two inputs is weighted by the adjustable synaptic gain factor g, and a response

threshold θ is subtracted. The firing rate r of the model neuron then is

$$r = R(f + f_{\text{add}}) = \begin{cases} r_{\text{high}} \cdot \tanh\left(\dfrac{g \cdot (f + f_{\text{add}}) - \theta}{r_{\text{high}}}\right) & \text{for } g \cdot (f + f_{\text{add}}) \geq \theta, \\ 0 & \text{otherwise,} \end{cases} \tag{7.10}$$

where $r_{\text{high}} = 300\,\text{Hz}$ is the highest possible firing rate of the model neuron. The gain factor g is set to 1 for the initial, healthy condition. The threshold θ is set to $\theta = f_{\text{add}}$ to ensure that in the healthy case ($g = 1$), the model neurons have the same response distribution for different firing rates of the additional input (see Figs. 3 and 5). The spontaneous firing rate of the model neuron is $r_{\text{sp}} = R(f_{\text{sp}} + f_{\text{add}})$, and the maximum firing rate is $r_{\text{max}} = R(f_{\text{max}} + f_{\text{add}})$.

The probability density function $q(r)$ of the model neuron's firing rates r is derived from the distribution $p_{\text{f}}(f)$ of AN responses and the response function R. The probability P_{sp} of spontaneous activity of the model neuron is the same as in the AN. In summary, we have

$$\begin{aligned} q(r) &= \frac{1}{R'\big(R^{-1}(r)\big)} p_{\text{f}}\big(R^{-1}(r)\big) \\ &= P_{\text{sp}} \cdot \delta(r - r_{\text{sp}}) + \begin{cases} \dfrac{p_{\text{d}}}{g} \cdot \dfrac{1}{1 - (r/r_{\text{high}})^2} & \text{for} \quad r_{\text{sp}} < r \leq r_{\text{max}} \\ 0 & \text{otherwise.} \end{cases} \end{aligned} \tag{7.11}$$

The mean firing rate of the model neuron is then given by

$$\begin{aligned} \langle r \rangle &= \int_{r_{\text{sp}}}^{r_{\text{max}}} \mathrm{d}r'\, r' \cdot q(r') \\ &= P_{\text{sp}} r_{\text{sp}} + \frac{p_{\text{d}}}{g} \int_{r_{\text{sp}}}^{r_{\text{max}}} \mathrm{d}r'\, \frac{r'}{1 - (r'/r_{\text{high}})^2} \\ &= P_{\text{sp}} r_{\text{sp}} + \frac{r_{\text{high}}^2 p_{\text{d}}}{2g} \ln \frac{r_{\text{high}}^2 - r_{\text{sp}}^2}{r_{\text{high}}^2 - r_{\text{max}}^2}, \end{aligned} \tag{7.12}$$

where r_{sp} and r_{max} depend on g (see above) so that $\langle r \rangle$ increases with increasing g.

7.7.5 Homeostatic Plasticity

Homeostatic plasticity serves to stabilize the mean activity of a neuron around a certain target level over long time scales on the order of days (Turrigiano, 1999; Burrone and Murthy, 2003). We model the effects homeostatic plasticity by a change in the gain factor g that is triggered by deviations of the mean activity $\langle r \rangle$ from a certain target rate r^*. We assume that the response function R is not affected by homeostatic plasticity, as in our model the adjustment of g is sufficient to mimic the changes in effective response gain by homeostatic scaling. The change of g that is necessary to restore the mean activity $\langle r \rangle$ in equation (7.12) to its target level r^* is computed numerically. The time-course of homeostatic plasticity is not considered. An upper limit of 3 (three times the normal gain) is imposed onto g to reasonably account for physiological constraints on synaptic strengths and excitability (see e.g. Turrigiano et al., 1998).

7.7.6 Additional Acoustic Stimulation

During the presentation of an acoustic stimulus at a suprathreshold intensity $I_{\text{stim}} > I_{\text{th}}$, the AN firing rate is $f_{\text{stim}} = f(I_{\text{stim}})$. If the stimulus is presented continuously, the spontaneous firing rate f_{sp} of the AN fiber population is to be replaced by $f_{\text{stim}} > f_{\text{sp}}$. The AN then fires at rate f_{stim} with probability $P_{\text{stim}} = \int_{-\infty}^{I_{\text{stim}}} \mathrm{d}I \; p_{\text{I}}(I)$, that is whenever I_{stim} is higher than the intensity I of an environmental stimulus with distribution p_{I}. The mean firing rate $\langle r \rangle$ of a second-order model neuron can then be calculated using equation (12) with P_{sp} and f_{sp} replaced by P_{stim} and f_{stim}. If $\langle r \rangle$ differs from the desired value r^*, homeostatic plasticity is activated, and g is changed. After homeostasis, the value of g depends also on I_{stim}. The required stimulus intensity I^*_{stim} to reverse hyperactivity (see Fig. 8) is such that $g(I^*_{\text{stim}})$ after homeostasis leads to a normal spontaneous firing rate $r_{\text{sp,healthy}}$ in the second-order neuron when the additional stimulation is turned off, namely $R(f_{\text{sp}}, g(I^*_{\text{stim}})) = r_{\text{sp,healthy}}$. The calculation of I^*_{stim} is carried out numerically, and separately for each frequency channel.

Chapter 8

Extension of the Model to Reproduce the Basic DCN Circuit

In the model presented in the last chapter we only considered excitatory input to cochlear nucleus neurons. However, the responses of many neuron types in the auditory brainstem are shaped by the interaction of excitatory and inhibitory inputs (Rhode and Greenberg, 1992; Irvine, 1992). The projection neurons of the DCN, for example, are excited by AN fibers and inhibited by various interneurons, many of which also receive excitation from the AN or from other sources like the somatosensory system (see, e.g., Davis et al., 1996b; Young and Davis, 2002; Shore, 2005, and Section 2.4). Many characteristics of the response properties of DCN projection neurons (PNs) can be explained by inhibition from two types of interneurons: type-II and wide-band inhibitor neurons (Young and Davis, 2002). Both interneurons receive excitation from AN fibers. The type-II neuron has a best frequency that is close to the PN's best frequency, and it inhibits the PN's response to pure tones or other narrow-band stimuli of high intensity. The wide-band inhibitor neuron, on the other hand, has a strong response to broad-band noise and only a weak response to pure tones. It inhibits DCN projection neurons as well as type-II neurons.

After hearing loss through cochlear damage, the excitatory input from the AN is reduced, which affects the projection neurons and the inhibitory interneurons in the DCN. This creates a situation where not only excitatory, but also inhibitory activity is decreased. Thus, the activity of DCN neurons can be changed in a complex way, depending on the connectivity and strength of the inhibitory connections. In the following, we are going to analyze the basic DCN circuit described above (see section 2.4 for more details). Briefly, we use a phenomenological network model with three types of model neurons: wide-band inhibitor (WBI) neurons, narrow-band inhibitor (NBI) neurons (type-II neurons), and projection neurons (PNs). We chose to call type-II neurons narrow-band inhibitors, due to their function of providing inhibition for narrow-band stimuli only.

The connection strengths in the circuit are adjusted such that essential features of the responses of these neuron types are reproduced. We determine how the responses of the PNs depend on the strength of the inhibitory projections form WBI and NBI neurons, and how the responses of all neurons in this circuit are changed by hearing loss. Then we evaluate the effects of a homeostatic stabilization of the mean rate of the projection neurons.

8.1 Auditory Nerve Model

The AN model used in this section is organized in frequency channels. Each frequency channel comprises AN fibers with similar characteristic frequencies, but different thresholds and spontaneous discharge rates. The small population of AN fibers in each frequency channel is described by a population firing rate as introduced in section 7.2.1 (see also Eq. 7.2). Each octave is divided into 10 frequency channels. Hearing loss through cochlear damage is implemented in this model by altering the AN rate-intensity functions in each frequency channel. A description of how the rate-intensity functions are changed to reproduce the effects of different kinds of cochlear damage can be found in section 7.2.2.

8.2 Model for Wide-Band Inhibitor Neurons

In the basic DCN circuit as proposed by Young and coworkers, the WBI neuron is the only neuron that receives only excitatory input from AN fibers. Our model WBI neuron receives input from AN fibers that span a wide range of characteristic frequencies (see Fig. 8.1a). It has a simple threshold-linear response function with a firing threshold θ_w. The firing rates of the afferent AN fibers are added, weighted by $1/x$, and θ_w is subtracted. In total, the firing rate w of the WBI neuron in response to AN input from x frequency channels firing at rates $f_1, \ldots, f_\mathrm{x}$ is given by

$$w = W(f_1, f_2, \ldots, f_\mathrm{x}) = \left[\frac{1}{x} \sum_{\mathrm{i}=1}^{x} f_\mathrm{i} - \theta_\mathrm{w} \right]_+ . \tag{8.1}$$

In our model, we consider input from $x = 10$ different AN frequency channels whose characteristic frequencies (CFs) span one octave. Moreover, we set the firing threshold to $\theta_\mathrm{w} = 100\,\mathrm{Hz}$. The resulting WBI model neuron is not spontaneously active and it does not respond to pure tones. It has a monotonic rate-intensity function for broad-band noise with a response threshold of 27 dB (Fig. 8.1b). The response threshold is determined by the minimum noise intensity I needed to evoke AN responses with $f_\mathrm{i}(I) = \theta_\mathrm{w}$. Cochlear damage thus increases the response threshold of the WBI neuron.

When we assume that the firing rates of AN fibers from different frequency channels are mutually independent, we can obtain the firing rate distribution of the WBI neuron from a convolution of the response distributions of the afferent AN fibers (see Methods, Eq. 8.7). In the healthy case, the resulting firing rate distribution of the model WBI neuron resembles a Gaussian distribution, with a delta peak at 0 Hz, as the WBI neuron is quiescent with probability 0.009. The WBI neuron's mean rate is 45 Hz (see Fig. 8.1c).

8.3 Model for Narrow-Band Inhibitor Neurons

Our model for a narrow-band inhibitor (NBI) neuron of the DCN is based on the response properties that have been reported for type-II neurons (see section 2.4). It receives excitation from AN fibers of a single frequency channel, and it is inhibited by a WBI neuron. We assume that the NBI neuron and the WBI neuron do not have shared inputs. The AN frequency channel that provides input to the NBI therefore does not make connections to the WBI (see Fig. 8.2a).

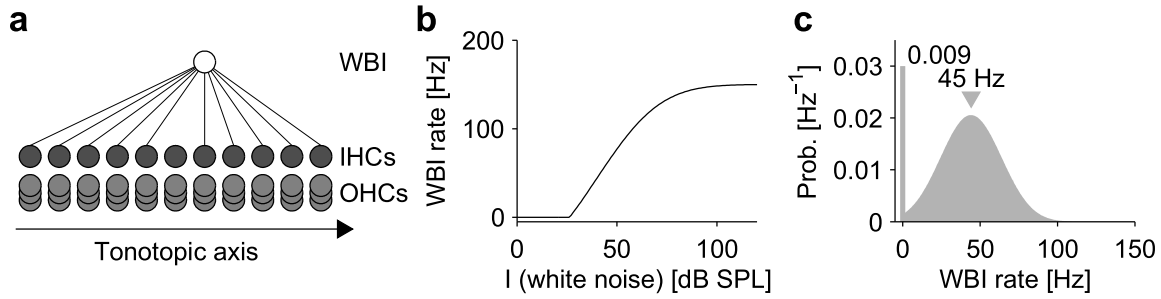

Figure 8.1: Wide-band inhibitor (WBI) model neuron. **a)** Schematic illustration of the WBI neuron's afferents. The WBI neuron has a large receptive field, it is excited by AN fibers (thin black lines) with a wide range of characteristic frequencies. **b)** Rate-intensity function of the WBI neuron for stimulation with white noise. The WBI neuron is not spontaneously active. Above threshold the discharge rate grows monotonically with increasing noise intensity and saturates for very high intensities. The WBI neuron does not respond to stimulation with pure tones. **c)** Firing-rate distribution of the WBI neuron. The neuron is quiescent with a probability of 0.009 (Delta-peak at 0 Hz), and it has a mean rate of 45 Hz.

The NBI neuron has a threshold-linear response function with a firing threshold θ_{n}. The firing rate n of the NBI neuron in response to AN input at rate f and WBI input at rate w is given by

$$n = N(f,w) = [f - g_{\mathrm{nw}} w - \theta_{\mathrm{n}}]_+ , \tag{8.2}$$

where the gain factor g_{nw} determines the strength of the inhibition from the WBI neuron. We set this gain factor to $g_{\mathrm{nw}} = 1.5$ and the firing threshold to $\theta_{\mathrm{n}} = \theta_{\mathrm{w}} = 100\,\mathrm{Hz}$ to ensure that the NBI neuron does not respond to broad-band noise. The gain factor for excitation from the AN is set to one for simplicity. Both gain factors are fixed, they are not regulated by homeostatic plasticity in our model. The response threshold of the NBI neuron for stimulation with pure tones is 27 dB, which is the intensity needed to evoke an AN response of $f = \theta_{\mathrm{n}}$. The NBI neuron has a monotonous rate-intensity function for pure tones (see Fig. 8.2b), and it does not respond to broad-band noise.

The NBI and the WBI neuron receive input from different AN frequency channels. Moreover, due to the WBI neuron's large receptive field, its afferent input is largely independent of the NBI neuron's input from a single AN frequency channel. Therefore, we assume that the firing rate of the NBI neuron's afferent AN fiber population and the firing rate of the WBI neuron are mutually independent, which provides a plausible and feasible approximation for further calculations. Assuming independence of the excitatory and the inhibitory input, the response distribution of the NBI model neuron can be calculated (Methods, Eq. 8.13). The resulting response distribution is shown in Fig. 8.2c. It has a delta peak at 0 Hz, as the NBI neuron is quiescent with probability 0.6. The mean firing rate of the NBI neuron is 19 Hz.

8.4 Model for Projection Neurons

In our model for a projection neuron (PN) of the DCN, we consider excitation by AN fibers from a single frequency channel, and inhibitory projections from a WBI and a NBI neuron. We assume that the NBI neuron receives excitatory input from AN fibers of the same frequency

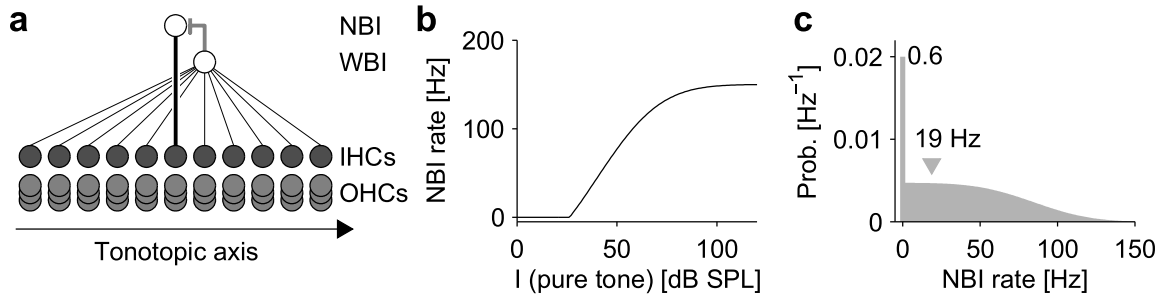

Figure 8.2: Narrow-band inhibitor (NBI) model neuron. **a)** Schematic illustration of the NBI's afferent connections. It receives excitation from AN fibers (thick black line) of a single frequency channel, and an inhibitory projection (thick gray line) from a WBI neuron. The WBI neuron's receptive field is approximately centered on the NBI neuron's characteristic frequency, and the two neurons have no shared inputs. **b)** Rate-intensity function of the NBI neuron for stimulation with pure tones at its characteristic frequency. The NBI neuron is not spontaneously active. Above threshold, the discharge grows monotonically with increasing sound intensity and saturates for very high intensities. The NBI neuron does not respond to broad-band noise. **c)** Firing-rate distribution of the NBI neuron. It is quiescent with probability 0.6, and its mean rate is 19 Hz.

channel as the PN. Moreover, we assume that both the PN and the NBI neuron are inhibited by the same WBI neuron (Fig. 8.3a). As our model neurons represent small populations of real neurons, these assumptions provide an approximation of the situation in the DCN, where PNs and type-II neurons each receive inhibition from WBI neurons with similar characteristics, but not necessarily from the same neurons.

The strength of the inhibitory projection from the WBI neuron onto the PN is regulated by the gain factor g_{w}, and the efficacy of inhibition from the NBI neuron is determined by the gain factor g_{n}. The gain factor g for input from the AN is set to $g = 1$ for simplicity. The PN neuron has a nonlinear response function with a firing threshold at 0 Hz, its firing rate response r is given by,

$$r = R(f,w) = r_{\mathrm{high}} \tanh\left(\frac{[f - g_{\mathrm{w}} w - g_{\mathrm{n}} N(f,w)]_+}{r_{\mathrm{high}}}\right) \tag{8.3}$$

where f is the firing rate of the afferent AN fiber population, w the firing rate of the WBI neuron, and r_{high} the maximum possible firing rate of the PN. The firing rate of the NBI neuron n is given as $n = N(f,w)$, as it depends on the same f and w as the PN's response due to their shared input.

8.4.1 Projection Neuron Responses to Tone- and Noise-Stimuli

In Figs. 8.3b-d we show how the response properties of the model PN are altered for different values of the two gain factors for the inhibitory inputs. When both g_{w} and g_{n} are set to low values, for example $g_{\mathrm{w}} = 0.6$ and $g_{\mathrm{n}} = 0.5$, the PN exhibits monotonous rate-intensity functions for both pure tones and broad-band noise (Fig. 8.3b). Moreover, the PN is inhibited by notched-noise. Note that, for our example, the notch in the noise spectrum is centered on the CF of the PN, and the notch depth is infinite. These responses resemble those of type-III neurons of the

DCN (Rhode and Greenberg, 1992; Young and Davis, 2002, see also Section 2.4 on page 10). When we increase the value of g_n to $g_n > 1$, the PN's rate-intensity function for pure tones becomes non-monotonous. For a parameter combination of $g_w = 0.6$ and $g_n = 1.3$, we observe an excitatory, monotonous response to noise and an inhibitory response to notched-noise. The response to pure tones is characterized by a non-monotonous rate-intensity function. The PN is excited by pure tones at low and medium intensities, whereas at high sound intensities, its response is close to the spontaneous rate (Fig. 8.3c). Such response properties resemble type-IV-T neurons of the DCN (Davis et al., 1996a). If we further increase both g_w and g_n, we can change the responses of the model projection neuron to resemble type-IV neurons (Young and Davis, 2002), an example for $g_w = 1.1$ and $g_n = 3$ is shown in Fig. 8.3d. The responses to pure tones are now strongly non-monotonous, the PN is strongly inhibited already at medium sound intensities. Moreover, also the responses to broad-band noise have become non-monotonous, but they are still excitatory at all sound intensities.

8.4.2 PN Responses to Arbitrary Combinations of AN and WBI Activity

The rate-intensity functions in the previous examples considered stimuli where only two of the three inputs to the PN were active: either AN fibers and the WBI neuron for broad-band noise, or AN fibers and the NBI neuron for pure tone stimuli. For more complex stimuli, however, the responses of the PN are determined by the combined effect of the inputs from the AN, the NBI, and the WBI neuron. As the PN and the NBI neuron receive input from the same AN fibers and the same WBI neuron, the response of the PN is a function of the firing rate f of the afferent AN fibers and the firing rate w of the WBI neuron (see Eq. 8.3). Figure 8.4 shows how the firing rate of the PN depends on f and w for different values of the inhibitory gain factors g_w and g_n.

For low values of g_w and g_n that lead to type-III response properties ($g_w = 0.6$ and $g_n = 0.5$ in Fig. 8.4a), most of the combinations of f and w have an excitatory effect on the PN. Inhibition is observed for high firing rates w of the WBI neuron in combination with low AN firing rates f. For $f > 100\,\text{Hz}$, the NBI neuron may be activate, but only when the firing rate of the WBI neuron is low. Therefore, we observe a two-fold effect of WBI activity for $f > 100\,\text{Hz}$: low rates of w have an excitatory effect on the PN, as the WBI neuron inhibits the NBI neuron, which in total leads to a disinhibition of the PN. Once the NBI neuron has ceased to fire, however, the net effect of further increases in WBI activity on the PN is inhibitory. The strength of the disinhibition effect depends on how strongly the NBI neuron is inhibited by the WBI neuron, which is determined by the value of the gain factor g_{nw}. Disinhibition is observed for $g_{nw} > g_w$.

When g_n is increased to obtain type-IV-T response properties in the PN, we see a different situation (Fig. 8.4b, $g_w = 0.6$ and $g_n = 1.3$). Still, most of the input combinations lead to excitatory responses of the PN, but in many cases the evoked firing rates are lower than for a type-III PN. Also the disinhibitory effect of WBI activity for $f > 100\,\text{Hz}$ has become more pronounced, as the PN is inhibited more strongly by the NBI neuron.

Finally, for type-IV response properties of the PN ($g_w = 1.1$ and $g_n = 3$, Fig. 8.4c), there are two large regions of inhibition, one at high f and low w, the other at high w and low f. In these regions, the PN is mostly silent. Excitation of the PN is only observed in a central region around $f = w + 100\,\text{Hz}$.

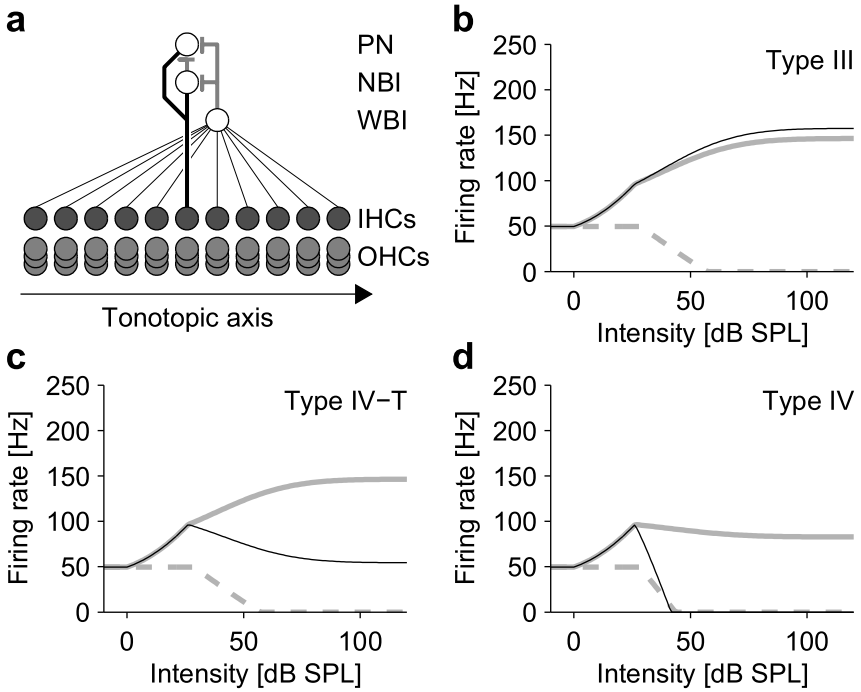

Figure 8.3: Properties of a projection neuron (PN). **a)** The PN receives excitation from a population of AN fibers (thick black line), and it is inhibited by a NBI and a WBI neuron (thick gray lines). The NBI neuron is excited by the same population of AN fibers as the PN, and inhibited by the same WBI neuron. **b)** Responses of a PN for $g_{\mathrm{n}} = 0.5$ and $g_{\mathrm{w}} = 0.6$. The PN shows excitatory responses to pure tones (thin black line) and broad-band noise (thick gray line), with monotonic rate-intensity functions. It is inhibited by notched-noise (dashed gray line). This behavior corresponds responses of type-III neurons in the DCN. **c)** PN responses for $g_{\mathrm{n}} = 1.3$ and $g_{\mathrm{w}} = 0.6$. For this parameter combination, we obtain type-IV-T response properties, with a nonmonotonic rate-intensity function for pure tones (black line), a monotonic rate-intensity function for broad-band noise (solid gray line), and inhibition through notched-noise (dashed gray line). **d)** PN responses for $g_{\mathrm{n}} = 3$ and $g_{\mathrm{w}} = 1.1$. This corresponds to type-IV response properties, with a strongly nonmonotonic rate-intensity function for pure tones, and also a non-monotonic rate-intensity function for noise.

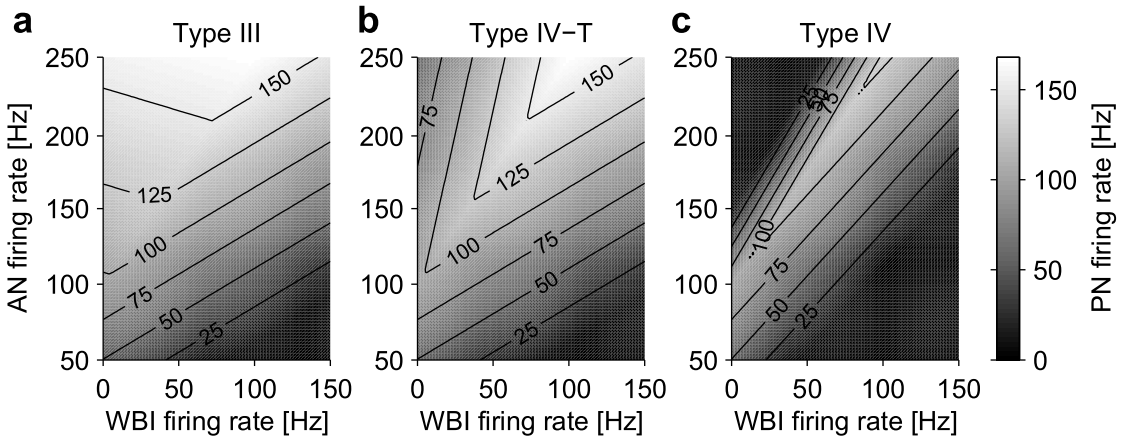

Figure 8.4: Firing rate of the projection neuron as a function of the input from the AN and the WBI neuron for different parameter values **a)** $g_{\mathrm{n}} = 0.5$ and $g_{\mathrm{w}} = 0.6$ (type III responses) **b)** $g_{\mathrm{n}} = 1.3$ and $g_{\mathrm{w}} = 0.6$ (type IV-T response properties) **c)** $g_{\mathrm{n}} = 3$ and $g_{\mathrm{w}} = 1.1$ (type IV responses).

8.4.3 Mean Firing Rates of the Projection Neurons

Now that we have established how the firing rate of the model PN depends on its inputs and on the strength of inhibition, we still need the joint probability distribution of the activity of the AN fibers and the WBI neuron before we can calculate the mean rate of the PN. If we assume that the firing rate of the AN fiber population that provides input to the PN and the NBI neuron, and the firing rate of the WBI neuron are mutually independent, the joint probability distribution of f and w is simply given by $p(f,w) = p_{\mathrm{f}}(f) \cdot p_{\mathrm{w}}(w)$, where $p_{\mathrm{f}}(f)$ is the probability distribution of the responses of the AN fiber population(see section 7.2.3 and Eq. 7.3), and $p_{\mathrm{w}}(w)$ the response distribution of the WBI neuron (see above and Methods Eq. 8.8). The mean firing rate of the PN can then be directly calculated (Methods, Eq. 8.15). As already discussed for the NBI neuron, the assumption of independence provides a plausible approximation of the relation between AN and WBI input. The general case with a stimulus-dependent relation between the two is much more difficult to handle, and the results can be expected to be highly sensitive to the kind of stimuli chosen to represent a natural acoustic environment.

The dependence of the mean rate of the PN on the strength of inhibition from the NBI and the WBI neuron is illustrated in Fig. 8.5. Without inhibition ($g_{\mathrm{w}} = g_{\mathrm{n}} = 0$), we obtain a mean rate of 130 Hz. Increasing g_{w} or g_{n} decreases the mean firing rate of the PN, and we find that the value of g_{w} has a stronger influence on the mean firing rate of the PN than the value of g_{n}. For high values of g_{w}, the mean rate of the PN can even be below the spontaneous rate (Fig. 8.5a). The parameter regions where the different DCN projection neuron response types are obtained are depicted in Fig. 8.5b. PNs with type-III and type-IV-T response characteristics have mean rates that are more than 1.5 times higher than the spontaneous firing rate, whereas the mean rate of type-IV PNs is either slightly above or even below the spontaneous rate. For our examples in Fig. 8.3b-d, the mean rates are 102 Hz for the type-III PN, 90 Hz for the PN with type-IV-T response properties, and 47 Hz for the type-IV PN.

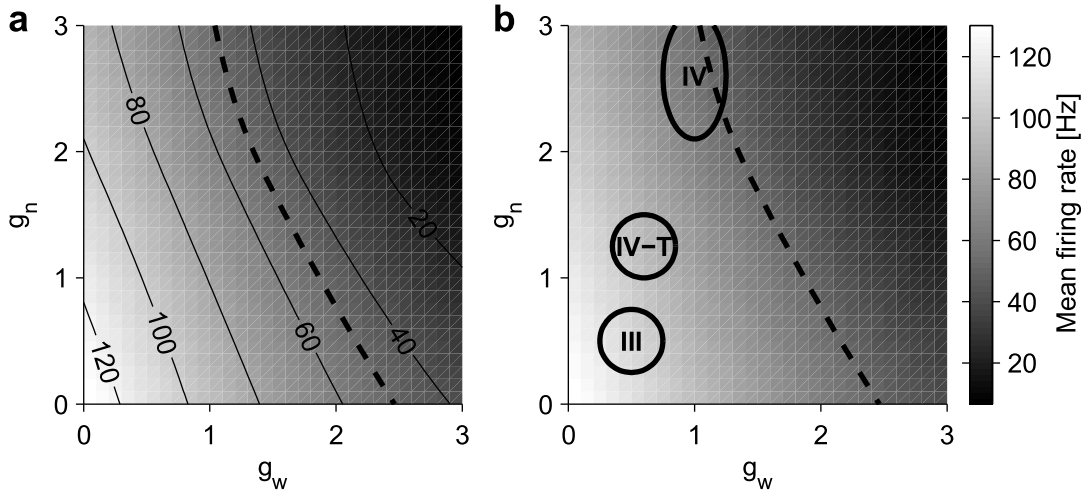

Figure 8.5: Mean firing rate of the PN in dependence upon the strength of narrow- and wide-band inhibition. **a)** Gray-scale coded plot of the projection neuron's mean rate. The thick dashed line in illustrates where the mean rate is equal to the spontaneous rate. The PN's mean rate is monotonically decreased when g_{w} and/or g_{n} are increased. **b)** The black ovals illustrate for which parameter combinations type-III, type-IV-T, and type IV response properties of the PNs are obtained.

8.4.4 Homeostatic Plasticity in Projection Neurons

We assume that the mean firing rates of DCN projection neurons are stabilized by homeostatic plasticity. For each PN type, i.e. each combination of the gain parameters g_{w} and g_{n}, the target firing rate that is stabilized by homeostasis is set to the mean firing rate obtained for input from healthy AN fibers (see Fig. 8.5). In this model, we consider homeostasis through global scaling of synapse strengths. Scaling is implemented through a homeostasis factor h which alters the gain of excitatory and inhibitory inputs in a multiplicative fashion. The gain of excitatory inputs is multiplied with h, and the gain of inhibitory inputs is divided by h (see also Methods, Eq. 8.16) to account for the opposite regulation of the strengths of excitatory and inhibitory inputs that has been observed in experiments. The response of a PN is then given by

$$r = R(f,w,h) = r_{\mathrm{high}} \tanh\left(\frac{h\cdot f - \frac{g_{\mathrm{w}}}{h}w - \frac{g_{\mathrm{n}}}{h}N(f,w)}{r_{\mathrm{high}}}\right). \tag{8.4}$$

In the healthy case, the homeostasis factor is one. When the mean rate of a PN is persistently decreased below its target level, h is increased until the mean rate has been restored. An increase in h strengthens excitatory and weakens inhibitory synapses. For persistent elevation of the mean rate above the healthy level, h is reduced, which decreases excitation and increases the effect of inhibition. In our model, the value of the homeostasis factor is limited to the range of $[0.3,3]$ to account for physiological constraints on synaptic strength.

8.5 Effects of Hearing Loss and Homeostatic Plasticity

In the following, we evaluate how the responses of neurons in our model DCN circuit are altered by hearing loss through different kinds and degrees of cochlear damage. We consider inner hair cell (IHC) loss, outer hair cell (OHC) loss, and stereocilia damage (SD). At this point, we restrict our analysis to the case where all AN frequency channels are affected by the same amount of cochlear damage. Finally, we analyze the effects of activity stabilization through homeostatic plasticity in the projection neuron. We assume that homeostatic mechanisms are not active in the NBI and WBI neurons. Experimental studies show that homeostatic mechanisms might regulate the activity of inhibitory interneurons in an opposite direction to the activity of principal cells (Turrigiano, 1999). In our model framework based on firing rates, this can be approximated by simply regulating the strengths of the inhibitory projections onto the projection neurons.

8.5.1 Inner Hair Cell Loss

As introduced in the previous chapter, we model the effects of IHC loss through scaling of the rate-intensity function of the AN population response. This leads to a reduction of the mean and the spontaneous rate in proportion to the degree of IHC loss (Fig. 8.6a). The resulting reduction of excitatory drive from the AN affects all neurons in our model DCN circuit. The WBI neuron's activity is strongly decreased by the loss of excitation after IHC loss. Its mean rate declines rapidly in proportion to the severity of IHC loss, and it ceases to fire when IHC loss exceeds approximately 45% (Fig. 8.6b). The NBI neuron presents a more complex situation: IHC loss reduces the excitatory input to this neuron, but due to the decrease in the activity of the WBI neuron, it also receives less inhibition. Hence, the NBI neuron's mean rate stays approximately constant for low IHC loss. At around 40% IHC loss, when the AN's mean rate drops below the NBI neuron's firing threshold, the mean rate of the NBI neuron also starts to decline, and for IHC loss of more than 60%, it remains quiescent (Fig 8.6c).

Let us now turn to the effect of IHC loss on the different types of PNs. After IHC loss, these neurons experience not only a reduction of excitatory input from the AN, but also decreased inhibition from the inhibitory interneurons.

For a type-III PN, for example, IHC loss of up to ca. 50% decreases the spontaneous rate more strongly than the mean rate: the decrease in mean activity of the inhibitory interneurons partly compensates for the decrease in mean excitation from the AN, whereas the spontaneous rate is only influenced by the reduction of excitatory AN input, as the inhibitory interneurons are not spontaneously active. Thus, the ratio between the mean and the spontaneous rate is increased for mild to moderate IHC loss. For more severe IHC loss, however, both the mean and the spontaneous rate are decreased proportionally (Fig. 8.6d, upper panel). We assume that the decrease in the projection neuron's mean rate activates homeostatic plasticity. Through the increase of the homeostasis factor h (Fig. 8.6d, middle panel), the strengths of excitatory synapses on the PN are increased, whereas inhibitory synapses are weakened (see above and Methods). Homeostasis can thus stabilize the mean rate of this type-III PN at its target value for up to 76% IHC loss. When IHC loss is more severe, homeostasis saturates at $h = 3$ and the mean rate declines. As the ratio between mean and spontaneous rate was increased by IHC loss, the spontaneous rate of the PN remains below its healthy value after homeostasis (Fig. 8.6d, lower panel).

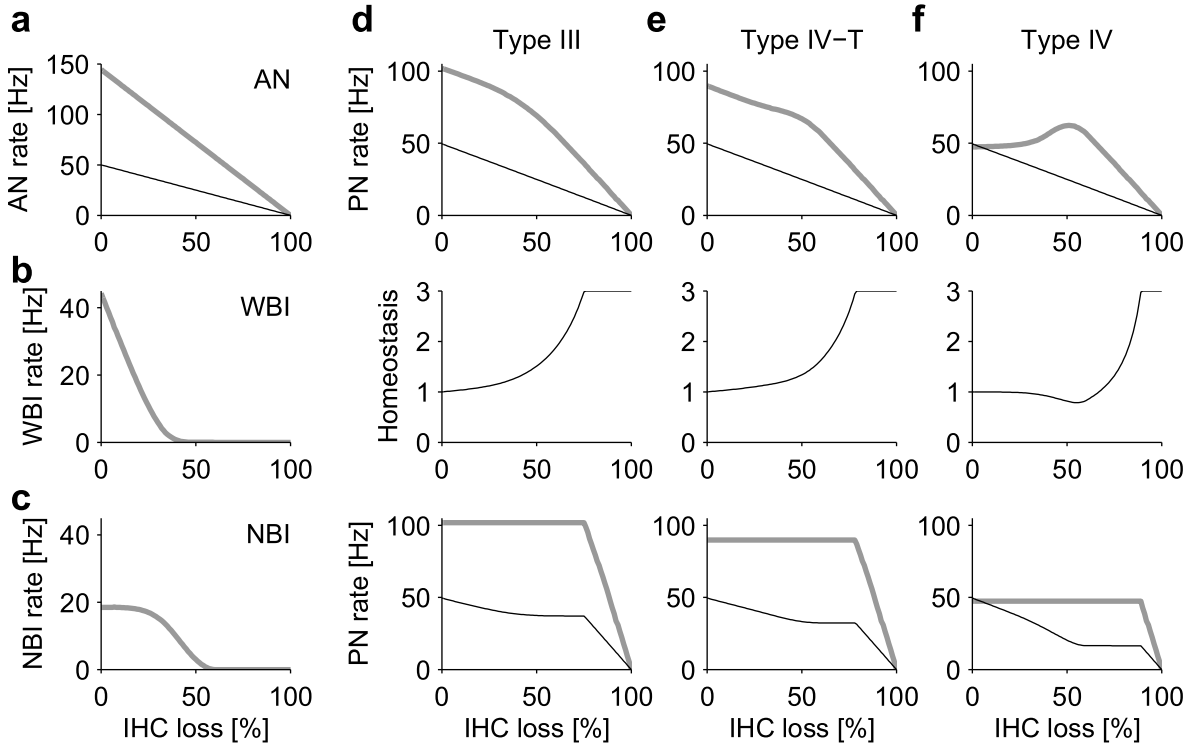

Figure 8.6: Effect of various degrees of IHC loss on the activity of AN fibers, WBI neurons, NBI neurons, and PNs, and consequences of homeostatic activity stabilization in the projection neurons. **a)** IHC loss decreases the mean (thick gray line) and the spontaneous firing rate (thin black line) of AN fibers. **b)** The mean firing rate of a WBI neuron is decreased by IHC loss, and it ceases to fire when IHC loss exceeds ca. 45%. **c)** For mild IHC loss, the mean firing rate of a NBI neuron stays approximately constant, because decreased excitation from the AN is compensated by decreased inhibition from the WBI. For medium IHC loss, the mean rate of the NBI neuron is decreased, and it remains quiescent when IHC loss exceeds ca. 60%. **d-f**) Responses of PNs tuned to type-III (d), type-IV-T (e), and type-IV characteristics (f). Responses immediately after IHC loss are shown in the top panels, the middle panels show the homeostasis factor, and the bottom panels show the PNs' responses after homeostasis. **d)** IHC loss decreases the mean and the spontaneous rate of a type-III PN. Homeostasis restores the mean rate to its target level for up to 76% IHC loss. The spontaneous rate is decreased below the normal level after homeostasis, as the ratio between mean and spontaneous rate was decreased by IHC loss. **e)** Also in a type-IV-T PN, mean and spontaneous firing rate are decreased by IHC loss. After homeostasis, the mean rate can be stabilized at the healthy value for up to 79% IHC loss, and the spontaneous rate is lower than in the healthy case. **f)** Medium IHC loss leads to an increase in the mean rate of a type-IV PN, because the activity of inhibitory is reduced. For severe IHC loss, the mean rate of the PN is strongly decreased. Homeostasis stabilizes the PN's mean rate until it saturates when IHC loss exceeds 90%. After homeostasis, the spontaneous rate is decreased.

In a PN with type-IV-T response characteristics, the effect of reduced inhibition after IHC loss is more pronounced than in a type-III PN. Although the mean rate still decreases monotonously for increasing IHC loss, the release from inhibition from the NBI neuron actually creates a small bump on the curve. As in the type-III PN, the ratio between mean and spontaneous rate is increased after IHC loss. (Fig. 8.6e, upper panel). Homeostasis (Fig. 8.6e, middle panel) is able to restore the mean rate of a type-IV-T PN for up to 79% IHC loss. The spontaneous rate, however, is below its healthy value after homeostasis (Fig. 8.6e, lower panel).

A type-IV-PN presents a different situation: In the healthy case, its mean rate is close to the spontaneous rate. After IHC loss, the effect of the loss of inhibition, especially from the NBI neuron, is so strong that the type-IV PN's mean rate is actually increased for moderate IHC loss. For severe IHC loss, on the other hand, it is also decreased similar to type-III and type-IV-T PNs (Fig. 8.6f, upper panel). As moderate IHC loss increases the type-IV PN's mean rate, homeostasis has to decrease the excitatory gain and increase the inhibitory gain, which is achieved by a homeostasis factor smaller than one (Fig. 8.6f, middle panel). After homeostasis, the mean firing rate is restored for up to 90% IHC loss, and the spontaneous firing rate is lower than before IHC loss (Fig. 8.6f, lower panel).

We conclude that also in the extended model with inhibitory interneurons, IHC loss does not lead to hyperactivity. In contrast to the simple model with excitation only, however, rescaling through homeostatic plasticity is not possible, and the spontaneous rate is decreased after homeostasis.

8.5.2 Outer Hair Cell Loss

The loss of outer hair cells increases the response threshold of the affected AN fibers, whereas the spontaneous and maximum firing rate remain unchanged (see section 7.2.2). The increase of the response threshold leads to a reduction of the mean AN firing rate (Fig. 8.7a). After OHC loss, the WBI neuron's mean rate is decreased in proportion to the severity of OHC loss, approaching 0 Hz for 100% OHC loss (Fig. 8.7b). The decrease in the WBI neuron's activity reduces the inhibition experienced by the NBI neuron. Its mean rate is increased for mild-to-moderate OHC loss, as in this range its inhibitory input is reduced more strongly than its excitatory input. When OHC loss gets more severe, the mean rate of the NBI neuron decreases, and for 100% OHC loss it reaches approximately two thirds of the original mean rate (Fig. 8.7c).

Type-III (Fig. 8.7d) and type-IV-T PNs (Fig. 8.7e) are affected by OHC loss in a similar way. In both neuron types, the mean firing rate is monotonously decreased by OHC loss, whereas the spontaneous rate stays constant (top panels). Homeostasis is able to restore the mean rates of both neuron types to their healthy values for all degrees of OHC loss. In both the type-III and the type-IV-T PN, the spontaneous rate is increased after homeostasis (bottom panels). Thus, in our model OHC loss can lead to hyperactivity in type-III and type-IV-T PNs.

In a type-IV PN, moderate OHC loss decreases the mean rate below the spontaneous rate. This is caused by the increase of the mean rate of the NBI neuron, which exerts a strong inhibitory influence on the type-IV PN. Thus, on average the type-IV PN experiences stronger inhibition from the NBI neuron after moderate OHC loss. After homeostasis, the mean rate of the type-IV PN is restored to its target value regardless of the severity of OHC loss. The spontaneous rate, however, is slightly increased for moderate-to-severe OHC loss (Fig. 8.7f). The maximum increase is about 12%, thus it might be considered strong enough to be called

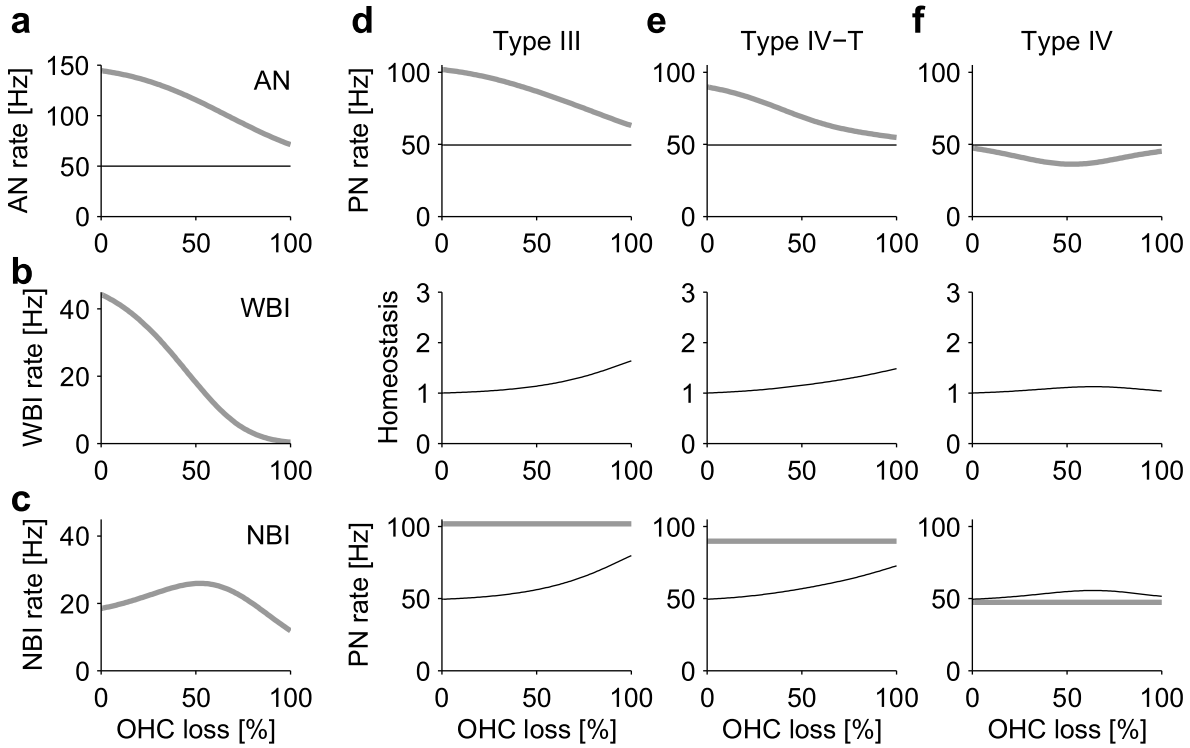

Figure 8.7: Effect of various degrees of OHC loss on the activity of AN fibers, WBI neurons, NBI neurons, and PNs, and consequences of homeostatic activity stabilization in the PNs. **a)** OHC loss decreases the mean rate (thick gray line) of the affected AN fibers, whereas the spontaneous rate (thin black line) stays constant. **b)** The mean rate of the WBI neuron is monotonously decreased for increasing OHC loss. **c)** The mean rate of the NBI neuron is a nonmonotonous function of the degree of OHC loss. **d-f**) PN responses, panels are arranged as in Fig. 8.6. **d)** The mean rate of a type-III PN is decreased after OHC loss (top panel). Gain adjustment through homeostatic plasticity (middle panel) can restore the mean rate to its target level, but increases the spontaneous firing rate (bottom panel). **e)** OHC loss also decreases the mean rate of type-IV-T PNs. After homeostasis, the mean rate is restored, but the spontaneous rate is elevated. **f)** In a type-IV PN, the mean rate is decreased below the spontaneous rate after OHC loss. Homeostatic activity stabilization can compensate for this, and elevates the spontaneous firing rate slightly.

hyperactivity.

To sum it up, OHC loss can lead to hyperactivity in all three projection neuron types, albeit only to a much weaker degree in type-IV compared to type-III and type-IV-T PNs.

8.5.3 Stereocilia Damage

Noise-induced damage to the stereocilia of inner and outer hair cells increases the response threshold and decreases the spontaneous firing rate of the corresponding AN fibers. Both changes conjointly reduce the mean AN firing rate (see Fig. 8.8a and section 7.2.2). The reduced input from the AN leads to a strong reduction of the WBI neuron's mean firing rate, and the neuron is inactivated when SD exceeds ca. 75%. The NBI neuron's mean rate, on the other hand, is increased by mild SD, as in this range the reduction of inhibition from the WBI neuron outweighs the decrease in excitation from the AN. However, when the mean AN rate is reduced below 100 Hz, the NBI neuron's mean rate starts to decline and is decreased below its healthy level for severe SD (Fig. 8.8c).

In all types of PNs, the mean firing rate is reduced in proportion to the severity of SD, and the reduction of the AN fibers' spontaneous rate is reflected in a reduction of the spontaneous rate of the PNs (Figs. 8.8d-f, top panels). Type-III (Fig. 8.8d) and type-IV-T PNs (Fig. 8.8e) are similar in that homeostasis is only able to restore the mean firing rate to its target level up to a critical degree of SD. In the model PN with type-III responses, homeostasis saturates at 78% SD, and in a type-IV-T PN at 84% SD (Figs. 8.8d,e, middle panels). After homeostasis, the spontaneous firing rates are slightly decreased for mild SD in both PN types, but increased above the healthy level for moderate-to-severe SD (Figs. 8.8d,e, bottom panels). The peak in the curve of spontaneous firing rate versus SD is created by the saturation of homeostasis (compare section 7.3.2 and Fig. 7.5c_3). In our model for a type-IV PN, the mean and the spontaneous rate are reduced to a similar degree by SD, and both remain close to each other (Fig. 8.8f, top panel). After homeostasis, the mean rate is stabilized at its target level regardless of the severity of SD (Fig. 8.8f, bottom panel), as homeostasis does not saturate (Fig. 8.8f, middle panel). The spontaneous firing rate of a type-IV PN, however, remains below its original level after homeostasis.

We conclude that SD can cause hyperactivity through homeostatic plasticity in DCN type-III and type-IV-T PNs, but not in type-IV PNs.

8.6 Discussion

In this section, we have extended our model to incorporate feedforward inhibition through inhibitory interneurons. Feedforward inhibition is a very common feature that shapes the responses of a variety of neuron types in the auditory brainstem (see, e.g., Rhode and Greenberg, 1992; Irvine, 1992, for reviews). We have implemented a phenomenological model of the basic DCN circuit (Young and Davis, 2002), and we have analyzed how hearing loss through cochlear damage changes the responses of the three model neuron types, wide-band inhibitor (WBI) neurons, narrow-band inhibitor (NBI) neurons, and projection neurons (PNs). Moreover, we have studied the effects of activity stabilization through homeostatic plasticity in the PNs.

Our modeling results show that hearing loss through cochlear damage can either increase

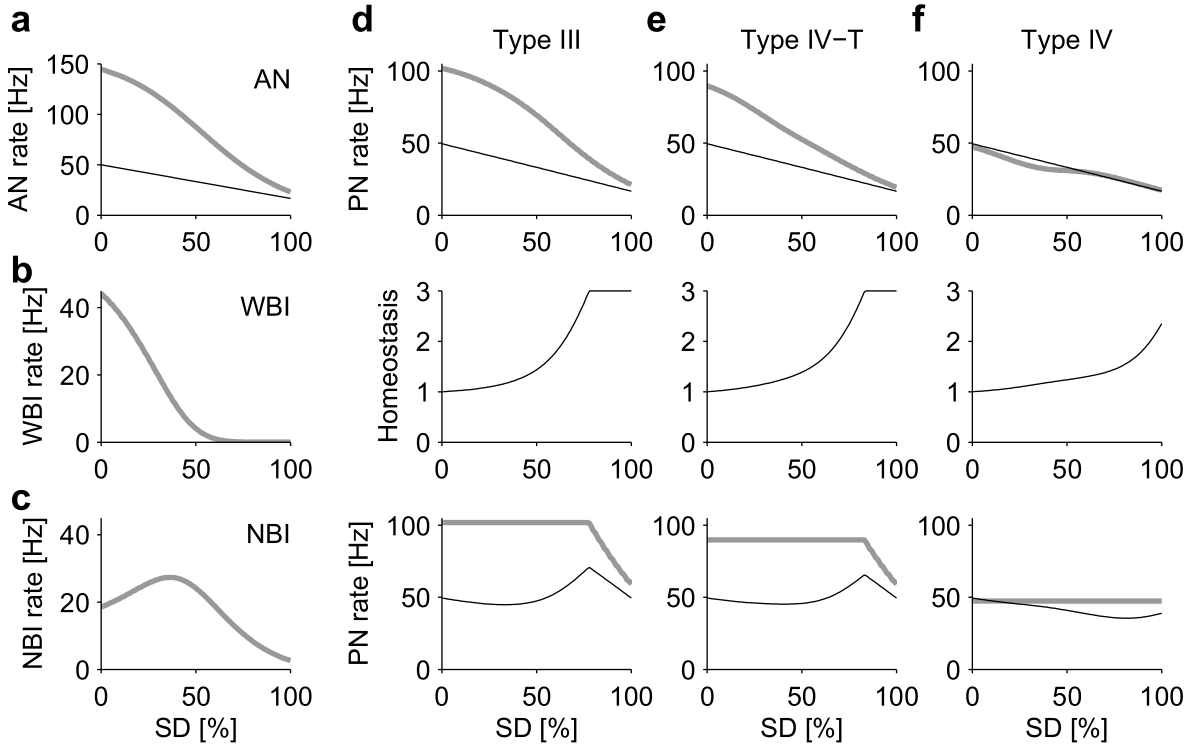

Figure 8.8: Effect of various degrees of SD on the activity of AN fibers, WBI neurons, NBI neurons, and PNs, and consequences of homeostatic activity stabilization in the PNs. **a)** The mean (thick gray line) and the spontaneous rate (thin black line) of AN fibers are decreased by SD. **b)** SD decreases the mean rate of the WBI neuron, which ceases to fire when SD exceeds ca. 75%. **c)** The NBI neuron's mean rate is increased for mild SD due to disinhibition, and decreased for severe SD. **d-f**) PN responses, panels are organized as in Fig. 8.6. **d)** The mean and the spontaneous rate of a type-III PN are decreased after SD. For up to 78% SD, the mean rate can be restored by homeostasis. The spontaneous firing rate is increased after homeostasis when SD exceeds 60%. **e)** SD also reduces the mean and spontaneous firing rate of a type-IV-T PN. Homeostasis restores the mean rate until it saturates at 84% SD. After homeostasis, the spontaneous rate is increased for more then 69% SD. **f)** After SD, the mean and spontaneous rate of a type-IV PN are both reduced by approximately the same degree. Homeostasis can restore the mean rate to its target value for all degrees of SD, whereas the spontaneous rate remains below its healthy level.

or decrease the mean rate of DCN neurons, depending on the strength and distribution of inhibitory inputs. For WBI neurons, we only observed a decrease in mean firing rate, regardless of the kind and severity of cochlear damage, reflecting the decrease in excitatory input from the AN. Increases in the mean rate were observed for NBI neurons after moderate OHC loss (Fig. 8.7c) and SD (Fig. 8.8c), and for type-IV PNs after moderate IHC loss (Fig. 8.6f, top panel). In these cases, the reduction in inhibitory input was stronger than the decrease in excitation from the AN. All other cases of cochlear damage led to a decrease in the mean firing rate. When the mean firing rate of PNs was stabilized by homeostatic plasticity, hyperactivity was observed in type-III and type-IV-T PNs after OHC loss and SD. Moreover, a small increase in spontaneous firing rates was also seen in type-IV PNs after OHC loss, whereas SD led to a decrease in the spontaneous firing rate of type-IV PNs after homeostasis. As in our previous model with excitation only, the development of hyperactivity depends on the relative change of the mean to the spontaneous firing rate after cochlear damage. Hyperactivity only develops when the ratio between mean and spontaneous firing rate is decreased. Moreover, hyperactivity is only a robust phenomenon when the healthy mean rate of a neuron is sufficiently above its spontaneous rate, i.e. when excitation dominates over inhibition. We found this to be the case in type-III and type-IV-T PNs, but not in type-IV PNs. Our example of a type-IV PN only became hyperactive for moderate OHC loss, and only to a small extent (Fig. 8.7f, bottom panel).

Our results offer a possibility to reconciliate contradicting experimental results on DCN hyperactivity: Brozoski et al. (2002) found increased spontaneous firing rates in putative fusiform cells of the chinchilla DCN after acoustic trauma, and also Kaltenbach and Falzarano (2002) reported hyperactivity to be strongest in the fusiform cell layer of the hamster DCN. On the other hand, Ma and Young (2006) found no indications of hyperactivity in principal cells of the cat DCN after acoustic trauma. Given our results, these discrepancies could be explained by differences in the prevailing PN response type in the DCNs of different animal species. In cats, the majority of PNs have been reported to possess type-IV response characteristics (Young, 1980), whereas the rate-intensity functions shown by Brozoski et al. (2002) for their recordings from chinchilla DCN were more reminiscent of type-III or type-IV-T responses. In our model, type-IV PNs do not become hyperactive after SD, whereas type-III and type-IV-T PNs develop increased spontaneous firing rates in the same situation (Fig. 8.8).

Evidences for homeostatic plasticity in the auditory system after hearing loss have already been discussed in the previous chapter. Given our results on homeostasis acting on excitation and inhibition, we postulate that activity stabilization could be the functional principle underlying the decreases in inhibition that have been observed at various stages of the auditory system (see, e.g., Suneja et al., 1998a,b; Potashner et al., 2000; Vale and Sanes, 2002, and also section 3.3).

The connection pattern between AN fibers, inhibitory interneurons, and PNs in our model is based on the basic circuit that has been proposed for the DCN (see Young and Davis, 2002, for a review). How this basic circuit can be employed to reproduce salient response properties of DCN projection neurons has been the focus of several modeling studies (Reed and Blum, 1995; Blum et al., 1995; Zheng and Voigt, 2006b,a). Our model is similar to the model of Reed and Blum (1995), as it is also rate-based, whereas the more recent model of Zheng and Voigt (2006a) employs spiking neurons. Our AN model, however, is simpler than the formalism employed by Reed and Blum (1995), as we consider AN responses only at the characteristic frequency (CF). By varying the strength of the inhibitory projections from the WBI neuron and

the NBI neuron onto the PN, we could tune the PN responses to reproduce the rate-intensity functions of different response classes of DCN principal cells (Fig. 8.3b-d). A possible extension of our model would be to employ a more detailed AN model that also captures the shape of the receptive fields of AN fibers. This would enable our model to reproduce also the response maps of DCN neurons, the weak response of WBI neurons to pure tones (Young and Davis, 2002) and the nonmonotonicity of the rate-intensity functions of NBI (type-II) neurons (Spirou et al., 1999). However, a more detailed AN model would strongly complicate the model and introduce details that are not relevant for the main conclusions. In our reduced model, most of the relevant features can be treated analytically.

A central assumption in our model is that the responses of AN fibers from different frequency channels are mutually independent. While this is certainly justified for fibers whose CFs are far apart, it might not be justified for nearby fibers, as their receptive fields overlap at high intensities. The assumption of independence is most crucial for determining the joint probability distribution of input from AN fibers and WBI neurons in PNs and NBI neurons. When a WBI neuron has a large receptive field and the CFs of most of its afferent AN fibers are far apart from the CF of those fibers that provide input to the corresponding PN and NBI neuron, the assumption of independence might provide a good approximation. In our model, the receptive field of the WBI unit spans one octave, whereas higher values are also found in physiological studies. A larger receptive field of the WBI neuron could be easily constructed in our model without changing the results by letting only every other frequency channel provide input to the WBI neuron. The afferent frequency channels would then be 0.2 octaves apart, also strengthening our independence assumption used in the derivation of the WBI neuron's response distribution. The only alternative to our analytical approach that rests on the assumption of independence would be to use a detailed AN model, and a large repertoire of natural sounds at different intensities as stimuli. However, there are currently no AN models that have been tuned to reproduce the effects of all the different kinds of hearing loss that we consider here. Moreover, the choice of stimuli will also have a significant effect on the results, as they would have to emulate a typical acoustic environment including behaviorally relevant stimuli. However, for animals such as hamsters, rats, or chinchillas that are often used in physiological studies on hyperactivity, little is known about typical acoustic environments and behaviorally relevant acoustic stimuli.

Another assumption in our model is that we included only type I AN fibers, which contact IHCs and constitute about 90-95% of all AN fibers. However, cochlear damage might also influence the activity of type II AN fibers which contact OHCs, and it has been suggested that reduced activity of type II AN fibers, for example after OHC loss, might be involved in the generation of DCN hyperactivity (Kaltenbach et al., 2002) and possibly also tinnitus (Jastreboff and Hazell, 1993): Reduced activity of type II AN fibers could influence DCN neurons via the parallel fiber system and lead to a disinhibition of PNs, thus increasing their spontaneous firing rates. This scenario could be implemented in our model by including an additional inhibitory input to the PNs, with the strength of inhibition reduced by OHC loss. This input would need to be spontaneously active so that its reduction can contribute to hyperactivity. However, as the responses and spontaneous firing rates of type II fibers in vivo have not been characterized yet (Robertson et al., 1999; Reid et al., 2004), we chose not to include them in our current model.

Our results show that activity stabilization by homeostatic plasticity after hearing loss need not automatically lead to the development of hyperactivity. The development of hyperactivity depends on the relative strength of excitatory and inhibitory inputs and on the statistics of the

input signal. Thus, only a fraction of neurons might become hyperactive. In general, the effects of activity stabilization by homeostatic plasticity will depend on the computations a certain neuron performs, how it encodes information, the input statistics it is normally adapted to, and how its input is changed in a pathological situation. In our model, we have assumed that neurons employ a rate code, i.e. all information is contained in the neuron's firing rate and not in the timing of individual action potentials, as our model neurons represent the average responses of small populations of real neurons. When the effects of hearing loss are investigated, a rate code might be a safe assumption: hearing loss predominantly affects the high-frequency range (section 3, Fig. 6.2), and phase-locking of AN spikes to the wave-form of acoustic stimuli breaks down above ca. 1.5 kHz (Cedolin and Delgutte, 2005), suggesting that the corresponding neurons in the early auditory pathway employ rate coding schemes.

Homeostatic plasticity is assumed to act on the single-neuron level in our model. Experimental studies show that there are different kinds of homeostatic mechanisms, single-neuron mechanisms that only regulate the activity of individual neurons (Burrone et al., 2002) and circuit-wide mechanisms that act via neurotrophic factors like e.g. BDNF (Desai et al., 1999a). Thus, also the activity of the inhibitory neurons could be adjusted in a circuit-wide mechanism. For simplicity, we have chosen to consider only homeostasis in the PNs. The effects of homeostatic plasticity in the inhibitory interneurons or homeostasis on the circuit level would be interesting projects for future investigations.

8.7 Methods

We set up a phenomenological model of the responses of AN fibers and DCN neurons. The model is phrased in terms of firing rates of small populations of AN fibers and DCN neurons.

8.7.1 Auditory Nerve Model

Our model of the AN is organized in frequency channels. Each channel comprises fibers with similar characteristic frequencies. We assume ten frequency channels per octave. The responses of the small population of AN fibers in each channel are captured by a population firing rate as described in section 7.7.2; see also Eq. 7.2. How the responses of AN fibers are changed by hearing loss through different kinds of cochlear damage is described in section 7.7.3.

In this framework, responses to pure-tone stimuli are captured by varying the sound intensity in one frequency channel, which leads to a firing rate response according to Eq. 7.2 in the corresponding AN fiber population. The AN fibers of all other frequency channels remain at their spontaneous rate. For broad-band noise, the sound intensity is set to the same value in all frequency channels. Consequently, the AN fiber populations of all frequency channels fire at the same rate in response to broad-band noise. AN responses to notched-noise are approximated by letting all AN fibers of all channels except those with CFs inside the notch fire at the same rate. The fibers with CFs in the notch fire at their spontaneous rate. This corresponds to stimulation by notch noise with an infinite notch depth.

8.7.2 Wide-Band Inhibitor Neuron

The wide-band inhibitor (WBI) neuron receives excitation from the AN fibers of x frequency channels (Fig. 8.1a). The synaptic weights that determine the efficacies for input from each of the x channels are all set to $1/x$. If we assume that the inputs interact linearly, input from x fiber populations firing at rates $f_1, f_2, \ldots, f_{\mathrm{x}}$ leads to a synaptic input s that is given by

$$s = \frac{1}{x} \sum_{\mathrm{i}=1}^{\mathrm{x}} f_{\mathrm{i}}. \tag{8.5}$$

The firing rate w of the WBI neuron is then

$$w = W(s) = [s - \theta_{\mathrm{w}}]_+ , \tag{8.6}$$

where θ_{w} is the firing threshold of the WBI neuron. Assuming that the activities of the AN fibers in different frequency channels are independent, we can obtain the probability distribution $p_{\mathrm{s}}(s)$ of the synaptic input s by convolving the firing rate distributions $p_{\mathrm{f}_1}, p_{\mathrm{f}_2} \ldots, p_{\mathrm{f}_{\mathrm{x}}}$ of all AN frequency channels and scaling by the synaptic weight factor:

$$\begin{aligned} p_{\mathrm{s}}(s) &= x \cdot (p_{\mathrm{f}_1} * p_{\mathrm{f}_2} * \cdots * p_{\mathrm{f}_{\mathrm{x}}})(s \cdot x) \\ &= x \cdot \int_{-\infty}^{\infty} \mathrm{d}f_1 \; p_{\mathrm{f}_1}(f_1) \int_{-\infty}^{\infty} \mathrm{d}f_2 \; p_{\mathrm{f}_2}(f_2) \ldots \int_{-\infty}^{\infty} \mathrm{d}f_{\mathrm{x}} \; p_{\mathrm{f}_{\mathrm{x}}}(s \cdot x - f_1 - f_2 - \cdots - f_{\mathrm{x\text{-}1}}) \end{aligned} \tag{8.7}$$

The convolution is carried out numerically using a MATLAB routine. To obtain the response distribution $p_{\mathrm{w}}(w)$ from the input distribution $p_{\mathrm{s}}(s)$ we apply the response threshold θ_{w}. The WBI neuron does not fire with probability $P_0 = \int_0^{\theta_{\mathrm{w}}} \mathrm{d}s \; p(s)$. In total, the response distribution of the WBI neuron is

$$p_{\mathrm{w}}(w) = P_0 \delta(w) + \begin{cases} p_{\mathrm{s}}(w + \theta_{\mathrm{w}}) & \text{for } 0 < w \le w_{\max} \\ 0 & \text{otherwise,} \end{cases} \tag{8.8}$$

where $w_{\max} = f_{\max} - \theta_{\mathrm{w}}$ is the maximum firing rate of the WBI neuron (with $f_{\max}$ being the maximum firing rate of the AN fibers). The mean rate $\langle w \rangle$ of the WBI neuron is then given by

$$\langle w \rangle = \int \mathrm{d}w \;\; w p_{\mathrm{w}}(w). \tag{8.9}$$

8.7.3 Narrow-Band Inhibitor Neuron

The narrow-band inhibitor (NBI) neuron is excited by AN fibers from a single frequency channel, and inhibited by a WBI neuron (Fig. 8.2a). The firing rate n of a NBI neuron thus depends on the firing rate f of its afferent AN fiber population and on the rate w of the WBI neuron,

$$n = N(f, w) = [f - g_{\mathrm{nw}} w - \theta_{\mathrm{n}}]_+ , \tag{8.10}$$

where $\theta_{\mathrm{n}} = 100\,\mathrm{Hz}$ is the response threshold of the NBI neuron, and $g_{\mathrm{nw}} = 1.5$ is the gain factor of the inhibitory input from the WBI neuron. We choose $g_{\mathrm{nw}} > 1$ and $\theta_{\mathrm{n}} = \theta_{\mathrm{w}}$ so that the NBI neuron does not respond to broad-band noise.

If we assume that the firing rate f of the AN fibers and the firing rate w of the WBI neuron are independent, then the joint probability distribution $p(f,w)$ of these inputs factorizes to $p(f,w) = p_\mathrm{f}(f)p_\mathrm{w}(w)$. The mean rate $\langle n \rangle$ of the NBI neuron is then given by

$$\langle n \rangle = \iint_{f\,w} \mathrm{d}w\,\mathrm{d}f\; p_\mathrm{f}(f)p_\mathrm{w}(w)N(f,w). \tag{8.11}$$

To obtain the response distribution $p_\mathrm{n}(n)$ of the NBI neuron, we first need to obtain the distribution of its effective synaptic input $s = f - g_\mathrm{nw}w$: We scale the distribution p_w of the WBI neuron's responses by the gain factor g_nw to obtain $p_{\mathrm{w}'}(w') = \frac{1}{g_\mathrm{nw}} p_\mathrm{w}(w'/g_\mathrm{nw})$. Then we convolve $p_{\mathrm{w}'}$ with the response distribution p_f of the afferent AN fiber population, which yields the distribution p_s of the effective synaptic input:

$$\begin{aligned} p_\mathrm{s}(s) &= (p_\mathrm{f} * p_{\mathrm{w}'})(s) \\ &= \int \mathrm{d}f\; p_\mathrm{f}(f)p_{\mathrm{w}'}(f-s) \end{aligned} \tag{8.12}$$

This operation is performed numerically using MATLAB. Applying the response function with its firing threshold θ_n then yields the distribution p_n of the NBI neuron's firing rate:

$$p_\mathrm{n}(n) = P_0\delta(n) + \begin{cases} p_\mathrm{s}(n+\theta_\mathrm{n}) & \text{for } 0 < n \le n_\mathrm{max} \\ 0 & \text{otherwise} \end{cases} \tag{8.13}$$

The NBI neuron does not fire with probability $P_0 = \int_0^{\theta_\mathrm{n}} \mathrm{d}s\; p(s)$, and $n_\mathrm{max} = f_\mathrm{max} - \theta_\mathrm{n}$ is its maximum firing rate.

8.7.4 Projection Neuron

The projection neuron (PN) receives excitation from AN fibers of a single frequency channel, and inhibition from a WBI and a NBI neuron. We assume that the PN and the NBI neuron are driven by AN fibers from the same frequency channel. Moreover, we assume that the PN and the NBI neuron are also inhibited by the same WBI neuron. Thus, the rate of the PN is a function of the rate f of the AN fiber population and the rate w of the WBI neuron. We assume a nonlinear response function R with a firing threshold at 0 Hz and a maximum firing rate response of $r_\mathrm{high} = 300\,\mathrm{Hz}$. The response r of the PN is then given by

$$r = R(f,w) = r_\mathrm{high} \tanh\left(\frac{[f - g_\mathrm{w}w - g_\mathrm{n}N(f,w)]_+}{r_\mathrm{high}}\right). \tag{8.14}$$

The gain factors g_w and g_n determine the strength of inhibition from the WBI and NBI neuron, respectively. The mean rate $\langle r \rangle$ of the PN can be calculated by

$$\langle r \rangle = \iint_{f\,w} \mathrm{d}w\,\mathrm{d}f\; p_\mathrm{f}(f)p_\mathrm{w}(w)R(f,w). \tag{8.15}$$

8.7.5 Homeostasis in the Projection Neuron

Homeostasis is assumed to stabilize the mean rate of only the PN. We consider homeostasis through synaptic scaling (Turrigiano et al., 1998; Kilman et al., 2002): the gain of excitatory inputs is multiplied by the homeostasis factor h, whereas the gain of inhibitory inputs is divided by h. The response r of a PN in dependence upon the value of the homeostasis factor is then given by

$$r = R(f,w,h) = r_{\text{high}} \tanh\left(\frac{h \cdot f - \frac{g_{\text{w}}}{h} w - \frac{g_{\text{n}}}{h} N(f,w)}{r_{\text{high}}}\right). \tag{8.16}$$

Thus, the mean rate of a PN can be adjusted by changing the value of h. The target mean rate r^* of homeostasis is defined as the mean rate obtained for input from an undamaged cochlea and $h = 1$. The exact value of h that is necessary to adjust the mean firing rate $\langle r \rangle$ of the projection neuron to the target level r^* is determined numerically. To account for physiological constraints on synaptic strength, h is limited to the interval $[0.3, 3]$.

Chapter 9

Predicting Tinnitus Pitch from Patients' Audiograms

In the previous chapters, we have shown that the pitch of the tinnitus sensation depends on the severity and frequency-extent of hearing loss (chapter 6), and we have developed a model of how hearing loss could lead to increased spontaneous firing rates in the auditory brainstem that might be perceived as tinnitus (chapters 7 and 8). We now test this model by applying it to data from patients with tone-like tinnitus. The model is used to predict changes in spontaneous firing rates of neurons in the auditory pathway from the audiograms of the patients. Then we assess whether the tinnitus pitch predictions derived from these patterns of spontaneous activity are consistent with the results of tinnitus pitch matching by the patients. Finally, we compare the pitch-prediction performance of our model to another model of tinnitus generation, the lateral-inhibition model of Gerken (1996).

To facilitate pitch prediction, we extend the model by introducing an additional layer of neurons. The neurons in this layer are connected by lateral inhibitory connections and could represent processing in higher auditory structures. Lateral inhibition leads to a sharpening of peaks and an exaggeration of edges in the activity patterns. The perceived pitch of an activity pattern in the model is then assumed to be determined by the characteristic frequency of the neuron with the highest spontaneous firing rate in the lateral inhibition layer.

9.1 Architecture of the Model for Pitch Prediction

The model we use for pitch prediction has three stages, first the auditory nerve (AN), then the dorsal cochlear nucleus (DCN), and finally a layer with lateral inhibition (LI) that represents processing in higher auditory structures. The model is organized in frequency channels that are arranged tonotopically from low to high frequencies (Fig. 9.1a). We assume 10 frequency channels per octave. As the model covers the six octaves of an audiogram from 125 Hz to 8 kHz, we have 61 frequency channels in total. We assume the same distribution of sound intensities for all frequency channels.

The activity of AN fibers in each frequency channel is described by a population firing rate as introduced in section 7.2.1. The properties of the population response are adjusted to capture the effects of the patients' hearing loss (see below). The AN stage provides input to the neurons of the DCN stage. In each frequency channel, we have three DCN neurons: a wide-band inhibitor (WBI) neuron, a narrow-band inhibitor (NBI) neuron, and a projection neuron

(PN), connected as described in the previous chapter. These model neurons represent average responses of small populations of real neurons. The PNs of the DCN stage provide input to the neurons of the LI layer.

The neurons of the LI layer are connected by lateral inhibitory connections. We assume a unimodal distribution of inhibitory projections. The connection pattern and the synaptic weights of the inhibitory projections of one neuron are illustrated in Fig. 9.1b. The strength of a connection depends on the distance between the neurons, and the shape of the distance dependence is given by a cosine function (dotted line in Fig. 9.1b, see Methods Eq. 9.2). The maximum width of the distribution is determined by the parameter σ, which we set to $\sigma = 3$ frequency channels, and the maximum weight is given by $w_{\max}$, which we set to $w_{\max} = 0.8$.

The lateral inhibition model of tinnitus generation proposed by Gerken (1996) can be reimplemented in our framework by disabling homeostatic plasticity in the cochlear nucleus stage and changing the weight distribution of the lateral inhibitory connections in the LI layer to a bimodal shape (Fig. 9.1c). The pattern of the lateral inhibitory connections is then governed by σ, $w_{\max}$ and additionally the offset parameter μ. For the Gerken-model, we chose the parameters to be $\sigma = 3$, $w_{\max} = 0.25$, and $\mu = 5$.

9.2 Modeling Human Hearing Loss

As a first step, we need to capture the patients' hearing loss with our auditory nerve model. All patients have noise-induced hearing loss. Therefore we assume that the underlying cochlear damage is noise-induced stereocilia damage (see section 3.1.1). From the patients' audiograms, we obtain the hearing thresholds and set the response thresholds of the model AN fiber populations of each frequency channel accordingly. Depending on the degree of threshold increase, we adjust the spontaneous firing rates of the AN fiber populations . To estimate the hearing thresholds at frequencies between the audiogram test tones (0.125, 0.25, 0.5, 1, 2, 3, 4, 6, and 8 kHz), we interpolate the audiograms linearly (see Methods). Our original model for stereocilia damage captures hearing loss of only up to 80 dB (section 7.2.1). Some patients, however, have greater hearing loss at some frequencies (see Fig. 6.1). We therefore extend our formalism to threshold increases of up to 120 dB (Eq. 9.1).

9.3 Predicting Tinnitus Pitch from a Patient's Audiogram

We now demonstrate how we use the model to derive a prediction of tinnitus pitch from an audiogram. Fig. 9.2a shows the audiogram of an example patient. This patient has noise-induced hearing loss exclusively in the high-frequency range above 1.5 kHz, and he matched his tinnitus pitch to a comparison tone of 4 kHz. As described above, the interpolated hearing thresholds obtained from the patient's audiogram are used to adjust the response properties of the model's AN stage to capture the patient's hearing loss. The resulting activity profiles of the model AN are shown in Fig. 9.2b. We find that the mean (thick gray line) and the spontaneous firing rates (thin black line) are reduced in the high-frequency range. This decrease in auditory nerve activity also decreases the excitatory drive for cochlear nucleus neurons.

In our example, we set the gain factors for the inhibitory inputs to the DCN projection neurons to $g_{\mathrm{n}} = 1.0$ for inhibition from the NBI neuron and $g_{\mathrm{w}} = 0.5$ for inhibition from the WBI neuron. This results in response properties that are in-between type-III and type-IV-T response

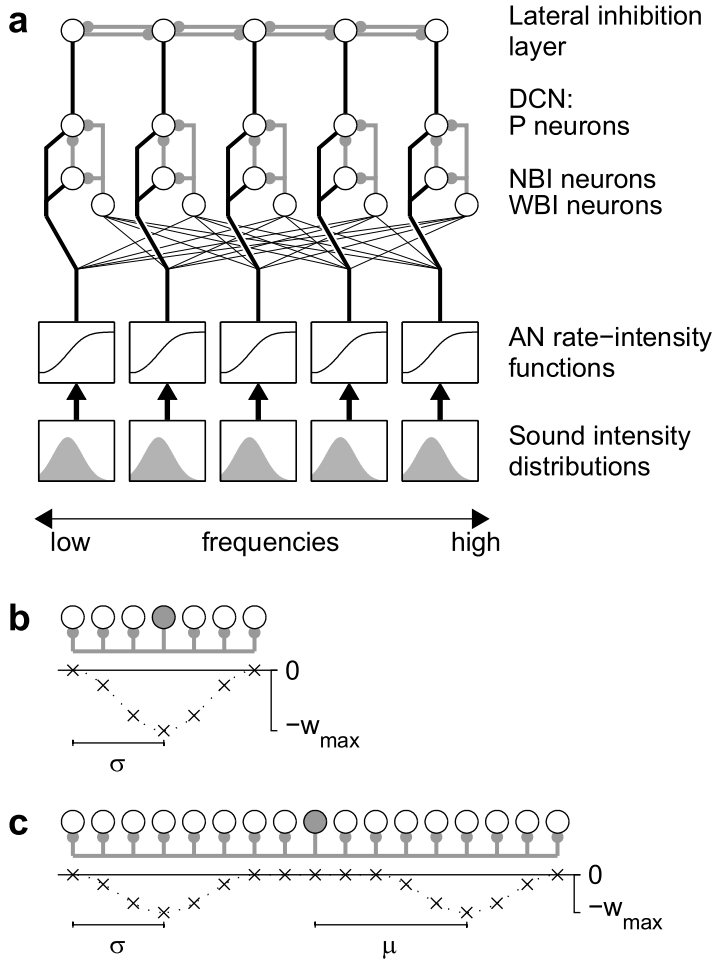

Figure 9.1: Architecture of the model for pitch prediction. **a)** Schematic picture of the model. Neurons are indicated by black circles, excitatory connections by black lines, and inhibitory connections by gray lines. The model is organized in frequency channels that are tonotopically arranged from low to high frequencies, 5 channels are shown. The distributions of sound intensity of all frequency channels form the acoustic environment. In each channel, sound intensity is transformed to AN activity by a rate-intensity function. The AN fibers provide excitatory input to neurons in the dorsal cochlear nucleus (DCN) stage of the model. There are projection neurons (PNs) and inhibitory interneurons (narrow-band inhibitor, NBI, and wide-band inhibitor, WBI). The P neurons of the DCN provide excitatory input to the neurons of the lateral inhibition layer. These neurons send lateral inhibitory projections to their neighbors. **b)** Illustration of the unimodal distribution of lateral inhibitory projections (gray lines) originating from any neuron (gray circle) in the lateral inhibition layer. The strength of the connections is indicated by the crosses, the dotted line depicts the shape of the synaptic weight function. The width of lateral inhibition is determined by the parameter σ, its maximum strength by $w_{\max}$. **c)** Illustration of the bimodal distribution of lateral inhibitory projections in the Gerken-model. The additional parameter μ determines the offset.

properties (see section 8.4.1), thus representing these classes of DCN neurons. Noise-induced hearing loss decreases the mean and spontaneous firing rates of these PNs, thus we observe a decrease in mean and spontaneous firing rates in the high-frequency range (Fig. 9.2c). The decrease in the mean firing rates activates homeostatic plasticity in the affected PNs. We assume that homeostasis acts on the single-neuron level, i.e. each PN individually tries to stabilize its mean firing rate. To counteract the reduction of a PN's mean firing rate after hearing loss, homeostasis increases the strength of excitatory synapses and decreases inhibitory synaptic strengths (see section 8.4.4). For our example patient, homeostasis is able to stabilize the mean firing rates of all CN PNs at their target level (Fig. 9.2d, thick gray line). The spontaneous firing rates, however, are increased after homeostatic plasticity in those PNs that receive input from the damaged parts of the cochlea (Fig. 9.2d, black line), and the degree to which the spontaneous firing rates are elevated in the PNs of each frequency channel depends on the severity of hearing impairment at this frequency. The shape of the resulting profile of spontaneous firing rates therefore 'mirrors' the shape of the audiogram.

The neurons of the LI layer, the next processing stage of the model, receive excitatory input from the projection neurons of the DCN. When the lateral inhibition layer is excited by the pattern of DCN spontaneous firing rates after homeostasis (Fig. 9.2e), the edge effect of lateral inhibition creates an even more distinct peak (Fig. 9.2f). The peak is located at a frequency above the audiogram edge, where hearing is impaired. If such a peak is interpreted as the basis for a tone-like tinnitus sensation, with a perceived pitch that corresponds to the characteristic frequency of the neuron with the highest firing rate, the model predicts a tinnitus pitch of 3.0 kHz. This prediction is 0.42 octaves lower than the patient's tinnitus pitch matching result of 4.0 kHz.

This tinnitus pitch prediction procedure is applied to all audiograms from all patients. The scatter plot in Fig. 9.3a shows the relation of model predictions to the observed tinnitus pitch. Many predictions deviate by less than 0.5 octaves. To assess the overall prediction quality of the model we calculate three quantities: First, the root mean squared deviation, that quantifies how far on average a prediction of the model deviates from the corresponding tinnitus pitch matching result and thus quantifies the average prediction error. Second, the mean deviation, which evaluates the prediction bias. Third, the correlation between predicted and observed tinnitus pitch. Although these quantities are related to each other (see Methods, Section 9.7.6), all values are given to allow for an easy judgement of the prediciton performance. We obtain an average prediction error of 0.6 octaves, which is comparable to the uncertainty of tinnitus pitch matching (Burns, 1984; Henry et al., 2004). The bias of the predictions is only -0.04 octaves, and the distribution of the deviations (black bars in Fig. 9.3c) is fairly symmetric. Finally, the correlation between predicted and observed pitch is 0.49 ($p = 0.0005$), which is higher than the value of 0.3 obtained for the correlation between audiogram edge frequency and tinnitus pitch

9.4 Homeostatic Plasticity is Essential for Tinnitus Pitch Prediction

The stabilization of the mean firing rate by homeostatic plasticity is an essential ingredient of the model, as this mechanism can lead to the development of increased spontaneous firing rates in the frequency-range where hearing is impaired. For comparison, we now evaluate the model without homeostatic plasticity. When we disable homeostasis in the DCN stage and change the

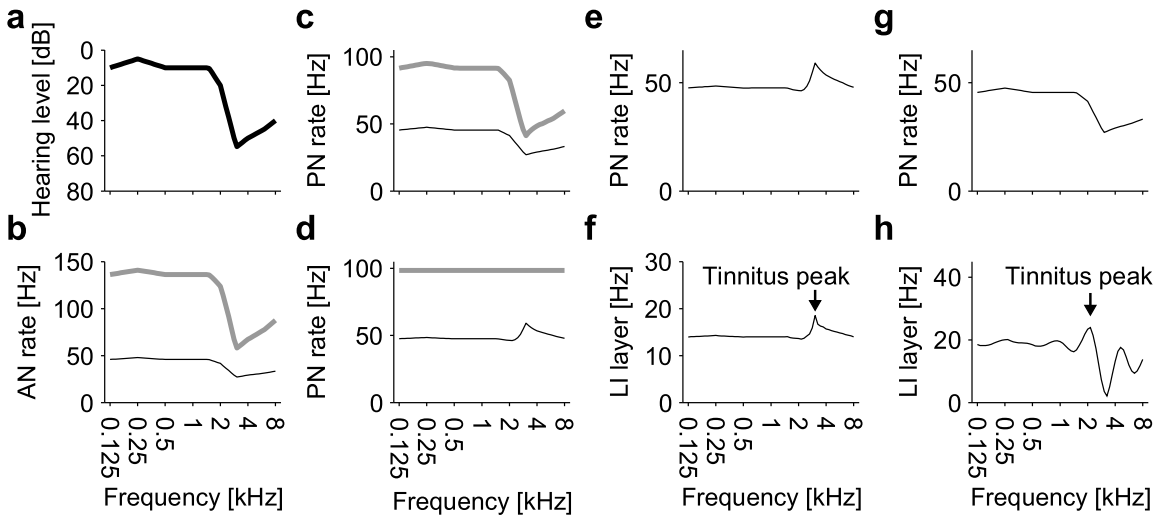

Figure 9.2: Illustration of tinnitus-pitch prediction. **a)** Example audiogram of a patient with noise-induced hearing loss and a tinnitus pitch of 4 kHz. **b)** Activity of model AN fibers adjusted to the patient's hearing loss: the mean (thick gray line) and the spontaneous firing rates (thin black line) are decreased in the frequency-range that is affected by hearing loss. **c)** Before homeostasis, the mean and spontaneous firing rates of PNs of the DCN are decreased in the high-frequency range. **d)** After homeostasis, the mean firing rates of the PNs are restored to their healthy levels, whereas the spontaneous firing rates are increased in the high-frequency range. **e)** Enlarged view of the pattern of PN spontaneous firing rates along the tonotopic axis of the DCN after homeostasis. **f)** When driven by the firing-rate pattern shown in e), the firing rates of the neurons of the lateral inhibition layer display a distinct peak. It corresponds to a characteristic frequency of 3 kHz, 0.42 octaves below the observed tinnitus pitch. **g)** Pattern of spontaneous firing rates of PNs along the tonotopic axis of the DCN in the reimplementation of the Gerken model. It is identical to the spontaneous firing rate profile shown in c. **h)** In the Gerken model, the most prominent activity peak in the lateral inhibition layer is located at 2 kHz, close to the audiogram edge and one octave lower than the observed tinnitus pitch.

pattern of lateral inhibition in the LI layer to a bimodal shape (Fig. 9.1c), the resulting model corresponds to the model of tinnitus generation proposed by Gerken (1996). The Gerken model assumes that tinnitus-like activity patterns can be generated when lateral inhibition exaggerates structures in the spontaneous activity in the auditory system: Noise-induced hearing loss, for example, decreases the spontaneous firing rates of AN fibers in the high-frequency range and thus creates an edge in the profile of the spontaneous firing rate of AN fibers along the tonotopic axis (see also Fig. 9.2a). If such a pattern of spontaneous activity excites a neuronal structure with lateral inhibitory connections in the central auditory system, lateral inhibition can create a peak that might be perceived as a tone (Gerken, 1996). The results of the Gerken model do not crucially depend on the pattern of lateral inhibition. A unimodal pattern yields similar results, with the most prominent activity peaks at frequencies near the audiogram edge (not shown). The bimodal pattern, however, produces more pronounced peaks than the unimodal pattern.

Figure 9.2g shows the profile of PN spontaneous firing rates in the DCN without homeostatic plasticity. The spontaneous firing rates are decreased in the high-frequency range, as observed also in the AN. If this profile of spontaneous firing rates excites the central layer of neurons with lateral inhibition, the edge effect of lateral inhibition also creates a peak (Fig. 9.2h), but the peak is located at frequencies close to the audiogram edge. The resulting tinnitus pitch prediction of 2.0 kHz is one octave lower than the patient's tinnitus pitch match. When we process all patients' audiograms with this model, the correlation between predicted and observed tinnitus pitch is 0.37 ($p = 0.01$). The average prediction error, however, is 1.46 octaves, and bias of the predictions is -1.28 octaves. The scatter plot of tinnitus pitch predicted by the Gerken model versus the observed pitch (Fig.9.3b) and the distribution of the Gerken model's predictions (Fig. 9.3c, gray bars) also show that tinnitus pitch is predicted systematically too low by this model. This is due to the fact that it predicts tinnitus pitch to be near the audiogram edge (Fig. 9.2h), whereas tinnitus pitch is matched to frequencies above the audiogram edge by almost all patients (Fig. 6.1b).

9.5 Performance of the Homeostasis Model for Different PN Types

In Chapter 8 we have demonstrated that the development of hyperactivity in the PNs of our DCN model depends on the relative strength of excitation and inhibition. After noise-induced stereocilia damage, hyperactivity only develops in type-III and type-IV-T PNs, and not in type-IV PNs. In type-III and type-IV-T neurons, excitation dominates over inhibition, leading to mean firing rates above the spontaneous firing rate, whereas type-IV responses are characterized by strong inhibition, which is reflected in a mean firing rate that is close to the spontaneous firing rate. To analyze the influence of inhibition on the model's ability to predict tinnitus pitch, we systematically vary the two inhibitory gain factors of the PNs: the gain factor g_{w} for inhibitory input from the WBI neuron is changed from 0 to 1.5 in steps of 0.5, and the gain factor g_{n} which regulates the efficacy of inhibition from the NBI neuron is varied from 0 to 3 in steps of 0.5. Thus, we obtain 28 different PN variants in total.

We perform the pitch prediction procedure described above for all 28 model variants with different PN response types. The performance of the model variants is judged against a simple estimator of tinnitus pitch, the frequency of the audiogram edge plus the mean distance between audiogram edge and tinnitus pitch. For this estimator, we obtain a root mean squared

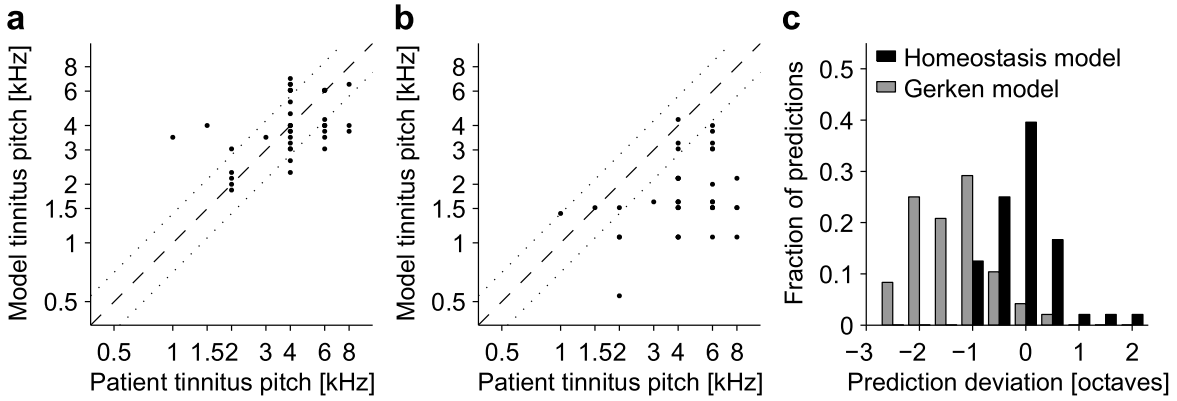

Figure 9.3: Pitch prediction performance of the homeostasis and the Gerken model. **a)** Scatter plot of tinnitus pitch predicted by the homeostasis model versus the tinnitus pitch matching results of the patients. The dotted lines indicate the interval of ± 0.5 octaves around the observed tinnitus pitch (dashed line). **b)** Scatter plot of tinnitus pitch predicted by the reimplementation of the Gerken model versus measured tinnitus pitch. **c)** Deviation of the tinnitus pitch predictions of the homeostasis model (black bars) and the Gerken model (gray bars) from the patients' tinnitus pitch matching results, same data as in a and b. The mean deviation of the Gerken model's predictions is -1.28 octaves, thus pitch is predicted systematically too low. The predictions of the homeostasis model have a mean deviation of -0.04 octaves from the observed pitch.

deviation of 0.81 octaves between predicted and measured tinnitus pitch, and a correlation of 0.3. Model variants yielding a higher correlation and a lower average prediction error than the simple estimator are indicated with a '+' in Fig. 9.4a. We find that the model predicts pitch with low prediction error and high correlation when the PNs receive low to medium inhibition. For strong inhibition, the model predictions are inconsistent with the data. The exact type of inhibition does not seem to be important, as demonstrated by the fact that accurate pitch prediction is possible from PNs receiving only wide-band inhibition, only narrow-band inhibition, or combinations of both kinds of inhibition. The highest correlation between predicted and observed tinnitus pitch is 0.52, and the lowest average prediction error is 0.6 octaves. When we pool the predictions from all those PN variants that yielded a better pitch prediction performance than the simple pitch estimator derived from the audiogram edge ('+' cases in Fig. 9.4a), we obtain a correlation of 0.40, an average prediction error of 0.69 octaves, and a prediction bias of -0.15 octaves.

We further analyze the performance of the model variants by plotting the correlation and the mean absolute deviation against the healthy ratio of the mean to the spontaneous rate (Fig. 9.4c,d). By 'healthy ratio' we mean the ratio between mean and spontaneous rate before hearing loss. Tinnitus pitch can be successfully estimated from the spontaneous firing rate profiles of those projection neurons whose mean-to-spontaneous ratio exceeds ca. 1.75. All of our model PN types have a healthy spontaneous rate of 50 Hz, thus the healthy mean rate must be higher than ca. 87.5 Hz, like for example in type-III and type-IV-T PNs.

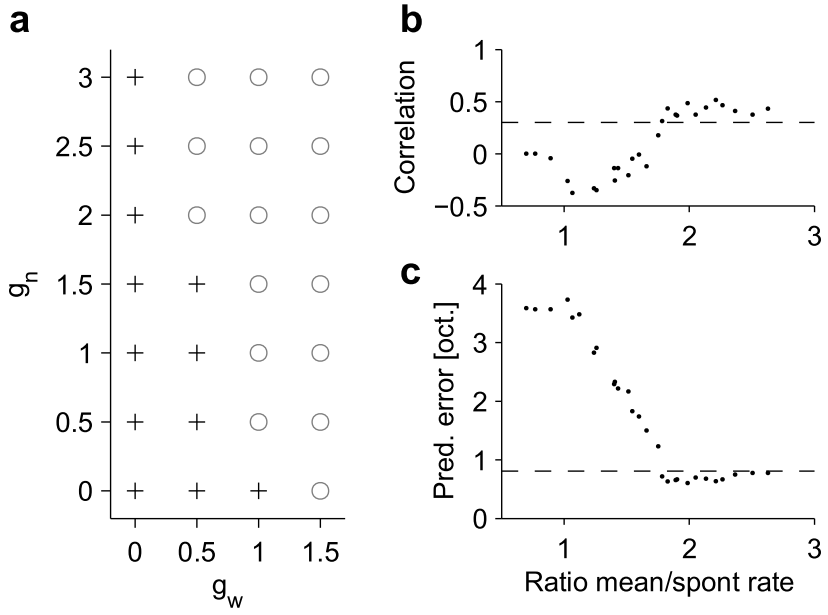

Figure 9.4: Pitch prediction and strength of inhibition in the DCN. **a)** Model performance for different values of the parameters g_w and g_n that lead to different response types of the PNs. The performance is compared to tinnitus pitch prediction from the audiogram edge frequency, which yields a correlation of 0.3 and a root mean squared deviation of 0.81 octaves between predicted and measured tinnitus pitch. A plus (+) sign indicates that for this parameter combination, the correlation exceeds 0.3, and the prediction error (root mean squared deviation) is lower than 0.81 octaves. Parameter combination with worse performance are indicated by circles (o). **b)** Correlation between predicted and observed tinnitus pitch versus the ratio between mean and spontaneous firing rate of the model PNs before hearing loss. The dashed line indicates the correlation between the audiogram edge and the tinnitus pitch. **c)** Prediction error of the model predictions versus the healthy ratio between mean and spontaneous firing rate. The dashed line gives the mean absolute deviation of tinnitus pitch prediction from the audiogram edge frequency.

9.6 Discussion

We have presented a computational model that predicts changes in the spontaneous firing rates of neurons in the auditory brainstem after hearing loss. When the model is applied to the audiograms of tinnitus patients, the predicted patterns of spontaneous firing are consistent with the pitch of the patients' tinnitus sensation. To our knowledge, this is the first model of tinnitus development that has been successfully applied to patient data.

All tinnitus patients had moderate to severe noise-induced hearing loss in the high-frequency range and tone-like tinnitus. This group of patients was chosen because the etiology of hearing loss was known, and the effects of noise overexposure on cochlear hair cells have been studied in detail in various animal studies (see, e.g., Liberman, 1984; Kaltenbach et al., 1992; Emmerich et al., 2005). Estimation of the cochlear damage underlying the observed hearing loss is crucial for applying the model to patient data, as the development of increased spontaneous firing rates in our model is sensitive to the exact type and extent of cochlear damage. For this patient sample, we captured the effects of noise-induced hearing loss using a model for the effects of noise-induced stereocilia damage. Our approach, however, was limited by the fact that no psychophysical tests were performed to determine whether some of our subjects had cochlear dead regions. These dead regions are assumed to be caused by IHC loss and are not necessarily visible in normal audiograms (Moore et al., 2000).

In our model, we assumed that increased spontaneous firing rates in neurons of the ascending auditory pathway may provide the basis for a tinnitus sensation. Moreover, we assumed that homeostatic plasticity after hearing loss can lead to the development of such increased spontaneous firing rates. Homeostasis was assumed to be active in the DCN, the first stage of the auditory pathway where tinnitus-related increases in spontaneous firing rate have been observed. To capture the responses of DCN neurons, we have employed a simplified phenomenological model of the DCN circuitry that can reproduce salient features of the responses of DCN projection neurons. As demonstrated in the previous chapter, the development of hyperactivity in the PNs of the DCN model depends on the type and severity of hearing loss as well as on the PN response type. Here, we obtained good pitch prediction results for type-III and type-IV-T PNs which develop robust hyperactivity. Tinnitus pitch prediction was not possible for type-IV PNs which do not become hyperactive after SD.

We have reimplemented the tinnitus model of Gerken (1996) for comparison. This model assumes that hearing loss induces discontinuities of the spontaneous AN activity along the tonotopic axis. These discontinuities are exaggerated by lateral inhibition in higher auditory structures to give rise to tinnitus-related activity peaks. The greatest discontinuity in AN activity after noise-induced hearing loss, however is around the audiogram edge. Therefore such a model predicts tinnitus pitch systematically too low (see Fig. 9.3). The main difference between the Gerken model and our model is activity stabilization through homeostatic plasticity. Thus, we could demonstrate that homeostatic plasticity is an essential ingredient for obtaining tinnitus pitch predictions that are consistent with patient data.

In our model, hyperactivity of DCN neurons gives rise to tinnitus-like activity patterns in higher auditory structures. This, however, does not mean that we propose DCN hyperactivity as the only cause for tinnitus. Our results are better interpreted such that homeostatic plasticity could lead to hyperactivity in a fraction of neurons in the auditory pathway. These neurons are characterized by a mean rate that is above the spontaneous rate. Moreover, only neurons that receive excitatory input from damaged parts of the cochlea can become hyperactive, thus

the spontaneous firing rates are only increased in those frequency channels where hearing loss is present. A model that incorporates activity stabilization through homeostatic plasticity thus automatically predicts changes in neuronal activity in a range of frequencies that is consistent with tinnitus pitch observed in patients.

The evaluation of tinnitus pitch in our model relies on the assumption of a rate-place code, i.e. the dominant pitch is assumed to be determined by the location of the neuron with the highest firing rate along the tonotopic axis. The pitch of a sound, however, could also be encoded in the temporal pattern of the neuronal discharge. As far as tinnitus is concerned, a rate-place code might be the more probable assumption, as tinnitus pitch is usually matched to comparison tones above 2 kHz (Henry et al., 1999; König et al., 2006). In this frequency range, temporal coding of pitch using interspike-interval representations is not possible (Cedolin and Delgutte, 2005) because phase-locking of AN activity breaks down above ca. 1 kHz. Moreover, pitch-sensitive neurons in the auditory cortex are arranged in an ordered, tonotopic fashion (Bendor and Wang, 2005), which also implies a place code for pitch in higher stages of auditory processing.

Tinnitus pitch matching can be highly variable (Burns, 1984; Henry et al., 2004), especially when pure tones are used as comparison stimuli, as these may strongly differ from the timbre of the tinnitus. Moreover, in the data we used for this study, clinical audiometers were used to generate the comparison stimuli for tinnitus pitch determination. As the tones produced by audiometers are spaced at intervals of approximately 0.5 octaves, this might have added to the error of tinnitus pitch determination. The result of an average prediction error of 0.69 octaves for our model compares well to the average range of 2.3 octaves that has been reported for tinnitus pitch matching results of individual subjects (compare also the distribution of the deviations of the model's predictions in Fig. 9.3). Thus, the prediction error of our model can be considered to be close to the error of tinnitus pitch determination itself. Moreover, for a wide range of parameters (see Fig. 9.4a), the accuracy of the model's pitch predictions exceeds the performance of a simple estimator that predicts tinnitus pitch based on the audiogram edge frequency. Within this parameter range, the prediction performance of the model is relatively constant. Outside the parameter range, however, the performance breaks down rapidly, so pitch prediction either works well or fails completely (Fig. 9.4b,c). Fitting of the parameters of the model's DCN stage in a sense of 'training' is not possible. Moreover, the parameters of lateral inhibition in the LI layer were kept constant for all different parameter combinations in the DCN stage.

A tinnitus sensation may be complex and it can consist of multiple components instead of just a pure tone. This is reflected for example in tinnitus spectra that are obtained when patients are asked to judge the contribution of comparison tones to their tinnitus sensation. These spectra usually span a broad frequency range (Noreña et al., 2002). For certain audiogram shapes, our model model predicts spontaneous activity patterns that are elevated over broad frequency ranges, with several peaks (not shown). Such patterns could constitute the basis for complex tinnitus sensations. The model, however, is limited by the limited accuracy of the audiometric data available, therefore we cannot predict the quality or timbre of the tinnitus sensation.

So far, our model considers activity stabilization only through plasticity in the auditory brainstem. After hearing loss, a variety of plastic changes has also been observed at other stages of the auditory system, for example reorganization of the tonotopic map in primary auditory cortex (Rajan et al., 1993; Irvine and Rajan, 1997). Such reorganization has been proposed to be involved in the generation of tinnitus (Rauschecker, 1999; Eggermont and Roberts,

2004). Nevertheless, already the patterns of increased spontaneous firing rates observed in the brainstem stage of our model are generally consistent with observed tinnitus pitch. We would thus expect similar results if reorganization was incorporated into the lateral inhibition stage of our model, as the location of activity maxima in the LI layer would still be determined by the activity patterns of the brain stem stage.

A future perspective would be to combine our model with a detailed model of cochlear processing. A realistic model of cochlear processing as a front-end to an extended, spike-based model of auditory processing and tinnitus development would enable us to present a variety of stimuli and to determine their effect on tinnitus-related hyperactivity. This would permit us to test the validity of our tinnitus model in more detail, for example masking curves could be obtained and compared to those measured in tinnitus patients. Moreover, we could implement a personalized tinnitus model for each tinnitus patient and determine the effects of various treatment strategies like for example hearing aids and masking devices with different settings. However, detailed high-resolution audiometry and psychophysical tests to characterize the status of the cochlear hair cells would be an essential prerequisite for such a project. We might then also be able to predict which kinds and characteristics of hearing loss lead to tinnitus.

9.7 Methods

9.7.1 Patients: Audiology and Tinnitus Pitch Matching

The sample of tinnitus patients used to evaluate the model comprises the patients with tone-like tinnitus of the patient data analysis presented in chapter 6. Therefore, see sections 6.1.1 and 6.1.2 for details on how audiograms were obtained and how tinnitus pitch matching was performed.

9.7.2 Interpolation of the Audiograms

The audiograms are interpolated linearly between the test frequencies of the clinical audiograms (0.125, 0.25, 0.5, 1, 1.5, 2, 3, 4, 6, and 8 kHz). The audiogram frequencies are first transformed to a logarithmic scale, and the hearing threshold for intermediate frequencies are given by a straight line fitted through the two adjacent audiogram points.

9.7.3 Auditory Nerve Model and Hearing Loss

We employ the AN model introduced in sections 7.7.2 and 7.7.3. We choose the framework for noise-induced stereocilia damage to capture the effects of noise-induced hearing loss on auditory nerve activity. The model is organized in frequency channels, and we employ 10 channels per octave. Thus, for the six octaves of an audiogram from 125 Hz to 8 kHz, we have 61 frequency channels in total. For each frequency channel, the response threshold I_{th} of the AN fiber population is set to the corresponding hearing threshold of the interpolated audiogram. To capture the effect of noise-induced stereocilia damage on the spontaneous rate of AN fibers, the spontaneous firing rate f_{sp} is decreased linearly according to the threshold increase:

$$f_{\mathrm{sp}}(I_{\mathrm{th}}) = f_{\mathrm{sp}} \cdot \left(1 - \frac{I_{\mathrm{th}}}{120\mathrm{dB}}\right) \tag{9.1}$$

For a threshold increase of 120 dB, the spontaneous firing rate is thus decreased to 0 Hz.

9.7.4 Dorsal Cochlear Nucleus Stage

We employ the model for the basic dorsal cochlear nucleus circuit derived in the previous chapter. To systematically test different PN response types, we vary g_{w} from 0 to 1.5 in steps of 0.5 and g_{n} from 0 to 3 in steps of 0.5. As in the previous chapter, we assume that homeostasis is only active in PNs.

9.7.5 Lateral Inhibition Layer

The neurons of the lateral inhibition layer receive excitatory input from the corresponding PNs of the DCN stage (see Fig. 9.1), and they are connected by inhibitory synapses. The pattern as well as the strength of the inhibitory connections are contained in the connection matrix $\mathbf{W}$, with the matrix component w_{ij} representing the strength of the synapse from neuron j to neuron i. For the arborization function of the lateral inhibition we use a cosine, the inhibition toward lower and higher frequencies is chosen to be symmetric. The weight w_{ij} for the inhibitory connection from neuron i to neuron j is then given by

$$w_{\mathrm{ij}} = \begin{cases} -w_{\max} \cdot \frac{1}{2}\left(1+\cos\left(\frac{\pi(i-j)}{\sigma}\right)\right) & \text{for } |i-j| \leq \sigma \\ 0 & \text{otherwise,} \end{cases} \tag{9.2}$$

where $w_{\max}$ denotes the maximum strength of the inhibitory synapse and σ the width of the arborization pattern of the inhibitory connections (see also Fig. 9.1b). We set the maximum strength to be $w_{\max} = 0.8$ and the with to be $\sigma = 3$ frequency channels.

To produce a bimodal distribution of inhibitory connections (Fig. 9.1c) as employed in the model by Gerken (1996), we introduce an additional offset parameter μ. The weights of the inhibitory connections are then given by

$$w_{\mathrm{ij}} = \begin{cases} -w_{\max} \cdot \frac{1}{2}\left(1+\cos\left(\frac{\pi(i-j-\mu)}{\sigma}\right)\right) & \text{for } |i-j-\mu| \leq \sigma \\ -w_{\max} \cdot \frac{1}{2}\left(1+\cos\left(\frac{\pi(i-j+\mu)}{\sigma}\right)\right) & \text{for } |i-j+\mu| \leq \sigma \\ 0 & \text{otherwise.} \end{cases} \tag{9.3}$$

For the reimplementation of the Gerken-model, we set the parameters to $w_{\max} = 0.25$, $\sigma = 3$, and $\mu = 5$.

To avoid edge effects at the lower and upper border of the neuronal structure, we extend the assembly of model neurons by three times its original size in both directions. The input patterns are also extended by assigning the firing rate of the last neuron at each border to all extra neurons in the corresponding direction.

In the absence of acoustic stimulation, the PNs of the model DCN fire at constant rate $\vec{r}_{\mathrm{sp}} = (r_1, r_2, ..., r_{61})$, with r_{i} being the firing rate of PN i. The activity $\vec{a}$ of the neurons in the LI layer then develops according to the differential equation

$$\tau \dot{\vec{a}} = -\vec{a} + [\vec{r}_{\mathrm{sp}} + \mathbf{W} \cdot \vec{a}]_+, \tag{9.4}$$

where $\tau = 10$ ms is the time-constant of the neurons, and $[...]_+$ denotes positive rectification. To obtain the steady-state activity, we implement the network using Matlab, initialize $\vec{a}$ with random values between 0 and 1, and simulate one second of activity.

9.7.6 Evaluation of Pitch Prediction Performance

The error of pitch prediction is quantified through the root mean squared deviation of the tinnitus frequencies predicted by the model from the pitch matching results of the patients. The deviation is measured in octaves. Thus, for the prediction error E_p, we have

$$E_\mathrm{p} = \sqrt{\frac{1}{n}\sum_{i=1}^{n}\left[\log_2(p_\mathrm{i}/t_\mathrm{i})\right]^2}, \tag{9.5}$$

with p_i being the tinnitus frequency (in kHz) predicted by the model for ear i, t_i the measured tinnitus pitch (in kHz) for this ear, and n the total number of ears.

The bias of pitch prediction is evaluated by computing the deviation of the mean predicted from the mean observed tinnitus pitch. For the bias B_p measured in octaves, we employ

$$B_\mathrm{p} = \frac{1}{n}\sum_{i=1}^{n}\log_2\left(p_\mathrm{i}/t_\mathrm{i}\right). \tag{9.6}$$

Finally, we calculate the correlation coefficient $C_\mathrm{p,t}$ to assess the correlation between predicted and observed tinnitus pitch:

$$C_\mathrm{p,t} = \frac{Cov(p,t)}{\sigma_\mathrm{p}\sigma_\mathrm{t}} \tag{9.7}$$

For this calculation, predicted and measured tinnitus pitch are converted to a logarithmic scale. The covariance $Cov(p,t)$ is then given by

$$Cov(p,t) = \frac{1}{n-1}\sum_{i=1}^{n}(\log_2 p_\mathrm{i} - \mu_\mathrm{p})(\log_2 t_\mathrm{i} - \mu_\mathrm{t}), \tag{9.8}$$

where $\mu_\mathrm{p} = \frac{1}{n}\sum_{i=1}^{n}\log_2 p_\mathrm{i}$ is the mean predicted and $\mu_\mathrm{t} = \frac{1}{n}\sum_{i=1}^{n}\log_2 t_\mathrm{i}$ the mean observed tinnitus pitch. The variance of the predicted tinnitus pitch is given by $\sigma_\mathrm{p}^2 = \frac{1}{n-1}\sum_{i=1}^{n}\left(\log_2 p_\mathrm{i} - \mu_\mathrm{p}\right)^2$, and the variance of the observed tinnitus pitch is calculated accordingly.

The three performance measures E_p, B_p, and $C_\mathrm{p,t}$ are related in the following way:

$$E_\mathrm{p}^2 = B_\mathrm{p}^2 + \frac{n}{n-1}\left(\sigma_\mathrm{p}^2 + \sigma_\mathrm{t}^2 - 2C_\mathrm{p,t}\sigma_\mathrm{p}\sigma_\mathrm{t}\right) \tag{9.9}$$

Chapter 10

Outlook

In this thesis we have addressed the relation between tinnitus and hearing loss. We have presented a theoretical model to explain how tinnitus-related activity patterns could arise in the auditory system after hearing loss. Our model is based on the physiology of the cochlea, the auditory nerve, and the auditory brainstem. It captures how the responses of auditory nerve fibers and cochlear nucleus neurons are changed after hearing loss through various kinds of cochlear damage. Moreover, the model evaluates the effects of a stabilization of the mean firing rate of cochlear nucleus neurons through homeostatic plasticity after hearing loss. Hearing loss can reduce the mean firing rate of neurons in the auditory pathway. In order to stabilize the mean rate at a certain target level, homeostatic plasticity increases excitatory synaptic strengths and neuronal excitability, and decreases inhibitory synaptic strengths. However, these changes can lead to increased spontaneous firing rates in a subpopulation of neurons. The results of our model are in agreement with data from animal studies on hyperactivity, and the predicted patterns of spontaneous firing rates are consistent with tinnitus pitch reported by patients. Thus, our model provides a biologically plausible theory of how hearing loss could lead to tinnitus. To our knowledge, this is the first model of tinnitus development that is consistent with patient data.

Current models of tinnitus generation like for example the 'Neurophysiological Model' by Jastreboff (1999) assume that tinnitus sensations are caused by altered activity patterns in the early auditory pathway. Our work provides a consistent framework that explains how the development of abnormal neuronal activity and thus tinnitus could be triggered by hearing loss. Moreover, our model also predicts that hyperactivity and possibly also tinnitus might be reduced through appropriate acoustic stimulation. This prediction is in accordance with recent results showing that an enhanced acoustic environment could prevent the development of increased spontaneous firing rates in the auditory cortex after acoustic trauma (Noreña and Eggermont, 2006). Moreover, it has also been demonstrated in the visual system that hyperactivity of cortical neurons could be induced through visual deprivation and reversed through restoring vision (Maffei et al., 2004). Restoring vision also reversed the observed homeostatic changes in excitatory and inhibitory synaptic strength. In our model, a complete renormalization of auditory nerve activity would completely reverse hyperactivity. This would correspond to a perfect hearing aid, but unfortunately this is not always possible with currently available technology. In section 7.4, we have derived a simpler strategy of matched-noise stimulation that might also be suitable for reversing hyperactivity. The spectrum of this matched-noise stimulus is similar to the enhanced acoustic environment used by Noreña and Eggermont (2006), and substantially

different from the unspecific white-noise stimuli that are currently used in tinnitus treatment.

Our theoretical results have direct implications for the treatment of tinnitus that is related to sensorineural hearing loss. For patients with tinnitus and hearing loss, the first objective should thus be to treat the symptoms of hearing loss by fitting a hearing aid. Alternatively, a noise generator producing a matched-noise stimulus as described in section 7.4 can be used. The spectrum of the noise needs to be adjusted to the patient's hearing loss. To test these predictions, a pilot study has been started in collaboration with Prof. Gross and Dr. König of the Charité Berlin. Depending on the severity of hearing loss, patients are fitted with a hearing aid or a noise generator.

Preliminary results look promising. In several patients, long-lasting suppression of tinnitus could be achieved: After using a hearing aid or a noise generator during the day, the patients were free of tinnitus for several hours in the evening. Usually, tinnitus returned until the next morning. The observed time-course indicates that the additional stimulation could indeed have influenced an activity-dependent gain control mechanism operating on a time-scale of hours. This result supports the basic assumptions of our model.

In our study, we use conventional hearing aids or noise generators. These devices are located behind the ear and use a plastic tube for sound conduction to the ear canal. This plastic tube inevitably acts as a low-pass filter and limits the highest possible output frequency of the devices to approximately 7 kHz. Several patients, however, matched their tinnitus pitch to a comparison tone of 8 kHz, sometimes stating that their tinnitus was even higher. For these patients, the stimulation devices do not provide stimulation around the tinnitus frequency. The model predicts that under these circumstances, additional stimulation should not be able to influence the tinnitus. This prediction is consistent with the result that none of these patients reported long-lasting suppression of tinnitus. Only a masking effect during stimulation was observed, with tinnitus returning immediately after the device had been turned off.

Our model predicts that it depends on the status of a patient's cochlea whether acoustic stimulation strategies can successfully reduce tinnitus. For stimulation to be effective, intact inner hair cells and auditory nerve fibers are required. So far, we have not been able to test whether our patients have cochlear dead regions, i.e. small regions in the cochlea where inner hair cells are absent. Unfortunately, cochlear dead regions are not detected by conventional audiometry (Moore et al., 2000). Such dead regions could severely limit the possibility of treating tinnitus through additional acoustic stimulation, as there is no way of stimulating deafferented auditory nerve fibers by means of acoustic stimuli. This could explain why some patients did not respond to the treatment, although in principle their tinnitus was in the right range to be reached by the stimulation devices.

So far, only the symptoms of hearing loss can be alleviated by means of hearing aids. A real cure for hearing loss is not yet available, because mammalian hair cells do not regenerate and hence damage to or loss of cochlear hair cells is irreversible. In birds, however, regeneration of hair cells has been observed after acoustic trauma or administration of ototoxic drugs (Corwin and Cotanche, 1988; Ryals and Rubel, 1988). Recently it has been demonstrated in cell culture that supporting cells of the mammalian cochlea retain the capacity to divide and transdifferentiate into hair cells (White et al., 2006). In vivo, cochlear supporting cells are prevented from re-entering the cell cycle by cell-cycle inhibitors. However, it is possible to stimulate the formation of hair cells through gene therapy: Delivery of the 'pro-hair-cell' gene *Atoh1* to the cochlea of guinea pigs stimulated the regeneration of hair cells after complete hair cell loss through ototoxic drugs (Izumikawa et al., 2005). The gene was delivered through adenovirus

vectors that were injected into the cochlea. The newly generated hair cells were functional and innervated by auditory nerve fibers, as demonstrated by near-normal thresholds of the acoustic brainstem response after treatment. These exciting results indicate that a cure for hearing loss and thus maybe also tinnitus might be available in a not so distant future. Until then, our results might improve tinnitus treatment and hopefully provide relief for many suffering patients.

Chapter 11

Deutsche Zusammenfassung

Tinnitus ist eine auditorische Illusion, eine Phantomwahrnehmung, zu der es keine entsprechende externe Schallquelle gibt. Das Tinnitusgeräusch kann dabei sowohl tonalen als auch rauschartigen Charakter haben. Typische Beschreibungen von Tinnitusgeräuschen sind Klingeln, Pfeifen, Summen, Brummen oder Rauschen. Dieses Phänomen ist weit verbreitet: Schätzungen gehen davon aus, dass bis zu 25% der Bevölkerung von Zeit zu Zeit eine Tinnitusepisode erleben. In den meisten Fällen handelt es sich dabei nur um ein kurzes Ereignis, das Sekunden bis Minuten dauert, in anderen Fällen jedoch ist der Tinnitus chronisch. Teilweise wird der Tinnitus von den Betroffenen so laut gehört, dass er von Umgebungsgeräuschen nicht überdeckt werden kann. Die Symptome können dabei so gravierend sein, dass die Lebensqualität der Betroffenen stark eingeschränkt ist. Hiervon sind in Deutschland etwa 1,5 Millionen Menschen betroffen.

Es gibt Anzeichen dafür, dass Tinnitus und Hörverlust zusammenhängen. Die Mehrheit der Tinnituspatienten hat ein eingeschränktes Hörvermögen. Die Tonhöhe des Tinnitus liegt dabei fast immer in Frequenzbereichen, die vom Hörverlust betroffen sind. Man nimmt deshalb an, dass eine Schädigung des Innenohres die Entwicklung von Tinnitus durch plastische Veränderungen in der Hörbahn begünstigen kann. Andererseits führt Hörverlust nicht automatisch zu Tinnitus. Da bislang nur eingeschränkte Erkenntnisse über die Pathogenese von Tinnitus beim Menschen vorliegen, gibt es derzeit keine kausale Therapie.

Das Tinnitusgeräusch wird wahrgenommen, obwohl kein entsprechender akustischer Schallreiz ans Ohr dringt. Die Ursache des Geräusches muss also in einer Veränderung der spontanen Aktivität von Nervenzellen im auditorischen System liegen. Die Muster der Spontantaktivität müssen dabei derart verändert sein, dass sie von Schallreizen hervorgerufener Nervenzellaktivität ähneln. So könnte zum Beispiel die spontane Entladungsrate von einzelnen Neuronen erhöht sein, oder eine Gruppe von Nervenzellen könnte ihre Spontanaktivität synchronisieren. Tinnitusartige Nervenzellaktivität wird nicht peripher im Innenohr, sondern im zentralen Hörsystem generiert. Entsprechend erfolglos waren frühere Versuche, Tinnitus in schwersten Fällen durch die Durchtrennung des Hörnervs zu behandeln.

Zur Erforschung der neurophysiologischen Grundlagen von Tinnitus wurden Tiermodelle entwickelt. Verhaltensversuche zeigten, dass auch Tiere Tinnitus empfinden können, zum Beispiel nach akustischem Trauma. In neurophysiologischen Experimenten mit verschiedenen Tierarten wurden keine Anzeichen von tinnitusartiger Nervenzellaktivität im Hörnerv nachgewiesen. Erhöhte spontane Entladungsraten als neurophysiologisches Korrelat von Tinnitus fand man jedoch im auditorischen Cortex, im Mittelhirn, sowie im Hirnstamm. Die früheste Stufe in

der Hörbahn, auf der tinnituskorrelierte Veränderungen der Spontanaktivität gefunden wurden, ist der cochleare Nukleus im Hirnstamm. Die Neurone im cochlearen Nukleus werden von den Hörnervfasern innerviert und stellen somit die erste zentrale Verarbeitungstufe der Hörbahn dar. Nach Schädigung der Cochlea durch akustisches Trauma war die spontane Feuerrate von Neuronen im dorsalen cochlearen Nukleus (DCN) signifikant erhöht. Die Stärke dieser 'Hyperaktivität' war zudem korreliert mit dem Verhalten von Versuchstieren bei Tinnitus-Tests. Die Entwicklung von Hyperaktivität im DCN nach Hörverlust stellt eine paradoxe Situation dar: Obwohl eine Schädigung der Cochlea die Aktivität der betroffenen Hörnervfasern und damit das Eingangssignal für den DCN reduziert, ist die spontane Feuerrate von DCN-Neuronen erhöht. Durch welchen Mechanismus diese Hyperaktivität entsteht ist jedoch noch weitgehend unklar.

Die vorliegende Arbeit befasst sich mit der Entstehung von Tinnitus, wobei der Fokus auf der Entwicklung von Tinnitus nach Hörverlust durch Schädigung des Innenohres liegt. Dabei wird folgenden Hauptfragen nachgegangen:

- Worin unterscheiden sich Tinnituspatienten mit Hörverlust von Patienten, die Hörverlust ohne Tinnitus haben?
- Wie entstehen erhöhte spontane Feuerraten im Hörsystem nach Hörverlust durch Schädigung der Cochlea?
- Kann ein Modell für die Entwicklung von erhöhten spontanen Feuerraten nach Hörverlust ausgehend von audiometrischen Daten die Tinnitustonhöhe vorhersagen?

Diese Fragestellungen sollen mithilfe theoretischer Modelle des auditorischen Systems sowie der Analyse audiometrischer Daten beantwortet werden.

Die Kapitel 2-5 beinhalten die Grundlagen. In Kapitel 2 wird zunächst ein Überblick über das auditorische System gegeben. Dabei wird ein besonderer Schwerpunkt auf die Physiologie des Hörnervs und des cochlearen Nukleus gelegt, da diese die Basis für die Modellierung in dieser Arbeit darstellen.

Kapitel 3 beschäftigt sich mit den Ursachen und Folgen von Hörverlust bei Mensch und Tier. Besonderes Augenmerk wird dabei auf den Zusammenhang zwischen Hörverlust und Schädigung der Cochlea, die Veränderung der Antworteigenschaften von Hörnervfasern nach Schädigung der Cochlea, sowie auf plastische Veränderungen im zentralen Hörsystem nach Hörverlust gelegt.

Dem Tinnitus beim Menschen und im Tiermodell widmet sich Kapitel 4. Zunächst werden Charakteristik und Epidemiologie von Tinnitus besprochen, dann werden Evidenzen für einen Zusammenhang zwischen Tinnitus und Hörverlust sowie für die Entstehung von Tinnitus im zentralen Hörsystem betrachtet. Im Abschnitt über Tiermodelle für Tinnitus werden die Ergebnisse von Verhaltensstudien zusammengefasst, die belegen, dass auch Tiere Tinnitus empfinden können. Dann folgt eine Besprechung der gefundenen neurophysiologischen Korrelate von Tinnitus im auditorischen Hirnstamm, Mittelhirn und Cortex. Eine Schädigung der Cochlea kann zu erhöhten spontanen Feuerraten von Neuronen entlang der Hörbahn führen. Im Cortex wurde außerdem auch erhöhte 'Synchronie' der neuronalen Aktivität gefunden.

Mechanismen aktivitätsabhängiger neuronaler Plastizität als mögliches Bindeglied zwischen Hörverlust und Tinnitus werden in Kapitel 5 besprochen. Es werden grundlegende Ergebnisse zur Langzeitpotenzierung und -depression von Synapsen vorgestellt. Bei diesen Mechanismen wird lokal die Stärke einzelner bzw. weniger Synapsen in Abhängigkeit von der neuronalen Aktivität verändert. Zum anderen besprechen wir homöostatische Mechanismen, von denen man annimmt, dass sie die Gesamtaktivität von Nervenzellen stabilisieren. Diese homöostatische Plastizität ist ein globaler Mechanismus, der die Stärke von allen inhibitorischen und exzitatorischen Synapsen eines Neurons skalieren und zusätzlich die Erregbarkeit der Nervenzelle verändern kann. Für das Vorhandensein von beiden Plastizitätsarten im Hörsystem tragen wir Evidenzen zusammen.

Die Kapitel 6-9 enthalten die Hauptergebnisse der vorliegenden Arbeit. In Kapitel 6, „Die Form des Audiogramms und das Auftreten von Tinnitus", widmen wir uns der Frage, wie sich die Audiogramme von Tinnituspatienten mit Hörverlust von denen von Patienten mit Hörverlust, aber ohne Tinnitus unterscheiden. Dafür analysieren wir audiometrische Daten von 71 Patienten mit berufsbedingter Lärmschwerhörigkeit (30 Patienten ohne Tinnitus, 24 mit tonalem und 17 mit rauschartigem Tinnitus). Wir stellen fest, dass sich die Audiogramme von Patienten mit und ohne Tinnitus in der Schwere des Hörverlusts, der Lage der Audiogrammkante sowie der maximalen Steilheit der Audiogramme unterscheiden. Im Vergleich zu Patienten ohne Tinnitus zeichnen sich Patienten mit Tinnitus im Mittel durch weniger Hörverlust, eine höhere Audiogrammkantenfrequenz sowie eine größere maximale Steilheit des Audiogramms aus. Die Unterschiede zwischen Patienten mit tonalem und rauschartigem Tinnitus hingegen sind nicht signifikant.

Kapitel 7, „Ein Modell für die Entwicklung von neuronaler Hyperaktivität", behandelt die Frage, wie sich erhöhte spontane Feuerraten im Hörsystem nach Hörverlust entwickeln können. Dazu benutzen wir ein phänomenologisches Modell, das die Antworten von Hörnervfasern und Neuronen des cochlearen Nukleus auf Schallreize, die Auswirkungen von verschiedenen Arten von cochlearer Schädigung sowie die Stabilisierung der mittleren Feuerrate von CN-Neuronen durch homöostatische Plastizität umfasst. Zunächst analysieren wir die Auswirkungen von Schädigung der Cochlea auf die Aktivität von Hörnervfasern und CN-Neuronen. Dabei stellen wir fest, dass Hörverlust eine dauerhafte Absenkung der mittleren Feuerrate von Hörnervfasern zur Folge hat, wodurch entsprechend auch die Aktvität von CN-Neuronen sinkt. Die Hauptannahme des Modells ist, dass eine derartige dauerhafte Veränderung der Aktivität homöostatische Plastizität in den CN-Neuronen aktiviert. Zur Stabilisierung der mittleren Feuerrate erhöht die Homöostase die neuronale Erregbarkeit und stärkt exzitatorische Synapsen. Diese Anpassung kann jedoch auch die spontane Feuerrate verändern und so die Entstehung von erhöhten spontanen Feuerraten bewirken. Hyperaktivität kann entstehen, wenn durch Schädigung der Cochlea das Verhältnis zwischen mittlerer und spontaner Feuerrate im Hörnerv reduziert ist. Im Modell entsteht Hyperaktivität nach dem Verlust von äußeren Haarzellen der Cochlea oder der Schädigung von Haarzell-Stereocilien. Des Weiteren kann Homöostase auch nichtauditorische Signale verstärken, welche dann zur Hyperaktivität beitragen. Schon dieses einfache Modell ohne freie Parameter liefert eine gute qualitative Übereinstimmung mit den Tierversuchsergebnissen zur Hyperaktivität im DCN.

In Kapitel 8, „Erweiterung des Modells zur Reproduktion der grundlegenden neuronalen Verschaltung des DCN", wird das Hyperaktivitätsmodell aus Kapitel 7 erweitert. Grundlage dafür ist die elementare neuronale Verschaltung des DCN, in der Projektionsneurone von zwei

verschiedenen Typen von inhbitorischen Interneuronen gehemmt werden. Durch Anpassen der Verbindungsstärken von den inhibitorischen Interneuronen zu den Projektionsneuronen können wir diese an die Antworteigenschaften von verschiedenen Typen von Projektionsneuronen des DCN wie zum Beispiel Typ-III und Typ-IV-Antworten anpassen. Dann untersuchen wir, wie die Aktivität der Modellneurone durch Schädigung der Cochlea verändert wird. Die mittlere Feuerrate der Modellneurone nach Hörverlust hängt ab von der Art und Schwere der Schädigung der Cochlea sowie der Stärke von Exzitation und Inhibition. Wir nehmen an, dass homöostatische Plastizität die mittlere Aktivität von Projektionsneuronen stabilisiert und dafür die Stärke von exzitatorischen und inhibitorischen Synapsen skaliert. Die spontane Feuerrate eines Projektionsneurons nach Hörverlust und Homöostase ist dann abhängig von der Art und Stärke der cochlearen Schädigung und dem Verhältnis von mittlerer zu spontaner Feuerrate vor Hörverlust. Nur Neurone, in denen Exzitation die Inhibition überwiegt, können hyperaktiv werden, weil hierdurch die mittlere Feuerrate über der Spontanrate liegt. Wir finden Hyperaktivität in Projektionsneuronen mit Typ-III- und Typ-IV-T-Antworteigenschaften, nicht jedoch in Typ-IV-Neuronen, deren mittlere Feuerrate nahe der spontanen Feuerrate ist.

In Kapitel 9, „Vorhersage der Tinnitustonhöhe aus Patientenaudiogrammen", wird unser Modell auf Daten von Patienten mit lärmbedingtem Hörverlust und tonalem Tinnitus angewandt. Für jeden Patienten modellieren wir ausgehend von seinem Audiogramm Veränderungen in der Spontanaktivität von Neuronen in der Hörbahn. Dann untersuchen wir, ob das im Modell auftretende Muster der Spontanaktivität mit der vom Patienten wahrgenommenen Tinnitustonhöhe konsistent ist. Die Ergebnisse zeigen, dass die Entwicklung von Hyperaktivität nach Hörverlust essentiell für eine korrekte Vorhersage der Tinnitustonhöhe ist. Gute Vorhersagen sind möglich auf Grundlage der Aktvität von Neuronen, in denen Exzitation die Inhibition überwiegt. In diesem Fall führt Aktivitätsstabilisierung durch homöostatische Plastizität zur Entwicklung von Hyperaktivität nach Hörverlust. Basierend auf den Hyperaktivitätsmustern liefert das Modell Vorhersagen mit niedrigem Vorhersagefehler (0,69 Oktaven), welcher der Unsicherheit der Tinnitusbestimmung beim Patienten vergleichbar ist. Außerdem zeichnen sich die Modellvorhersagen durch eine niedrige systematische Abweichung (-0,15 Oktaven) und hohe Korrelation (im Mittel 0,4) zwischen vorhergesagter und vom Patienten bestimmter Tinnitustonhöhe aus. Zum Vergleich implementieren wir ein anderes Modell der Tinnitusentstehung, das Hirnstammmodell von Gerken (1996). Dieses Modell ohne Homöostase sagt die Tinnitustonhöhe systematisch zu niedrig voraus, im Mittel um etwa 1,3 Oktaven.

Die Schlussfolgerungen und Konsequenzen, die sich aus den Ergebnissen der vorliegenden Arbeit ergeben, werden in Kapitel 10 zusammengefasst. Unser Modell für die Entstehung von neuronaler Hyperaktivität durch homöostatische Plastizität nach Hörverlust ist zum einen konsistent mit Daten aus Tierversuchen. Zum anderen sagt es auf der Basis von Patientenaudiogrammen Aktivitätsmuster vorher, die gut mit der von den jeweiligen Patienten empfundenen Tinnitustonhöhe übereinstimmen. Damit stellt es ein plausibles Modell für die Entstehung von Tinnitus nach Hörverlust dar. Soweit uns bekannt, ist es außerdem das erste Tinnitusmodell, dessen Vorhersagen konsistent mit Patientendaten sind. Aus dem Modell lassen sich direkte Konsequenzen für die Behandlung von Tinnitus ableiten. Wenn Tinnitus durch zentrale Kompensation für verringerte Hörnervaktivität nach Hörverlust entsteht, so sollte die Tinnitusbehandlung auf eine Renormalisierung der Hörnervaktivität abzielen, um so die Entstehung von Hyperaktivität rückgängig zu machen. Die dafür notwendige zusätzliche Reizung kann dabei durch Hörgeräte oder an den Hörverlust angepasste Rauschgeräte geschehen. Basierend auf dieser Vorhersage haben wir bereits eine Patientenstudie begonnen, deren erste Resultate er-

folgversprechend sind.

Acknowledgments

I would like to thank all those people without whom this work would not have been possible. First and foremost I would like to express my gratitude towards Richard Kempter. He gave me the opportunity to pursue my research in his research group and constantly supported me during these years. I would like to thank him for the inspiration, encouragement, and constructive criticism he gave me, and for the numerous discussions about my work. Apart from that, I would like to thank him for creating a research group with a good community spirit.

I would like to thank Christian Leibold for many discussions about my work, for always asking critical questions, and for mathematical support.

I am grateful to Manfred Gross and Ovidiu König for providing me with the audiometric data used in this thesis and for giving me the possibility to collaborate with them on the treatment of tinnitus patients. This gave me the opportunity of confronting my theoretical concepts with reality. In this context, I also would like to thank Dirk Hornig for devising a simple way to implement matched-noise stimulation.

Moreover, I would like to thank all those people who patiently read and commented on my manuscripts: Christian Leibold, Martin Stemmler, Andreas Herz, Samuel Glauser, Paula Kuokkanen, Robert Schmidt, Ed Hagen, Michael Kranert, and Antje Fürstenberg.

The ITB in Berlin has been an excellent place for my scientific work, and I would like to thank all its members for talks, discussions, and the great atmosphere. Especially, I would like to thank Jan Benda, Branka Bernard, Samuel Bernard, Roberto Fernandez-Galan, Matthias Flor, Matthias Franzius, Samuel Glauser, Ed Hagen, Kirsten Hilgenböcker, Paula Kuokkanen, Tim Oppermann, Robert Schmidt, susanne Schreiber, and Henning Sprekeler for scientific and non-scientific discussions, jokes, mensa, and coffee.

Last but not least, I would like to thank all my friends, my parents, and Antje.

Figure Acknowledgments

I would like to thank the American Physiological Society for granting me the permission to use Figure 2.3 from Taberner and Liberman (2005) and Figure 3.3 from Dallos and Harris (1978). I am grateful to Springer and to William Rhode, Kevin Davis, and Eric Young for allowing me to use Figure 2.5 from Rhode and Greenberg (1992) and Figs. 2.6 and 2.7 from Young and Davis (2002). The permission to use Figure 2.4 from Pollak et al. (2003) and Figure 3.1 from Chen and Fechter (2003) was granted to me by Elsevier. Furthermore, I would like to thank James Kaltenbach and Michael Heinz for allowing me to use their data to produce Figures 4.2 and 3.2.

List of Abbreviations

AN	auditory nerve
CF	characteristic frequency
CN	cochlear nucleus
DCN	dorsal cochlear nucleus
EPSC	excitatory postsynaptic current
IC	inferior colliculus
IPSC	inhibitory postsynaptic current
IHC	inner hair cell
LL	lateral lemniscus
LSO	lateral superior olive
LTD	long-term depression
LTP	long-term potentiation
MGB	medial geniculate body
MNTB	medial nucleus of the trapezoid body
MSO	medial superior olive
NBI	narrow-band inhibitor
OHC	outer hair cell
PN	projection neuron
WBI	wide-band inhibitor

Bibliography

A. A. Aarnisalo, U. Pirvola, X. Q. Liang, J. Miller, and J. Ylikoski. Apoptosis in auditory brainstem neurons after a severe noise trauma of the organ of corti: intracochlear BDNF treatment reduces the number of apoptotic cells. *ORL J. Otorhinolaryngol. Relat. Spec.*, 62:330–334, 2000.

J. C. Adams and B. D. Schulte. Histopathological observations of the aging gerbil cochlea. *Hear. Res.*, 104: 101–111, 1997.

C. D. Aizenmann, P. B. Manis, and D. J. Linden. Polarity of long-term synaptic gain change is related to postsynaptic spike firing at a cerebellar inhibitory synapse. *Neuron*, 21:827–835, 1998.

L. A. Anderson, M. S. Malmierca, M. N. Wallace, and A. R. Palmer. Evidence for a direct, short latency projection from the dorsal cochlear nucleus to the auditory thalamus in the guinea pig. *Eur. J. Neurosci*, 24:491–498, 2006.

G. Andersson. Tinnitus loudness matching in relation to annoyance and grading of severity. *Auris Nasus Larynx*, 30:129–133, 2003.

D. M. Baguley, P. Axon, I. M. Winter, and D. A. Moffat. The effect of vestibular nerve sectioning upon tinnitus. *Clin. Otolaryngol.*, 27:219–226, 2002.

D. Basta and A. Ernst. Effects of salicylate on spontaneous activity in inferior colliculus brain slices. *Neurosci. Res.*, 50:237–243, 2004.

D. Basta, B. Tzschentke, and A. Ernst. Noise-induced cell death in the mouse medial geniculate body and primary auditory cortex. *Neurosci. Lett.*, 381:199–204, 2005.

D. Bendor and X. Wang. The neuronal representation of pitch in primate auditory cortex. *Nature*, 436:1161–1165, 2005.

A. M. Berglund, T. E. Benson, and M. C. Brown. Synapses from labeled type II axons in the mouse cochlear nucleus. *Hear. Res.*, 94:31–46, 1996.

G. Q. Bi and M. M. Poo. Synaptic modifications in cultured hippocampal neurons: dependence on spike timing, synaptic strength, and postsynaptic cell type. *J. Neurosci.*, 18:10464–10472, 1998.

T. V. Bliss and T. Lomo. Long-lasting potentiation of synaptic transmission in the dentate area of the anaesthetized rabbit following stimulation of the perforant path. *J. Physiol.*, 232:331–356, 1973.

J. J. Blum, M. C. Reed, and J. M. Davies. A computational model for signal processing by the dorsal cochlear nucleus. II. Responses to broadband and notch noise. *J. Acoust. Soc. Am.*, 98:181–191, 1995.

T. J. Brozoski and C. A. Bauer. The effect of dorsal cochlear nucleus ablation on tinnitus in rats. *Hear. Res.*, 206: 227–236, 2005.

T. J. Brozoski, C. A. Bauer, and D. M. Caspary. Elevated fusiform cell activity in the dorsal cochlear nucleus of chinchillas with psychophysical evidence of tinnitus. *J. Neurosci.*, 22:2383–2390, 2002.

E. D. Buras, A. G. Holt, R. D. Griffith, M. Asako, and R. A. Altschuler. Changes in glycine immunoreactivity in the rat superior olivary complex following deafness. *J. Comp. Neurol.*, 494:179–189, 2006.

E.M. Burns. A comparison of variability among measurements of subjective tinnitus and objective stimuli. *Audiology*, 23:426–440, 1984.

J. Burrone and V. N. Murthy. Synaptic gain control and homeostasis. *Curr. Opin. Neurobiol.*, 13:560–567, 2003.

J. Burrone, M. O'Byrne, and V. N. Murthy. Multiple forms of synaptic plasticity triggered by selective suppression of activity in individual neurons. *Nature*, 420:414–418, 2002.

N. B. Cant. The cochlear nucleus: neuronal types and their synaptic organization. In B. D. Webster, A. N. Popper, and R. R. Fay, editors, *The Mammalian Auditory Pathway: Neuroanatomy*, chapter 3, pages 66–116. Springer, New York, 1992.

N. B. Cant and K. C. Gaston. Pathways connecting the right and left cochlear nuclei. *J. Comp. Neurol.*, 212: 313–326, 1982.

D. M. Caspary, T. A. Schatteman, and L. F. Hughes. Age-related changes in the inhibitory response properties of dorsal cochlear nucleus output neurons: role of inhibitory inputs. *J. Neurosci.*, 25:10952–10959, 2005.

J. H. Casseday, T. Fremouw, and E. Covey. The inferior colliculus: a hub for the central auditory system. In D. Oertel, R. R. Fay, and A. N. Popper, editors, *Integrative Functions in the Mammalian Auditory Pathway*, volume 15 of *Springer Handbook of Auditory Research*, chapter 7, pages 238–318. Springer, New York, 2002.

L. Cedolin and B. Delgutte. Pitch of complex tones: rate-place and interspike interval representations in the auditory nerve. *J. Neurophysiol.*, 94:347–362, 2005.

G. D. Chen and L. D. Fechter. The relationship between noise-induced hearing loss and hair cell loss in rats. *Hear. Res.*, 177:81–90, 2003.

G.-d. Chen and P.J. Jastreboff. Salicylate-induced abnormal activity in the inferior colliculus of rats. *Hear. Res.*, 82:158–178, 1995.

K. Chen, X. Song, and D. A. Godfrey. Effects of sodium salicylate on spontaneous activity of dorsal cochlear nucleus neurons. *Assoc. Res. Otolaryngol. Abs.*, page 45, 2003.

D.Y. Chung, R.P. Gannon, and K. Mason. Factors affecting the prevalence of tinnitus. *Audiology*, 23:441–452, 1984.

J. T. Corwin and D. A. Cotanche. Regeneration of sensory hair cells after acoustic trauma. *Science*, 240:1772–1774, 1988.

P. Dallos and D. Harris. Properties of auditory nerve responses in absence of outer hair cells. *J. Neurophysiol.*, 41:365–383, 1978.

G. W. Davis. Homeostatic control of neural activity: From phenomenology to molecular design. *Annu. Rev. Neurosci.*, 29:307–323, 2006.

H. Davis, R. W. Benson, W. P. Covel, C. Fernandez, R. Goldstein, Y. Katsuki, J. P. Legioux, D. R. McAuliffe, and I. Tasaki. Acoustic trauma in guinea pig. *J. Acoust. Soc. Am.*, 25:1180–1189, 1953.

K. A. Davis. Contralateral effects and binaural interactions in dorsal cochlear nucleus. *J. Assoc. Res. Otolaryngol.*, 6:280–296, 2005.

K. A. Davis, J. Ding, T. E. Benson, and H. F. Voigt. Response properties of units in the dorsal cochlear nucleus of unanesthetized decerebrate gerbils. *J. Neurophysiol.*, 75:1411–1431, 1996a.

K. A. Davis, R. L. Miller, and E. D. Young. Effects of somatosensory and parallel-fiber stimulation on neurons in dorsal cochlear nucleus. *J. Neurophysiol.*, 76:3012–3024, 1996b.

K. A Davis and E. D. Young. Pharmacological evidence of inhibitory and disinhibitory neuronal circuits in dorsal cochlear nucleus. *J. Neurophysiol.*, 83:926–940, 2000.

S. Dazert, M. L. Feldman, and E. M. Keithley. Cochlear spiral ganglion cell degeneration in wild-caught mice as a function of age. *Hear. Res.*, 100:101–106, 1996.

I. Dean, N. S. Harper, and D. McAlpine. Neural population coding of sound level adapts to stimulus statistics. *Nat. Neurosci.*, 8:1684–1689, 2005.

N. S. Desai, L. C. Rutherford, and G. G. Turrigiano. BDNF regulates the intrinsic excitability of cortical neurons. *Learn. Mem.*, 6:284–291, 1999a.

N. S. Desai, L. C. Rutherford, and G. G. Turrigiano. Plasticity in the intrinsic excitability of cortical pyramidal neurons. *Nat. Neurosci.*, 2:515–520, 1999b.

J. Ding, T. E. Benson, and H. F. Voigt. Acoustic and current-pulse responses of identified neurons in the dorsal cochlear nucleus of unanesthetized, decerebrate gerbils. *J. Neurophysiol.*, 82:3434–3457, 1999.

R. A. Dobie. Overview: Suffering from tinnitus. In J. B. Snow, editor, *Tinnitus: Theory and Management*, pages

1–15. B.C. Decker, Hamilton, London, 2004.

M. Dominguez, S. Becker, I. Bruce, and H. Read. A spiking neuron model of cortical correlates of sensorineural hearing loss: Spontaneous firing, synchrony, and tinnitus. *Neural Comput.*, 18:2942–2958, 2006.

J. J. Eggermont and L. E. Roberts. The neuroscience of tinnitus. *Trends. Neurosci.*, 27:676–682, 2004.

E. Emmerich, F. Richter, V. Linss, and W. Linss. Frequency-specific cochlear damage in guinea pig after exposure to different types of realistic industrial noise. *Hear. Res.*, 201:90–98, 2005.

M. A. Escabi, L. M. Miller, H. L. Read, and C. E. Schreiner. Naturalistic auditory contrast improves spectrotemporal coding in the cat inferior colliculus. *J. Neurosci.*, 23:11489–11504, 2003.

R. L. Folmer and J. R. Carroll. Long-term effectiveness of ear-level devices for tinnitus. *Otolaryngol. Head Neck Surg.*, 134:132–137, 2006.

C. Formby, L. P. Sherlock, and S. L. Gold. Adaptive plasticity of loudness induced by chronic attenuation and enhancement of the acoustic background. *J. Acoust. Soc. Am.*, 114:55–58, 2003.

H. W. Francis, D. K. Ryugo, M. J. Gorelikow, C. A. Prosen, and B. J. May. The functional age of hearing loss in a mouse model of presbycusis. II. neuroanatomical correlates. *Hear. Res.*, 183:29–36, 2003.

J. M. P. Franosch, R. Kempter, H. Fastl, and J. L. van Hemmen. Zwicker tone illusion and noise reduction in the auditory system. *Phys. Rev. Lett.*, 90:178103, 2003.

R. C. Froemke and Y. Dan. Spike-timing-dependent synaptic modification induced by natural spike trains. *Nature*, 416:433–438, 2002.

K. Fujino and D. Oertel. Bidirectional synaptic plasticity in the cerebellum-like mammalian dorsal cochlear nucleus. *Proc. Natl. Acad. Sci. USA*, 100:265–270, 2003.

J.-L. Gaiarsa, O. Caillard, and Y. Ben-Ari. Long-term plasticity at GABAergic and glycinergic synapses: mechanisms and functional significance. *Trends Neurosci.*, 25:564–570, 2002.

W. Y. Gao, D. L. Ding, X. Y. Zheng, F. M. Ruan, and Y. J. Liu. A comparison of changes in the stereocilia between temporary and permanent hearing losses in acoustic trauma. *Hear. Res.*, 62:27–41, 1992.

G. A. Gates and J. H. Mills. Presbycusis. *Lancet*, 366:1111–1120, 2005.

C. D. Geisler. *From sound to synapse*. Oxford University Press, New York, 1998.

G. M. Gerken. Central tinnitus and lateral inhibition: an auditory brainstem model. *Hear. Res.*, 97:75–83, 1996.

W. Gerstner, R. Kempter, J. L. van Hemmen, and H. Wagner. A neuronal learning rule for sub-millisecond temporal coding. *Nature*, 383:76–81, 1996.

A. L. Giraud, S. Chery-Croze, G. Fischer, C. Fischer, M. C. Vighetto, A. amd Gregoire, F. Lavenne, and L. Collet. A selective imaging of tinnitus. *Neuroreport*, 10:1–5, 1999.

J. J. Guinan and M. L. Gifford. Effects of electrical stimulation of efferent olivocochlear neurons on cat auditory-nerve fibers. *Hear. Res.*, 33:97–127, 1988.

R. Gütig, R. Aharonov, S. Rotter, and H. Sompolinsky. Learning input correlations through nonlinear temporally asymmetric hebbian plasticity. *J. Neurosci.*, 23:3697–3714, 2003.

J. S. Haas, T. Nowotny, and H. D. Abarbanel. Spike-timing-dependent plasticity of inhibitory synapses in the entorhinal cortex. *J. Neurophysiol.*, Aug 23:Epub ahead of print, 2006.

R. V. Harrison. Rate-versus-intensity functions and related AP responses in normal and pathological guinea pig and human cochleas. *J. Acoust. Soc. Am.*, 70:1036–1044, 1981.

R. V. Harrison, D. Ibrahim, and R. J. Mount. Plasticity of tonotopic maps in auditory midbrain following partial cochlear damage in the developing chinchilla. *Exp. Brain Res.*, 123:449–460, 1998.

J. W. P. Hazell. The TRT method in practice. In J. W. P. Hazell, editor, *Proceedings of the Sixth International Tinnitus Seminar*, pages 92–98. The Tinnitus and Hyperacusis Centre, London, 1999.

D. O. Hebb. *The organization of behavior: A neuropsychological theory*. Wiley, New York, 1949.

H. E. Heffner and I. A. Harrington. Tinnitus in hamsters following exposure to intense sound. *Hear. Res.*, 170: 83–95, 2002.

H. E. Heffner and G. Koay. Tinnitus and hearing loss in hamsters (mesocricetus auratus) exposed to loud sound. *Behav. Neurosci.*, 119:734–742, 2005.

M. G. Heinz and E. D. Young. Response growth with sound level in auditory nerve fibers after noise-induced hearing loss. *J. Neurophysiol.*, 91:784–794, 2004.

M. F. Heller and M. Bergman. Tinnitus aurium in normally hearing persons. *Ann. Otol. Rhinol. Laryngol.*, 62: 73–93, 1953.

J. A. Henry, C. L. Flick, A. Gilbert, R. M. Ellingson, and S. A. Fausti. Comparison of manual and computer-automated procedures for tinnitus pitch-matching. *J. Rehabil. Res. Dev.*, 41:121–138, 2004.

J. A. Henry, M. Meikle, and A. Gilbert. Audiometric correlates of tinnitus pitch: insights from the Tinnitus Data Registry. In J. Hazell, editor, *Proceedings of the Sixth International Tinnitus Seminar*, pages 51–57. The Tinnitus and Hyperacusis Centre, London, 1999.

H. J. Hoffman and G. W. Reed. Epidemiology of tinnitus. In J. B. Snow, editor, *Tinnitus: Theory and Management*, pages 16–41. B.C. Decker, Hamilton, London, 2004.

J. J. Hopfield. Neural networks and physical systems with emergent collective computational abilities. *Proc. Natl. Acad. Sci. USA*, 79:2554–2558, 1982.

J. W. House and D. E. Brackmann. Tinnitus: surgical treatment. *Ciba Found. Symp.*, 85:204–216, 1981.

A. R. Houweling, M. Bazhenov, I. Timofeev, M. Steriade, and T. J. Sejnowski. Homeostatic synaptic plasticity can explain post-traumatic epileptogenesis in chronically isolated neocortex. *Cereb. Cortex*, 15:834–845, 2005.

D. R. Irvine and R. Rajan. Injury-induced reorganization of frequency maps in adult auditory cortex: the role of unmasking of normally-inhibited inputs. *Acta Otolaryngol. Suppl.*, 532:39–45, 1997.

D. R. Irvine, R. Rajan, and S. Smith. Effects of restricted cochlear lesions in adult cats on the frequency organization of the inferior colliculus. *J. Comp. Neurol.*, 467:354–374, 2003.

D. R. F. Irvine. Physiology of the auditory brainstem. In A.N. Popper and R.R. Fay, editors, *The Mammalian Auditory Pathway: Neurophysiology*, chapter 4, pages 153–231. Springer, New York, 1992.

J. Ito and J. Sakakihara. Suppression of tinnitus by cochlear implantation. *Am. J. Otolaryngol.*, 15:145–148, 1994.

M. Izumikawa, R. Minoda, K. Kawamoto, K. A. Abrashkin, D. L. Swiderski, D. F. Dolan, D. E. Brough, and Y. Raphael. Auditory hair cell replacement and hearing improvement by atoh1 gene therapy in deaf mammals. *Nat. Med.*, 11:271–276, 2005.

P. Jackson. A comparison of the effects of eighth nerve sectioning with lidocaine on tinnitus. *J. Laryngol. Otol.*, 99:663–666, 1985.

A. V. Jacomme, F. R. Nodal, V. M. Bajo, Y Manunta, J. M. Edeline, A. Babalian, and E. M. Rouiller. The projection from auditory cortex to cochlear nucleus in guinea pigs: an in vivo anatomical and in vitro electrophysiological study. *Exp. Brain Res.*, 153:467–476, 2003.

M. M. Jastreboff and P. J. Jastreboff. How TRT derives from the neurophysiological model. In J. W. P. Hazell, editor, *Proceedings of the Sixth International Tinnitus Seminar*, pages 87–91. The Tinnitus and Hyperacusis Centre, London, 1999.

P. J. Jastreboff. The neurophysiological model of tinnitus and hyperacusis. In J. W. P. Hazell, editor, *Proceedings of the Sixth International Tinnitus Seminar*, pages 32–38. The Tinnitus and Hyperacusis Centre, London, 1999.

P. J. Jastreboff, J. F. Brennan, J. K. Coleman, and C. T. Sasaki. Phantom auditory sensation in rats: an animal model for tinnitus. *Behav. Neurosci.*, 102:811–822, 1988.

P. J. Jastreboff and J. W. P. Hazell. A neurophysiological approach to tinnitus: clinical implications. *Br. J. Audiol.*, 27:7–17, 1993.

P. J. Jastreboff and M. M. Jastreboff. Tinnitus retraining therapy (TRT) as a method for treatment of tinnitus and hyperacusis patients. *J. Am. Acad. Audiol.*, 11:162–177, 2000.

P. J. Jastreboff and C. T. Sasaki. An animal model for tinnitus: a decade of development. *Am. J. Otol.*, 15:19–27, 1994.

P. J. Jastreboof and C. T. Sasaki. Salicylate-induced changes in spontaneous activity of single units in the inferior

colliculus of the guinea pig. *J. Acoust. Soc. Am.*, 80:1384–1391, 1986.

R. L. Jenison. A computational model of reorganization in the auditory cortex in response to cochlear lesions. In W. Jesteadt, editor, *Modeling Sensorineural Hearing Loss*. Lawrence Earlbaum Associates, Hillsdale, NJ, 1997.

J. A. Kaltenbach, D. A. Godfrey, J. B. Neumann, D. L. McCaslin, C. E. Afman, and J. Zhang. Changes in spontaneous neural activity in the dorsal cochlear nucleus following exposure to intense sound: relation to threshold shift. *Hear. Res.*, 124:78–84, 1998.

J. A. Kaltenbach and C. E. Afman. Hyperactivity in the dorsal cochlear nucleus after intense sound exposure and its resemblance to tone-evoked activity: a physiological model for tinnitus. *Hear. Res.*, 140:165–172, 2000.

J. A. Kaltenbach, J. M. Czaja, and C. R. Kaplan. Changes in the tonotopic map of the dorsal cochlear nucleus following induction of cochlear lesion by exposure to intense sound. *Hear. Res.*, 59:213–223, 1992.

J. A. Kaltenbach and P. R. Falzarano. DCN hyperactivity induced by previous intense sound exposure: origin with respect to cell layer. In *Assoc. Res. Otolaryngol. Abs.*, page 208, 2002.

J. A. Kaltenbach, D. A. Godfrey, J. B. Neumann, D. L. McCaslin, C. E. Afman, and J. Zhang. Changes in spontaneous neural activity in the dorsal cochlear nucleus following exposure to intense sound: relation to threshold shift. *Hear. Res.*, 124:78–84, 1998.

J. A. Kaltenbach and D. L. McCaslin. Increases in spontaneous activity in the dorsal cochlear nucleus following exposure to high intensity sound: a possible neural correlate for tinnitus. *Audit. Neurosci.*, 3:57–78, 1996.

J. A. Kaltenbach, J. D. Rachel, T. A. Mathog, J. Zhang, P. R. Falzarano, and M. Lewandowski. Cisplatin-induced hyperactivity in the dorsal cochlear nucleus and its relation to outer hair cell loss: relevance to tinnitus. *J. Neurophysiol.*, 88:699–714, 2002.

J. A. Kaltenbach, M. A. Zacharek, J. Zhang, and S. Frederick. Activity in the dorsal cochlear nucleus of hamsters previously tested for tinnitus following intense tone exposure. *Neurosci. Lett.*, 355:121–125, 2004.

J. A. Kaltenbach, J. Zhang, and C. E. Afman. Plasticity of spontaneous neural activity in the dorsal cochlear nucleus after intense sound exposure. *Hear. Res.*, 147:282–292, 2000.

M. R. Kamke, M. Brown, and D. R. Irvine. Plasticity in the tonotopic organization of the medial geniculate body in adult cats following restricted unilateral cochlear lesions. *J. Comp. Neurol.*, 459:355–367, 2003.

P. O. Kanold and P. B. Manis. A physiologically based model of discharge pattern regulation by transient K+ currents in cochlear nucleus pyramidal cells. *J. Neurophysiol.*, 85:523–538, 2001.

P. O. Kanold and E. D. Young. Proprioceptive information from the pinna provides somatosensory input to cat dorsal cochlear nucleus. *J. Neurosci.*, 21:7848–7858, 2001.

E. M. Keithley and M. L. Feldman. Spiral ganglion cell counts in an age-graded series of rat cochleas. *J. Comp. Neurol.*, 188:429–442, 1979.

E. M. Keithley and M. L. Feldman. Hair cell counts in an age-graded series of rat cochleas. *Hear. Res.*, 8:249–262, 1982.

R. Kempter, W. Gerstner, and J.L. van Hemmen. Hebbian learning and spiking neurons. *Phys. Rev. E*, 59:4498–4514, 1999.

N. Y. Kiang, M. C. Liberman, and R. A. Levine. Auditory-nerve activity in cats exposed to ototoxic drugs and high-intensity sounds. *Ann. Otol. Rhinol. Laryngol.*, 85:752–768, 1976.

V. Kilman, M. C. W. van Rossum, and G. G. Turrigiano. Activity deprivation reduces miniature IPSC amplitude by decreasing the number of postsynaptic $GABA_a$ receptors clustered at neocortical synapses. *J. Neurosci.*, 22: 1328–1337, 2002.

K. C. Koerber, R. R. Pfeiffer, W. B. Warr, and N. Y. Kiang. Spontaneous spike discharges from single units in the cochlear nucleus after destruction of the cochlea. *Exp. Neurol.*, 16:119–130, 1966.

H. Komiya and J. J. Eggermont. Spontaneous firing activity of cortical neurons in adult cats with reorganized tonotopic map following pure-tone trauma. *Acta Otolaryngol.*, 120:750–756, 2000.

O. König, R. Schaette, R. Kempter, and M. Gross. Course of hearing loss and occurrence of tinnitus. *Hear. Res.*, 221:59–64, 2006.

V. C. Kotak, S. Fujisawa, F. A. Lee, O. Karthikeyan, C. Aoki, and D. H. Sanes. Hearing loss raises excitability in the auditory cortex. *J. Neurosci.*, 25:3908–3918, 2005.

V. C. Kotak and D. H. Sanes. Long-lasting inhibitory synaptic depression is age- and calcium-dependent. *J. Neurosci.*, 20:5820–5826, 2000.

M. Kudoh, M. Sakai, and K. Shibuki. Differential dependence of ltd on glutamate receptors in the auditory cortical synapses of cortical and thalamic inputs. *J. Neurophysiol.*, 88:3167–3174, 2002.

M. Kudoh and K. Shibuki. Long-term potentiation in the auditory cortex of adult rats. *Neurosci. Lett.*, 25:21–23, 1994.

M. Kudoh and K. Shibuki. Long-term potentiation of supragranular pyramidal outputs in the rat auditory cortex. *Exp. Brain Res.*, 110:21–27, 1996.

G. Langner and E. Wallhäusser-Franke. Computersimulation of a tinnitus model based on labeling of tinnitus activity in the auditory cortex. In J. W. P. Hazell, editor, *Proceedings of the Sixth International Tinnitus Seminar*, pages 20–25. The Tinnitus and Hyperacusis Centre, London, 1999.

S. Laughlin. A simple coding procedure enhances a neuron's information capacity. *Z. Naturforsch.*, 36:910–912, 1981.

R. A. Levine. Somatic (craniocervical) tinnitus and the dorsal cochlear nucleus hypothesis. *Am. J. Otolaryngol.*, 20:351–362, 1999.

R. A. Levine, M. Abel, and H. Cheng. Cns somatosensory-auditory interactions elicit or modulate tinnitus. *Exp. Brain Res.*, 153:643–648, 2003.

M. C. Liberman. Auditory-nerve response from cats raised in a low-noise chamber. *J. Acoust. Soc. Am.*, 63: 442–455, 1978.

M. C. Liberman. Single-neuron labeling and chronic cochlear pathology. I. Threshold shift and characteristic-frequency shift. *Hear. Res.*, 16:33–41, 1984.

M. C. Liberman and L. W. Dodds. Single-neuron labeling and chronic cochlear pathology. II. Stereocilia damage and alterations of spontaneous discharge rates. *Hear. Res.*, 16:43–53, 1984a.

M. C. Liberman and L. W. Dodds. Single-neuron labeling and chronic cochlear pathology. III. Stereocilia damage and alterations of threshold tuning curves. *Hear. Res.*, 16:55–74, 1984b.

M. C. Liberman and N. Y. Kiang. Single-neuron labeling and chronic cochlear pathology. IV. Stereocilia damage and alterations in rate- and phase-level functions. *Hear. Res.*, 16:75–90, 1984.

D. J. Lim. Ultrastructural cochlear changes following acoustic hyperstimulation and ototoxicity. *Ann. Otol. Rhinol. Laryngol.*, 85:740–751, 1976.

A. H. Lockwood, R. J. Salvi, and R. F. Burkland. Tinnitus. *N. Engl. J. Med.*, 347:904–910, 2002.

A. H. Lockwood, R. J. Salvi, M. L. Coad, M. L. Towsley, D. S. Wack, and B. W. Murphy. The functional neuroanatomy of tinnitus: evidence for limbic system links and neural plasticity. *Neurology*, 51:647–648, 1998.

W. L. Ma, H. Hidaka, and B. J. May. Spontaneous activity in the inferior colliculus of CBA/J mice after manipulations that induce tinnitus. *Hear. Res.*, 212:9–21, 2006.

W. L. Ma and E. D. Young. Dorsal cochlear nucleus response properties following acoustic trauma: response maps and spontaneous activity. *Hear. Res.*, 216-217:176–188, 2006.

A. Maffei, S. B. Nelson, and G. G. Turrigiano. Selective reconfiguration of layer 4 visual cortical circuitry by visual deprivation. *Nat. Neurosci*, 7:1353–1359, 2004.

M. S. Malmierca, M. A. Merchan, C. K. Henkel, and D. L. Oliver. Direct projections from cochlear nuclear complex to auditory thalamus in the rat. *J. Neurosci.*, 22:10891–10897, 2002.

Y. Manabe, S. Yoshida, H. Saito, and H. Oka. Effects of lidocaine on salicylate-induced discharge of neurons in the inferior colliculus of the guinea pig. *Hear. Res.*, 103:192–198, 1997.

E. Marder and A. A. Prinz. Modeling stability in neuron and network function: the role of activity in homeostasis. *BioEssays*, 24:1145–1154, 2002.

H. Markram, J. Lübke, M. Frotscher, and B. Sakman. Regulation of synaptic efficacy by coincidence of postsynaptic APs and EPSPs. *Science*, 275:213–215, 1997.

S. J. Martin, P. D. Grimwood, and R. G. Morris. Synaptic plasticity and memory: an evaluation of the hypothesis. *Annu. Rev. Neurosci.*, 23:649–711, 2000.

T. E. Mast. Binaural interaction and contralateral inhibition in dorsal cochlear nucleus of the chinchilla. *J. Neurophysiol.*, 33:108–115, 1970.

T. E. Mast. Dorsal cochlear nucleus of the chinchilla: excitation by contralateral sound. *Brain Res.*, 62:61–70, 1973.

H. J. McDermott, M. Lech, M. S. Kornblum, and D. R. F. Irvine. Loudness perception and frequency discrimination in subjects with steeply sloping hearing loss: possible correlates of neural plasticity. *J. Acoust. Soc. Am.*, 104:2314–2325, 1998.

S. L. McFadden, C. Kasper, J. Ostrowski, D. Ding, and R. J. Salvi. Effects of inner hair cell loss on inferior colliculus evoked potential thresholds, amplitudes and forward masking functions in chinchillas. *Hear. Res.*, 120:121–132, 1998.

D. P. McShane, M. L. Hyde, and P.W. Alberti. Tinnitus prevalence in industrial hearing loss compensation claimants. *Clin. Otolaryngol. Allied Sci.*, 13:323–330, 1988.

R. J. Meleca, J. A. Kaltenbach, and P. R. Falzarano. Changes in the tonotopic map of the dorsal cochlear nucleus in hamsters with hair cell loss and radial nerve bundle degeneration. *Brain Res.*, 750:201–213, 1997.

J. C. Milbrandt, T. M. Holder, M. C. Wilson, R. J. Salvi, and D. M. Caspary. Gad levels and muscimol binding in rat inferior colliculus following acoustic trauma. *Hear. Res.*, 147:251–260, 2000.

A. R. Møller. *Hearing – Its Physiology and Pathophysiology*. Academic Press, San Diego, 2000.

B. C. Moore, M. Huss, D. A. Vickers, B. R. Glasberg, and J. L. Alcantara. A test for the diagnosis of dead regions in the cochlea. *Br. J. Audiol.*, 34:205–224, 2000.

J. E. Mossop, M. J. Wilson, D. M. Caspary, and D. R. Moore. Down-regulation of inhibition following unilateral deafening. *Hear. Res.*, 147:183–187, 2000.

W. Mühlnickel, T. Elbert, E. Taub, and H. Flor. Reorganization of auditory cortex in tinnitus. *Proc. Natl. Acad. Sci. USA*, 95:10340–10343, 1998.

S. M. Muly, J. S. Gross, and S. J. Potashner. Noise trauma alters D-[3H]aspartate release and AMPA binding in chinchilla cochlear nucleus. *J. Neurosci. Res.*, 75:585–596, 2004.

V. N. Murthy, T. Schikorski, C. F. Stevens, and Y. Zhu. Inactivity produces increases in neurotransmitter release and synapse size. *Neuron*, 20:673–682, 2001.

J. B. Jr. Nadol. Electron microscopic findings in presbycusic degeneration of the basal turn of the human cochlea. *Otolaryngol. Head Neck Surg.*, 87:818–836, 1979.

K. Needham and A. G. Paolini. Fast inhibition underlies the transmission of auditory information between cochlear nuclei. *J. Neurosci.*, 23:6357–6361, 2003.

I. Nelken. Feature detection by the auditory cortex. In D. Oertel, R. R. Fay, and A. N. Popper, editors, *Integrative Functions in the Mammalian Auditory Pathway*, volume 15 of *Springer Handbook of Auditory Research*, chapter 9, pages 358–416. Springer, New York, 2002.

C. Nicolas-Puel, R.L. Faulconbridge, M. Guitton, J. L. Puel, M. Mondain, and A. Uziel. Characteristics of tinnitus and etiology of associated hearing loss: a study of 123 patients. *Int. Tin. J.*, 8:37–44, 2002.

A. Noreña, C. Micheyl, S. Chery-Croze, and L. Collet. Psychoacoustic characterization of the tinnitus spectrum: implications for the underlying mechanisms of tinnitus. *Audiol. NeuroOtol.*, 7:358–369, 2002.

A. J. Noreña and J. J. Eggermont. Changes in spontaneous neural activity immediately after an acoustic trauma: implications for neural correlates of tinnitus. *Hear. Res.*, 183:137–153, 2003.

A. J. Noreña and J. J. Eggermont. Enriched acoustic environment after noise trauma reduces hearing loss and prevents cortical map reorganization. *J. Neurosci.*, 25:699–705, 2005.

A. J. Noreña and J. J. Eggermont. Enriched acoustic environment after noise trauma abolishes neural signs of

tinnitus. *Neuroreport*, 17:559–563, 2006.

A. J. Noreña, M. Tomita, and J.J. Eggermont. Neural changes in cat auditory cortex after a transient pure-tone trauma. *J. Neurophysiol.*, 90:2387–2401, 2003.

R. J. O'Brien, S. Kambol, M. D. Ehlers, K. R. Rosen, G. D. Fischbach, and R. L. Huganir. Activity-dependent modulation of synaptic ampa receptor accumulation. *Neuron*, 21:1067–1078, 1998.

K. Ochi, T. Ohashi, and M. Kenmochi. Hearing impairment and tinnitus pitch in patients with unilateral tinnitus: comparison of sudden hearing loss and chronic tinnitus. *Laryngoscope*, 113:427–431, 2003.

S. Oleskevich and B. Walmsley. Synaptic transmission in the auditory brainstem of normal and congenitally deaf mice. *J. Physiol.*, 540:447–455, 2002.

L. C. Parra and B. A. Pearlmutter. Illusory percepts from auditory adaptation. *J. Acoust. Soc. Am.*, 121:1632–1641, 2007.

W.H. Phoon, H.S. Lee, and S.E. Chia. Tinnitus in noise-exposed workers. *Occup. Med. (London)*, 43:35–38, 1993.

M. Pilgramm, R. Rychlick, Lebisch H, H. Siedentrop, G. Goebel, and D. Kirchhoff. Tinnitus in the Federal Republic of Germany: a representative epidemological study. In J. W. P. Hazell, editor, *Proceedings of the Sixth International Tinnitus Seminar*, pages 64–67. The Tinnitus and Hyperacusis Centre, London, 1999.

R. J. Pinchoff, R. F. Burkard, R. J. Salvi, M. L. Coad, and A. H. Lockwood. Modulation of tinnitus by voluntary jaw movements. *Am. J. Otol.*, 19:785–789, 1998.

G. D. Pollak, R. M. Burger, and A. Klug. Dissecting the circuitry of the auditory system. *Trends Neurosci.*, 26: 33–39, 2003.

S. J. Potashner, S. K. Suneja, and C. G. Benson. Altered glycinergic synaptic activities in guinea pig brain stem auditory nuclei after unilateral cochlear ablation. *Hear. Res.*, 147:125–136, 2000.

C. Qiu, R. Salvi, D. Ding, and R. Burkard. Inner hair cell loss leads to enhanced response amplitudes in auditory cortex of unanesthetized chinchillas: evidence for increased system gain. *Hear. Res.*, 139:153–171, 2000.

N. Quaranta, S. Wagstaff, and D. M. Baguley. Tinnitus and cochlear implantation. *Int. J. Audiol.*, 43:245–251, 2004.

J. D. Rachel, J. A. Kaltenbach, and J. Janisse. Increases in spontaneous neural activity in the hamster dorsal cochlear nucleus following cisplatin treatment: a possible basis for cisplatin-induced tinnitus. *Hear. Res.*, 164: 206–214, 2002.

R. Rajan. Receptor organ damage causes loss of cortical surround inhibition without topographic map plasticity. *Nat. Neurosci.*, 1:138–143, 1998.

R. Rajan and D. R. Irvine. Absence of plasticity of the frequency map in dorsal cochlear nucleus of adult cats after unilateral partial cochlear lesions. *J. Comp. Neurol.*, 399:35–46, 1998a.

R. Rajan, D. R. Irvine, L. Z. Wise, and P. Heil. Effect of unilateral partial cochlear lesions in adult cats on the representation of lesioned and unlesioned cochleas in primary auditory cortex. *J. Comp. Neurol.*, 338:17–49, 1993.

R. Rajan and D. R. F. Irvine. Neuronal responses across cortical field A1 in plasticity induced by peripheral auditory organ damage. *Audiol. NeuroOtol.*, 3:123–144, 1998b.

A. Rao and A. M. Craig. Activity regulates the synaptic localization of the nmda receptor in hippocampal neurons. *Neuron*, 19:801–812, 1997.

J. P. Rauschecker. Auditory cortical plasticity: a comparison with other sensory systems. *Trends Neurosci.*, 22: 74–80, 1999.

G. F. Reed. An audiometric study of 200 cases of subjective tinnitus. *Arch. Otolaryngol.*, 71:94–104, 1960.

M. C. Reed and J. J. Blum. A computational model for signal processing by the dorsal cochlear nucleus. I. Responses to pure tones. *J. Acoust. Soc. Am.*, 97:425–438, 1995.

M. A. Reid, J. Flores-Otero, and R. L. Davis. Firing patterns of type-II spiral ganglion neurons *in vitro*. *J. Neurosci.*, 24:733–742, 2004.

S. A. Reyes, R. J. Salvi, R. F. Burkard, M. L. Coad, D. S. Wack, P. J. Galantowicz, and A. H. Lockwood. Brain imaging of the effects of lidocaine on tinnitus. *Hear. Res.*, 171:43–50, 2002.

W. S. Rhode and S. Greenberg. Physiology of the cochlear nuclei. In A.N. Popper and R.R. Fay, editors, *The Mammalian Auditory Pathway: Neurophysiology*, chapter 3, pages 94–152. Springer, New York, 1992.

L. E. Roberts, G. Moffat, and D. J. Bosnyak. Residual inhibition functions in relation to tinnitus spectra and auditory threshold shifts. *Acta Otolaryngol. Suppl.*, 556:27–33, 2006.

D. Robertson and D. R. F. Irvine. Plasticity of frequency organization in auditory cortex of guinea pigs with partial unilateral deafness. *J. Comp. Neurol.*, 282:456–471, 1989.

D. Robertson, P. M. Sellick, and R. Patuzzi. The continuing search for outer hair cell afferents in the guinea pig spiral ganglion. *Hear. Res.*, 136:151–158, 1999.

B.M. Ryals and E.W. Rubel. Hair cell regeneration after acoustic trauma in adult coturnix quail. *Science*, 240: 1774–1776, 1988.

D. K. Ryugo. The auditory nerve: peripheral innervation, cell body morphology, and central projections. In D.B. Webster, A.N. Popper, and R.R. Fay, editors, *The Mammalian Auditory Pathway, Neuroanatomy*, chapter 2, pages 23–65. Springer, New York, 1992.

M. B. Sachs and P. J. Abbas. Rate versus level functions for auditory-nerve fibers in cats: tone-burst stimuli. *J. Acoust. Soc. Am.*, 56:1835–1847, 1974.

T. Saito, Y. Manabe, N. Honda, T. Yamada, T. Yamamoto, and H. Saito. Semiquantitative analysis by scanning electron microscopy of cochlear hair cell damage by ototoxic drugs. *Scanning Microsc.*, 9:271–281, 1995.

R. J. Salvi, J. Wang, and D. Ding. Auditory plasticity and hyperactivity following cochlear damage. *Hear. Res.*, 147:261–274, 2000.

R. Schaette and R. Kempter. Development of tinnitus-related neuronal hyperactivity through homeostatic plasticity after hearing loss: a computational model. *Eur. J. Neurosci.*, 23:3124–3138, 2006.

R. A. Schmiedt and J. J. Zwislocki. Effects of hair cell lesions on responses of cochlear nerve fibers. II. Single- and two-tone intensity functions in relation to tuning curves. *J. Neurophysiol.*, 43:1390–1405, 1980.

B. A. Schneider and S. J. Hamstra. Gap detection thresholds as a function of tonal duration for younger and older listeners. *J. Acoust. Soc. Am.*, 106:371–380, 1999.

E. Schneider, K. M. Hocker, H. Lebisch, and M. Pilgramm. Does systematic noise stimulation improve tinnitus habituation? In J. W. P. Hazell, editor, *Proceedings of the Sixth International Tinnitus Seminar*, pages 391–393. The Tinnitus and Hyperacusis Centre, London, 1999.

J. W. Schnupp and A. J. King. Coding for auditory space in the nucleus of the brachium of the inferior colliculus in the ferret. *J. Neurophysiol.*, 78:2717–2731, 1997.

A. H. Seidl and B. Grothe. Development of sound localization mechanisms in the mongolian gerbil is shaped by early acoustic experience. *J. Neurophysiol.*, 94:1028–1036, 2005.

S. Seki and J. J. Eggermont. Changes in cat primary auditory cortex after minor-to-moderate pure-tone induced hearing loss. *Hear. Res.*, 173:172–186, 2002.

S. Seki and J. J. Eggermont. Changes in spontaneous firing rate and neural synchrony in cat primary auditory cortex after localized tone-induced hearing loss. *Hear. Res.*, 180:28–38, 2003.

S. H. Sha and J. Schacht. Stimulation of free radical formation by aminoglycoside antibiotics. *Hear. Res.*, 128: 112–118, 1999.

Y. Shiomi, J. Tsuji, Y. Naito, N. Fujiki, and N. Yamamoto. Characteristics of DPOAE audiogram in tinnitus patients. *Hear. Res.*, 108:83–88, 1997.

S. E. Shore. Multisensory integration in the dorsal cochlear nucleus: unit responses to acoustic and trigeminal ganglion stimulation. *Eur. J. Neurosci.*, 21:3334–3348, 2005.

S. E. Shore, D. A. Godfrey, R. H. Helfert, R. A. Altschuler, and S. C. Jr. Bledsoe. Connections between the cochlear nuclei in guinea pig. *Hear. Res.*, 62:16–26, 1992.

S. E. Shore, C. J. Sumner, S. C. Bledsoe, and J. Lu. Effects of contralateral sound stimulation on unit activity of

ventral cochlear nucleus neurons. *Exp. Brain Res.*, 153:427–435, 2003.

D. Sindhusake, M. Golding, P. Newall, G. Rubin, K. Jakobsen, and P. Mitchell. Risk factors for tinnitus in a population of older adults: the Blue Mountains Hearing Study. *Ear Hear.*, 24:501–507, 2003.

D. Sindhusake, M. Golding, D. Wigney, P. Newall, K. Jakobsen, and P. Mitchell. Factors predicting severity of tinnitus: a population-based assessment. *J. Am. Acad. Audiol.*, 15:269–280, 2004.

T. Sirimanna, D. Stephens, and T. Board. Tinnitus and audioscan notches. *J. Audiol. Med.*, 5:38–48, 1996.

P. H. Smith and G. A. Spirou. From the cochlea to the cortex and back. In D. Oertel, R. R. Fay, and A. N. Popper, editors, *Integrative Functions in the Mammalian Auditory Pathway*, volume 15 of *Springer Handbook of Auditory Research*, chapter 2, pages 6–71. Springer, New York, 2002.

S. Song and L. F. Abbott. Cortical development and remapping through spike timeing dependent plasticity. *Neuron*, 32:339–350, 2001.

S. Song, K. D. Miller, and L. F. Abbott. Competitive Hebbian learning through spike-timing dependent synaptic plasticity. *Nat. Neurosci.*, 3:919–926, 2000.

S. Soucek, L. Michaels, and A. Frohlich. Evidence for hair cell degeneration as the primary lesion in hearing loss of the elderly. *J. Otolaryngol.*, 15:175–183, 1986.

G. A. Spirou, K. A. Davis, I. Nelken, and E. D. Young. Spectral integration by type II interneurons in dorsal cochlear nucleus. *J. Neurophysiol.*, 82:648–663, 1999.

G. A. Spirou and E. D. Young. Organization of dorsal cochlear nucleus type IV unit response maps and their relationship to activation by bandlimited noise. *J. Neurophysiol.*, 66:1750–1768, 1991.

A. Spoor. Presbycusis values in relation to noise-induced hearing loss. *Int. Audiol.*, 6:48–57, 1967.

O. Stuhlmann. *An introduction to biophysics*. Wiley, New York, 1943.

C. J. Sumner, L. P. O'Mard, E. A. Lopez-Poveda, and R. Meddis. A nonlinear filter-bank model of the guinea-pig cochlear nerve: rate responses. *J. Acoust. Soc. Am.*, 113:3264–3274, 2003.

C. J. Sumner, D. L. Tucci, and S. E. Shore. Responses of ventral cochlear nucleus neurons to contralateral sound after conductive hearing loss. *J. Neurophysiol.*, 94:4234–4243, 2005.

S. K. Suneja, C. G. Benson, and S. J. Potashner. Glycine receptors in adult guinea pig brain stem auditory nuclei: regulation after unilateral cochlear ablation. *Exp. Neurol.*, 154:473–488, 1998a.

S. K. Suneja, S. J. Potashner, and C. G. Benson. Plastic changes in glycine and GABA release and uptake in adult brain stem auditory nuclei after unilateral middle ear ossicle removal and cochlear ablation. *Exp. Neurol.*, 151: 273–288, 1998b.

R. K. Surr, J. A. Kolb, M. T. Cord, and N. P. Garrus. Tinnitus handicap inventory (THI) as a hearing aid outcome measure. *J. Am. Acad. Audiol.*, 10:489–495, 1999.

A. M. Taberner and M. C. Liberman. Response properties of single auditory nerve fibers in the mouse. *J. Neurophysiol.*, 93:557–569, 2005.

H. Thai-Van, C. Micheyl, B. C. J. Moore, and L. Collet. Enhanced frequency discrimination near the hearing loss cut-off: a consequence of central auditory plasticity induced by cochlear damage? *Brain*, 126:2235–2245, 2003.

H. Thai-Van, C. Micheyl, A. Noreña, and L. Collet. Local improvement in auditory frequency discrimination is associated with hearing-loss slope in subjects with cochlear damage. *Brain*, 125:524–537, 2002.

D. A. Tucker, S. L. Phillips, R. A. Ruth, W. A. Clayton, E. Royster, and A. D. Todd. The effect of silence on tinnitus perception. *Otolaryngol. Head. Neck. Surg.*, 132:20–24, 2005.

G. G. Turrigiano. Homeostatic plasticity in neuronal networks: the more things change, the more they stay the same. *Trends Neurosci.*, 22:221–227, 1999.

G. G. Turrigiano, K. R. Leslie, N. S. Desai, L. C. Rutherford, and S. B. Nelson. Activity-dependent scaling of quantal amplitude in neocortical neurons. *Nature*, 391:892–896, 1998.

G. G. Turrigiano and S. B. Nelson. Hebb and homeostasis in neuronal plasticity. *Curr. Opin. Neurobiol.*, 10: 358–364, 2000.

T. Tzounopoulos, Y. Kim, D. Oertel, and L. O. Trussell. Cell-specific, spike timing-dependent plasticities in the dorsal cochlear nucleus. *Nat. Neurosci.*, 7:719–725, 2004.

C. Vale and D. H. Sanes. The effect of bilateral deafness on excitatory and inhibitory synaptic strength in the inferior colliculus. *Eur. J. Neurosci.*, 16:2394–2404, 2002.

M. W. van Ruijven, J. C. de Groot, S. F. Klis, and G. F. Smoorenburg. The cochlear targets of cisplatin: an electrophysiological and morphological time-sequence study. *Hear. Res.*, 205:241–248, 2005.

M. W. van Ruijven, J. C. de Groot, and G. Smoorenburg. Time sequence of degeneration pattern in the guinea pig cochlea during cisplatin administration. A quantitative histological study. *Hear. Res.*, 197:44–54, 2004.

D. Waldvogel, H. P. Mattle, M. Sturzenegger, and G. Schroth. Pulsatile tinnitus – a review of 84 patients. *J. Neurol.*, 245:137–142, 1998.

J. Wang, D. Ding, and R. J. Salvi. Functional reorganization in chinchilla inferior colliculus associated with chronic and acute cochlear damage. *Hear. Res.*, 168:238–249, 2002a.

J. Wang, N. L. Powers, P. Hofstetter, P. Trautwein, D. Ding, and R. Salvi. Effects of selective inner hair cell loss on auditory nerve fiber threshold, tuning and spontaneous and driven discharge rate. *Hear. Res.*, 107:67–82, 1997.

Y. Wang, K. Hirose, and M. C. Liberman. Dynamics of noise-induced cellular injury and repair in the mouse cochlea. *J. Assoc. Res. Otolaryngol.*, 3:248–268, 2002b.

D. L. Weedman and D. K. Ryugo. Pyramidal cells in primary auditory cortex project to cochlear nucleus in rat. *Brain Res.*, 706:97–102, 1996.

N. Weisz, T. Hartmann, K. Dohrmann, W. Schlee, and A. Norena. High-frequency tinnitus without hearing loss does not mean absence of deafferentation. *Hear. Res.*, 222:108–114, 2006.

P. M. White, A. Doetzlhofer, Y. S. Lee, A. K. Groves, and N. Segil. Mammalian cochlear supporting cells can divide and trans-differentiate into hair cells. *Science*, 441:984–987, 2006.

J. A. Winer. The functional architecture of the medial geniculate body and the primary auditory cortex. In D.B. Webster, A.N. Popper, and R.R. Fay, editors, *The mammalian auditory pathway: neuroanatomy*, pages 222–409. Springer, New York, 1992.

R. L. Winslow and M. B. Sachs. Effect of electrical stimulation of the crossed olivocochlear bundle on auditory nerve response to tones in noise. *J. Neurophysiol.*, 57:1002–1021, 1987.

E. D. Young. Identification of response properties of ascending axons from dorsal cochlear nucleus. *Brain Res.*, 200:23–37, 1980.

E. D. Young and K. A. Davis. Circuitry and function of the dorsal cochlear nucleus. In D. Oertel, R. R. Fay, and A. N. Popper, editors, *Integrative Functions in the Mammalian Auditory Pathway*, volume 15 of *Springer Handbook of Auditory Research*, chapter 5, pages 121–157. Springer, New York, 2002.

M. A. Zacharek, J. A. Kaltenbach, T. A. Mathog, and J. Zhang. Effects of cochlear ablation on noise induced hyperactivity in the hamster dorsal cochlear nucleus: implications for the origin of noise induced tinnitus. *Hear. Res.*, 172:137–144, 2002.

J. Zhang, J. A. Kaltenbach, J. Wang, and C. Davis. Origin of intense sound exposure induced hyperactivity in the dorsal cochlear nucleus of hamsters. *Assoc. Res. Otolaryngol. Abs.*, page 44, 2003.

L. I. Zhang, H. W. Tao, C. E. Holt, W. A. Harris, and M.-m. Poo. A critical window for cooperation and competition among developing retinotactical synapses. *Nature*, 395:37–44, 1998.

X. Zhang, M. G. Heinz, I. C. Bruce, and L. H. Carney. A phenomenological model for the responses of auditory nerve fibers: I. nonlinear tuning with compression and suppression. *J. Acoust. Soc. Am.*, 109:648–670, 2001.

Y. Zhang and S. H. Wu. Long-term potentiation in the inferior colliculus studied in rat brain slice. *Hear. Res.*, 147:92–103, 2000.

X. Zheng and H. F. Voigt. Computational model of response maps in the dorsal cochlear nucleus. *Biol. Cybern.*, 95:233–242, 2006a.

X. Zheng and H. F. Voigt. A modeling study of notch noise responses of type III units in the gerbil dorsal cochlear nucleus. *Ann. Biomed. Eng.*, 34:697–708, 2006b.

J. Zhou and S. Shore. Projections from the trigeminal nuclear complex to the cochlear nuclei: a retrograde and anterograde tracing study in the guinea pig. *J. Neurosci. Res.*, 78:901–907, 2004.

Selbständigkeitserklärung

Hiermit erkläre ich, dass ich die Dissertation selbständig verfasst und keine anderen als die angegebenen Hilfsmittel benutzt habe.

Berlin, den 15. Februar 2007